

Title: Attenuated evolution of mammals through the Cenozoic

Authors: Anjali Goswami^{1,2*}, Eve Noirault¹, Ellen J. Coombs^{1,2,3}, Julien Clavel⁴, Anne-Claire Fabre^{1,5,6}, Thomas J.D. Halliday^{1,7}, Morgan Churchill⁸, Abigail Curtis⁹, Akinobu Watanabe^{1,10,11}, Nancy B. Simmons¹², Brian L. Beatty^{10,13}, Jonathan H. Geisler^{10,13}, David L. Fox¹⁴, Ryan N. Felice^{1,2,15}

Affiliations:

¹Department of Life Sciences, Natural History Museum; London, United Kingdom

²Department of Genetics, Evolution, and Environment, University College London; London, United Kingdom

³Department of Vertebrate Zoology, National Museum of Natural History, Smithsonian Institution; Washington, DC, United States

⁴Université Lyon, Université Claude Bernard Lyon 1, CNRS, ENTPE, UMR 5023 LEHNA, F-69622, Villeurbanne, France

⁵Naturhistorisches Museum Bern; Bern, Switzerland

⁶Institute of Ecology and Evolution, University of Bern; Bern, Switzerland

⁷School of Geography, Earth and Environmental Sciences, University of Birmingham; Birmingham, United Kingdom

⁸Department of Biology, University of Wisconsin Oshkosh; Oshkosh, WI, USA

⁹Department of Biology, University of Washington; Seattle, WA, USA

¹⁰Department of Anatomy, College of Osteopathic Medicine, New York Institute of Technology; Old Westbury, NY, USA

¹¹Division of Paleontology, American Museum of Natural History; New York, NY, USA

¹²Department of Mammalogy, Division of Vertebrate Zoology, American Museum of Natural History; New York, NY, USA

¹³ Department of Paleobiology, National Museum of Natural History, Smithsonian Institution; Washington, DC, United States

¹⁴Department of Earth and Environmental Sciences, University of Minnesota; Minneapolis, MN, USA

¹⁵Centre for Integrative Anatomy, Department of Cell and Developmental Biology, University College London; London, United Kingdom

*Corresponding author. Email: a.goswami@nhm.ac.uk

Abstract: The Cenozoic diversification of placental mammals is the archetypal adaptive radiation. Yet, discrepancies between molecular divergence estimates and the fossil record fuel ongoing debate around the timing, tempo, and drivers of this radiation. Analysis of a high-dimensional 3D skull dataset for living and extinct placental mammals demonstrates that evolutionary rates peak early and attenuate quickly. This long-term decline in tempo is punctuated by bursts of innovation that decrease in amplitude over the past 66 million years. Social, precocial, aquatic, and herbivorous species evolve fastest, especially whales, elephants, sirenians, and extinct ungulates. Slow rates in rodents and bats indicate dissociation of taxonomic and morphological diversification. Frustratingly, highly similar ancestral shape estimates for placental mammal superorders suggest that their earliest representatives may continue to elude unequivocal identification.

One-Sentence Summary: Short bursts of innovation punctuate long-term decline in the rate of placental mammal skull evolution through the “Age of Mammals”.

Introduction

Placental mammals make up 94% of extant mammalian diversity, with over 6100 recognized extant species (1). This richness in species numbers is paired with an immense variation in ecology and morphology, with fully volant to fully aquatic forms spanning six orders of magnitude in size. Much diversification of placental mammals is thought to have been achieved quickly in the early Cenozoic, in the aftermath of the Cretaceous-Paleogene (K/Pg) mass extinction that removed non-avian dinosaurs from global ecosystems (2). However, despite a wealth of data from extant and fossil species, the timing, tempo, and drivers of the placental mammal morphological radiation have remained contentious. Studies of body size evolution variably support an early burst (3), accelerating rates linked to climate (4), or stable rates following the initial superordinal divergences. These studies often suggest that the K/Pg event had little impact on placental mammal evolution (5). In contrast, studies of tooth morphology or discrete character data suggest either that morphological diversification post-dated the K/Pg extinction (6, 7) or that rates of evolution increased rapidly at K/Pg boundary (8). Some of this uncertainty is due to ongoing debate on the timing of origin of Placentalia and its proximity to the K/Pg mass extinction (9–16). Two additional critical factors contribute to this uncertainty, 1) the exclusion of fossils from most studies, despite wholly extinct lineages dominating the initial post-K/Pg fauna (10), and 2) the limited phenotypic data used in most analyses of the morphological diversification of placentals. Phenotype is the object of natural selection, as the interface between organisms and their environment, but most studies reduce complex morphologies to highly simplified metrics, such as body size (11, 12) or discrete binary

characters (9, 13), hindering robust understanding of the influence of social, ecological, and developmental factors on morphological evolution.

Here we reconstruct the pattern and drivers of the morphological diversification of Placentalia with the first quantitative analysis of cranial evolution that samples the full breadth of living and extinct placental mammal diversity. Our dense 3D morphometric dataset (757 landmarks and sliding semi-landmarks) for 322 species spans the Cenozoic Era and represents every extant family and a majority of extinct orders (Fig. 1-2, fig. S1, table S1, data S1). We focus on the cranium because it is a feature-rich structure that performs several critical functions implicated in placental mammal success, from feeding, fighting, and communication to housing and protecting sensory structures and the brain. Given the ongoing debate on the timing of placental mammal diversification and the phylogenetic positions of some extinct clades, we perform these analyses across 1800 evolutionary trees, using multiple topologies and divergence estimates spanning from 100 to 70 million years ago, thereby incorporating the impact of this chronological and phylogenetic uncertainty on our understanding of placental mammal evolution. We summarized our results by binning these phylogenetic frameworks into a total of 18 sets, divided by tree topology and 5-million-year intervals for the placental mammal root age; for example, 100 trees use tree topology 2 and a divergence estimate for Placentalia ranging between 80-85 million years ago. With these analyses, we reconstructed the tempo and mode of evolution of the placental mammal skull to robustly test the hypothesis that placental mammals radiated quickly in the aftermath of the K/Pg mass extinction and to assess the primary social, developmental, and ecological factors associated with their morphological diversification.

Results

Cranial variation across placental mammals

Despite the vast ecological range of placental mammals, skull variation is overwhelmingly concentrated into a single region of morphospace, suggesting extensive conservation or convergence of cranial form across all placental mammal superorders (Fig. 1, fig. S2). There are two other clusters observed, but each is populated by single clades, specifically whales and rodents. PC1 (34.1% of the total variation) is dominated by shifts associated with the land-to-water transition of whales, with two distinct concentrations representing “terrestrial” and “aquatic” adaptive peaks. Extreme elongation of the premaxilla and maxilla and retraction of the nasals in Cetacea drives change along this axis, with early whales overlapping substantially with terrestrial Laurasian “ungulates” including Litopterna, Perissodactyla, and Artiodactyla. Several other lineages converge on aspects of this morphology, particularly the retraction of the nasals, including Sirenia, Desmostylia, Proboscidea, and Embrithopoda. The opposite extreme of PC1 is dominated by short-faced, globular euarchontaglirans, particularly Rodentia and Primates. Whales span the full breadth of PC2 (14.9% of the total variation), with the unusual extinct walrus-like whale *Odobenocetops* defining the maximum end of the axis, and the early archaeocete *Pakicetus* at the opposite extreme. Many placental mammal lineages are better discriminated along this axis, with extremely dolicocephalic armadillos occupying lower PC2 values, and brachycephalic primates, bats, and elephants at the positive end. Rodents are further distinguished on PC3, where they form a distinct concentration of variation separate from other terrestrial placental mammals (Fig. 1, fig. S2), driven largely by the height of facial region, size of the nasals, and orientation of the occipital region. Extant and extinct taxa largely overlap in cranial morphospace, with Paleogene to Recent taxa occupying similar positions on the principal axes. Fossil forms fill the gap between the terrestrial and aquatic clusters on PC1, but they also define the extremes of most principal axes, demonstrating the exceptional extinct diversity of

placentals. In contrast, the pale fox (*Vulpes pallida*) is closest to the average cranial shape of extant placental mammals, with an extinct confamilial, the borophagine dog *Desmocyon matthewsi* possessing a skull most similar to the average shape among the sampled living and extinct mammals.

Tempo of cranial evolution across placental mammals

Bayesian analysis using a reversible-jump Markov chain Monte Carlo algorithm supported variable-rates Brownian motion with a lambda tree transformation ($\lambda = 0.629-0.741$) as the best supported model of evolution across every phylogenetic topology and divergence time bin sampled in this study (fig. S3). Despite vast differences in the estimated root age for placentals, ranging from 100 to 70 million years in the phylogenetic hypotheses included here, results are remarkably consistent, with little to no difference in positions of rate shifts or relative rates of evolution across the placental mammal tree (Fig. 2; fig. S4). Rate shifts are clustered at the base of Placentalia, varying slightly in whether they occur at the basal nodes for each superorder or more inclusive nodes (e.g. Boreoeutheria and Atlantogenata) and demonstrating an increase in rate from stem to crown Placentalia (fig. S4). High rates are also concentrated at the base of many orders, reflecting the rapid accumulation of ecological and morphological diversity early in the placental mammal radiation. Multiple rate increases occur along the stem of Cetacea, with particularly fast rates of evolution on the branches leading to fully aquatic whales (basilosaurid archaeocetes + crown cetaceans), as well as to odontocetes. High rates of evolution are also observed at or near the base of Paenugulata (and/or Sirenia, depending on phylogenetic tree), Cingulata, Primates (and/or Catarrhini), Rodentia, and Chiroptera. There are relatively fewer high rates of evolution observed in less-inclusive clades, but high rates are observed on the

branches leading to hominids, sabre-toothed cats, pinnipeds, beavers, camels, yangochiropteran bats, and the extinct large-bodied brontothere perissodactyls (Fig. 2, fig. S4).

Placing evolutionary rates in temporal context necessarily depends heavily on the divergence estimates of the phylogenetic framework. Nonetheless, the distribution of evolutionary rates across a range of phylogenetic hypotheses is strongly indicative that the tempo of cranial evolution increased rapidly early in placental mammal evolution, proximal to the end-Cretaceous mass extinction, and fell equally rapidly, in contrast to studies of body size evolution in extant taxa (4, 5). This initial burst is followed by long term decline, but this decline is punctuated by multiple smaller peaks throughout the Cenozoic, a pattern that we describe as “attenuated evolution”, indicating decreasing amplitude of peaks in evolutionary rate along a backdrop of declining rates. The initial radiation and declining rates are consistent with an early burst model (18), but the presence of numerous intermediate peaks in evolutionary rates distinguishes this pattern from a standard early burst. The declining size of those peaks likely reflects increasingly limited niche space with distance from the K/Pg mass extinction, while their timing, allowing for the aforementioned uncertainties, likely reflects subsequent bursts of diversification associated with major climatic and geologic events. Several scenarios reconstruct a large peak in rates in the early to middle Eocene and smaller peaks near the Eocene-Oligocene and Oligocene-Miocene boundaries, all of which are associated with transitions between warmer and cooler climates (Fig. 3). In contrast, the impact of the rapid warming event at the Paleocene-Eocene boundary (PETM) on evolutionary rates is ambiguous, with sharp declines, small increases, or little change in rate during this interval, depending on the estimated root age of Placentalia.

Both the slowest and the fastest evolving clades in this study are wholly extinct lineages that straddle the end-Cretaceous mass extinction (Fig. 3, fig. S5). Stem placental mammals with

unambiguous Late Cretaceous origins and a rich fossil record evolved much more slowly than all crown placental mammals in every phylogenetic framework. “Archaic” and South American native ungulates, both of which first appear in the fossil record in the Paleocene in the aftermath of the mass extinction, display the fastest rates of evolution in every scenario. Comparing overall rates of cranial evolution across orders also demonstrates a clear dissociation of taxonomic diversification and morphological evolution in the crown placental mammal radiation.

Irrespective of topology and divergence estimates, laurasiatherian and afrotherian clades display the fastest rates of cranial evolution (Fig. 3; fig. S5), while the most speciose placental mammal orders, Rodentia and Chiroptera, show some of the lowest evolutionary rates for cranial shape.

The relative ranking among the five orders with the fastest rates of cranial evolution varies depending on topology and divergence time bin, but always includes: Cetacea, Proboscidea, Sirenia, and the extinct orders Litopterna and “Amblypoda” (a likely paraphyletic grouping of early Cenozoic large-bodied ungulates). Interestingly, members of the defunct, paraphyletic “Insectivora”, including Afrosoricida, Macroscelidea, Scandentia, and Eulipotyphla, consistently show some of the slowest rates of evolution, which may have contributed to the long-standing difficulties with ascertaining their phylogenetic relationships based on morphology alone.

Among extant superorders, Euarchontoglires is consistently the slowest evolving, with all clades, including rodents and primates, exhibiting some of the slowest evolutionary rates among placentals. The xenarthran clades all consistently display an intermediate rate of evolution relative to other placentals, while laurasiatherians show the broadest range of evolutionary rates across orders. Other than the fast-evolving aquatic or extinct ungulates and slow-evolving bats noted above, the other laurasiatherians show a division between herbivorous ungulate orders (Artiodactyla, Perissodactyla, and Notoungulata) that evolve at moderate rates, while

carnivorous laurasiatherians, including Carnivora and the extinct creodonts, display relatively slow rates of evolution. While we do not quantify taxonomic diversification in this study, our results do suggest that the expected close association of rates of speciation and rates of phenotypic evolution may not extend cleanly to the placental mammal skull. This expectation stems from theories of positive coupling between lineage splitting and adaptation to new niches via phenotypic evolution (19). In contrast, numerous examples exist of taxonomic diversification occurring in the absence of ecological or morphological divergence (20). Recent study of rates of body size evolution and speciation in several vertebrate clades identified a general relationship between these two rates within each vertebrate class, but noted that the strength of this association varied widely in subclades within each class. Moreover, some smaller clades displayed a negative relationship between rate of speciation and that of body size evolution (20). Similarly, the lack of a clear association between taxonomic diversity and rate of cranial evolution across placental mammals does not preclude a stronger association existing within placental mammal clades. A focused analysis of this relationship, taking into account ongoing debate on the ability to accurately estimate rates of taxonomic diversification (21), is needed, but it is worth considering whether the likely drivers of non-adaptive radiations, such as geographic isolation, may be more pronounced in smaller taxa, such as those that dominate the two most speciose placental mammal clades, Rodentia and Chiroptera.

Drivers of cranial evolution in placental mammals

We further examined the influences of size, diet, and locomotion on skull shape and rate of cranial evolution using multivariate phylogenetic linear models fitted by penalized likelihood, across the same distribution of phylogenetic tree topologies and divergence time bins described above. The additional factors of habitat, development (altricial/precocial), diel activity pattern,

and social structure (social/solitary) were further examined for the 207 extant species (data S1). When limited to extant taxa, size and diet were the only factors consistently supported as significantly influencing cranial shape and significantly interacting with each other across all phylogenetic frameworks and time bins ($p < 0.05$; table S2). Locomotion has a significant, albeit lower, effect on skull shape in all but the youngest divergence time bin (70-75Ma), whereas habitat type was supported as a significant factor in a minority of analyses. Analyses including extinct taxa are congruent with these results, including diet and size showing the strongest and most consistent influence on cranial shape, as well as having a significant interaction (table S2). Shape changes associated with increased size are concentrated in the elongation of the rostral region (fig. S6), as suggested by previous studies (22). Large size is additionally associated with retraction of the nasals, noted in numerous lineages as described above. Variation associated with dietary categories also reflects traits long identified as informative for ecomorphological analyses, including a larger sagittal crest in carnivores, reduced zygomatics in social insectivores, and rostrum elongation and cranial telescoping in bulk invertivores (a category composed entirely of cetaceans).

Although most of the factors we examined are not significantly associated with cranial shape, there are substantial differences in the rate of cranial evolution associated with these factors, which could be informative for modelling species response to environmental change. In particular, diet, locomotion, social structure, and development show significant differences in cranial rate among character states (Fig. 4, fig. S7). Dietary categories dominated by aquatic taxa, specifically bulk invertivores and piscivores, evolve the fastest, followed by herbivores. Aquatic and semi-aquatic mammals evolve fastest among locomotor categories, with arboreal and semi-arboreal showing comparatively slow evolution. Aquatic mammals similarly

dominated among habitat categories, whereas desert taxa exhibit a broad range of rates. Notably, social animals evolve significantly faster than solitary animals, potentially due to pressure for elaborate cranial ornamentation in many social species. Precocial species also evolve at a strikingly faster rate than altricial mammals, suggesting that extended parental care of young may result in overall slower rates of evolution. Placental mammals without a fixed period of activity, a category dominated by fast-evolving whales and proboscideans, evolve more rapidly than diurnal, nocturnal, or crepuscular species, but there are surprisingly no significant differences among taxa displaying these latter three activity patterns. Some of these patterns, such as fast rates in bulk invertivores, are clearly driven by cetaceans. However, several of the character states exhibited by some or most cetaceans are shared with other placentals, and these non-cetacean taxa also display higher rates of evolution. For example, aquatic mammals in this dataset include cetaceans, pinnipeds, sirenians, and desmostylians, all of which display elevated rates of skull evolution. Other character states associated with higher rates of evolution, such as precociality, sociality, and cathemeral activity pattern, are observed across placentals. In particular, these states are exhibited by many terrestrial herbivores (another fast-evolving ecological group), as well as cetaceans (fig. S8), demonstrating that these results are not solely driven by a single, fast-evolving clade.

Although not considered explicitly here, we may expect postcranial systems to diverge from the patterns observed here, particularly in terms of the differences across clades. Specifically, we may expect higher rates of postcranial evolution in bats and euarchontans, as well as in arboreal and semi-arboreal taxa more generally, in contrast to the low rates of cranial evolution observed for these groups here. More similarity in temporal pattern of cranial and postcranial evolution is likely, as those are likely driven by extrinsic phenomenon, such as mass extinctions or large-

scale environmental change. However, some of the most extreme postcranial transitions, associated with the appearance of fully aquatic or fully volant mammals, occur during the Eocene. Quantifying postcranial evolution would thus likely increase the amplitude of evolutionary rates during that interval, but further work along these lines is needed to test this hypothesis.

Ancestral estimations of the earliest placental mammals and implications for resolving their origins

Finally, we used our extensive sample of living and extinct placental mammals to estimate cranial shapes for the most recent common ancestor (MRCA) of placental mammals and of each of the four placental mammal superorders (Fig. 3). Regardless of the starting 3-D mesh used (shown here for *Vulpes pallida*, the most average extant placental mammal in this sample), ancestral estimates for the four superorders are remarkably similar, with only the euarchontogliran MRCA distinguished by a broader vault and a shorter and narrower rostrum. Subtle differences among all superordinal MRCAs exist, largely in the breadth and tapering of the rostrum. However, the similarities in these ancestral reconstructions may explain the persistent difficulties with identifying unambiguous Cretaceous crown placentals, despite the near certain divergence of the superorders in advance of the end-Cretaceous mass extinction. Rather than reflecting shortcomings of the fossil record or phylogenetic methodologies, this uncertainty may be due to the lack of clear morphological differences among the earliest representatives of the placental mammal superorders (7). This more pernicious source of uncertainty may be unresolvable, but, fortunately, our results demonstrate that reconstructions of the tempo and drivers of the exceptional morphological diversification of placental mammals are

robust to considerable uncertainty in both phylogenetic topology and the timing of their initial radiation.

Materials and Methods

Our dataset samples 322 crown and stem placental mammals, including 207 extant and 115 extinct species. 66 3D landmarks and 69 semi-landmark curves were collected for the left side of the skull using Stratovan Checkpoint (Stratovan, Davis, CA, USA). Landmarks and semi-landmarks were imported into R for analysis, where curves were resampled to a common number of semi-landmarks, slid to minimize bending energy, and registered with Generalised Procrustes Analysis, resulting in a total of 757 3D landmarks and sliding semi-landmarks. Data on diet, locomotion, habitat, development, social structure, and activity pattern were collected from the published literature.

In the absence of a well-resolved phylogenetic hypothesis that samples all living and extinct taxa in our dataset, we constructed an extensive range of alternative phylogenies. Starting with a set of node-dated trees from the posterior distribution of a recent species-level molecular analysis of placental mammal relationships (14), we binned these trees into six 5-million-year bins (70-75Ma, 75-80Ma, 80-85Ma, 85-90Ma, 90-95Ma, and 95-100Ma). We then grafted in fossil taxa based on a suite of recent morphological phylogenetic analyses (see Supplementary Materials), focusing on three alternative topologies that capture the major points of uncertainty, and generating 419,400 alternative trees to capture uncertainty in divergence estimates. Finally, we subsampled this set to 1800 trees, 100 for each of the six 5-million-year root-age bins for each of the three topologies, which was used in subsequent analyses.

Macroevolutionary analyses

To examine the overall pattern of cranial variation across placentals, we conducted a principal components analysis using Procrustes-aligned 3D data and reconstructed wireframe models for the minimum and maximum shapes on the primary axes of variation. We further estimated the ancestral shape for the placental MRCA and each superordinal MRCA by maximum likelihood and warping of a reference shape to the ancestral estimates.

We assessed 10 alternative evolutionary models (variable- and single-rate models for Brownian motion, Ornstein-Uhlenbeck, and BM with lambda, kappa, or delta tree transformations) for cranial evolution using phylogenetic PC scores representing 95% of the total variation in the dataset and a reversible-jump Markov Chain Monte Carlo (MCMC) algorithm implemented in BayesTraits v. 3 (5). For the best supported model, we binned rates by geological time and plotted their pattern through time for one randomly selected tree from 18 alternative tree topologies and divergence estimate bins. We further extracted rates for the terminal branches and plotted them by clade to assess differences in mean rate across clades.

We assessed the association of life history and ecological traits on cranial variation and evolutionary rates using Type II phylogenetic MANOVAs (phylogenetic regressions) on the Procrustes coordinates with log centroid size and each of the six factors as predictors across the same 18 trees. We conducted one analysis of size, diet, and locomotion for the full dataset of living and extinct species ($n = 322$) and a second one of all six factors for just the extant taxa ($n = 207$). Finally, we used a state-specific Brownian motion (BMM) model to estimate rates of evolution for each ecological and life history state across the full suite of 1800 trees. Further details of all materials and methods are provided in Supplementary Materials.

References and Notes:

1. C. J. Burgin, J. P. Colella, P. L. Kahn, N. S. Upham, How many species of mammals are there? *J. Mammal.* **99**, 1–14 (2018).
2. G. G. Simpson, The beginning of the age of mammals. *Biol. Rev.* **12**, 1–46 (1937).
3. N. Cooper, A. Purvis, Body size evolution in mammals: Complexity in tempo and mode. *Am. Nat.* **175**, 727–738 (2010).
4. J. Clavel, H. Morlon, Accelerated body size evolution during cold climatic periods in the Cenozoic. *Proc. Natl. Acad. Sci. U.S.A.* **114**, 4183–4188 (2017).
5. C. Venditti, A. Meade, M. Pagel, Multiple routes to mammalian diversity. *Nature.* **479**, 393–396 (2011).
6. D. M. Grossnickle, E. Newham, Therian mammals experience an ecomorphological radiation during the Late Cretaceous and selective extinction at the K–Pg boundary. *Proc. R. Soc. B.* **283**, 20160256 (2016).
7. N. Brocklehurst, E. Panciroli, G. L. Benevento, R. B. J. Benson, Mammaliaform extinctions as a driver of the morphological radiation of Cenozoic mammals. *Curr. Biol.* **31**, 2955–2963.e4 (2021).
8. T. J. D. Halliday, P. Upchurch, A. Goswami, Eutherians experienced elevated evolutionary rates in the immediate aftermath of the Cretaceous–Palaeogene mass extinction. *Proc. R. Soc. B.* **283**, 20153026 (2016).
9. R. M. D. Beck, M. S. Y. Lee, Ancient dates or accelerated rates? Morphological clocks and the antiquity of placental mammals. *Proc. R. Soc. B.* **281**, 20141278 (2014).
10. M. S. Springer, C. A. Emerling, R. W. Meredith, J. E. Janečka, E. Eizirik, W. J. Murphy, Waking the undead: Implications of a soft explosive model for the timing of placental mammal diversification. *Mol. Phylo. Evol.* **106**, 86–102 (2017).

11. R. W. Meredith *et al.*, Impacts of the Cretaceous terrestrial revolution and K/Pg extinction on mammal diversification. *Science*. **334**, 521–524 (2011).
12. S. Álvarez-Carretero *et al.*, A species-level timeline of mammal evolution integrating phylogenomic data. *Nature*. **602**, 263–267 (2022).
13. M. A. O’Leary *et al.*, The placental mammal ancestor and the post–K-Pg radiation of placentals. *Science*. **339**, 662–667 (2013).
14. T. J. D. Halliday, M. dos Reis, A. U. Tamuri, H. Ferguson-Gow, Z. Yang, A. Goswami, Rapid morphological evolution in placental mammals post-dates the origin of the crown group. *Proc. R. Soc. B*. **286**, 20182418 (2019).
15. N. S. Upham, J. A. Esselstyn, W. Jetz, Inferring the mammal tree: Species-level sets of phylogenies for questions in ecology, evolution, and conservation. *PLOS Biol*. **17**, e3000494 (2019).
16. N. M. Foley, M. S. Springer, E. C. Teeling, Mammal madness: is the mammal tree of life not yet resolved? *Phil. Trans. R. Soc. B*. **371**, 20150140 (2016).
17. T. R. Lyson *et al.*, Exceptional continental record of biotic recovery after the Cretaceous–Paleogene mass extinction. *Science*. **366**, 977–983 (2019).
18. L. J. Harmon *et al.*, Early bursts of body size and shape evolution are rare in comparative data. *Evol*. **64**, 2385–2396 (2010).
19. G. G. Simpson, *The Major Features of Evolution*. (Columbia University Press, New York, 1953).
20. C. R. Cooney, G. H. Thomas, Heterogeneous relationships between rates of speciation and body size evolution across vertebrate clades. *Nat. Ecol. Evol*. **5**, 101–110 (2021).
21. S. Louca, M. W. Pennell, Extant timetrees are consistent with a myriad of diversification histories. *Nature*. **580**, 502–505 (2020).

22. A. Cardini, P. D. Polly, Larger mammals have longer faces because of size-related constraints on skull form. *Nat. Commun.* **4**, 2458 (2013).
23. T. J. D. Halliday, P. Upchurch, A. Goswami, Resolving the relationships of Paleocene placental mammals. *Biol. Rev.* **92**, 521–550 (2017).
24. C. Bardua, R. N. Felice, A. Watanabe, A.-C. Fabre, A. Goswami, A practical guide to sliding and surface semilandmarks in morphometric analyses. *Integ. Org. Biol.* **1** (2019), doi:10.1093/iob/obz016.
25. S. Schlager, in *Statistical Shape and Deformation Analysis*, G. Zheng, S. Li, G. Székely, Eds. (Academic Press, 2017), pp. 217–256.
26. E. K. Baken, M. L. Collyer, A. Kaliontzopoulou, D. C. Adams, geomorph v4.0 and gmShiny: Enhanced analytics and a new graphical interface for a comprehensive morphometric experience. *Meth. Ecol. Evol.* **12**, 2355–2363.
27. J. M. Ryan, G. K. Creighton, L. H. Emmons, Activity patterns of two species of *Nesomys* (Muridae: Nesomyinae) in a Madagascar rain forest. *J. Trop. Ecol.* **9**, 101–107 (1993).
28. A. Orr, thesis, California State University Fresno (1998).
29. R. M. Nowak, E. P. Walker, *Walker's Mammals of the World* (Johns Hopkins University Press, Baltimore, 5th ed., 1991).
30. B. J. MacFadden, Cenozoic mammalian herbivores from the Americas: reconstructing ancient diets and terrestrial communities. *Annu. Rev. Ecol. Syst.* **31**, 33–59 (2000).
31. J. Kennis, C. Laurent, N. D. Amundala, A. M. Dudu, H. Leirs, Survival and movement of the Congo forest mouse (*Deomys ferrugineus*): a comparison of primary rainforest and fallow land in Kisangani, Democratic Republic of Congo. *Afric.Zool.* **47**, 147–159 (2012).
32. M. Kamoun, P. Steinmetz, Feeding behaviour, intake and digestion of the *Camelus dromedarius* at pasture. *Opt. Méditerr. B.* **13**, 51–57 (1995).

33. C. N. Jacques, J. D. Sievers, C. L. Sexton, D. E. Roddy, Evaluating diet composition of pronghorn in Wind Cave National Park, South Dakota, *Prairie Nat.* **12**, 239-250 (2006).
34. IUCN, The IUCN Red List of Threatened Species. Version 2021-3 (2021).
35. G. Guo, E. Zhang, Diet of the Chinese water deer (*Hydropotes inermis*) in Zhoushan Archipelago, China. *Acta Therio. Sin.* **25**, 122–130 (2005).
36. S. Giri, A. Aryal, R. K. Koirala, B. Adhikari, D. Raubenheimer, Feeding ecology and distribution of Himalayan serow (*Capricornis thar*) in Annapurna Conservation Area, Nepal. *World J. Zool.* **6**, 80-85 (2011).
37. C. Gebert, H. Verheyden-Tixier, Variations of diet composition of Red Deer (*Cervus elaphus* L.) in Europe. *Mamm. Rev.* **13**, 189-201 (2001).
38. W. W. Dalquest, thesis, Louisiana State University (1953).
39. L. Costeur, O. Maridet, S. Peigné, E. P. J. Heizmann, Palaeoecology and palaeoenvironment of the Aquitanian locality Ulm-Westtangente (MN2, Lower Freshwater Molasse, Germany). *Swiss J. Palaeontol.* **131**, 183–199 (2012).
40. J. F. Connor, The mammals of the Tug Hill Plateau, New York. *NY State Mus. Sci. Ser. Bull.* **406**, 1–82 (1966).
41. A. M. Candela, L. L. Rasia, M. E. Pérez, in *Early Miocene Paleobiology in Patagonia*, S. F. Vizcaíno, R. F. Kay, M. S. Bargo, Eds. (Cambridge University Press, ed. 1, 2012), pp. 287–305.
42. D. E. Wilson, S. Ruff, Eds., *The Smithsonian Book of North American Mammals* (Smithsonian Institution Press, Washington, 1999).
43. J. R. Schuette, D. M. Leslie, R. L. Lochmiller, J. A. Jenks, Diets of hartebeest and roan antelope in Burkina Faso: Support of the long-faced hypothesis. *Journal of Mammalogy.* **79**, 426–436 (1998).
44. J. D. Schmerge, thesis, University of Kansas (2015).

45. F. Reid, *A Field Guide to the Mammals of Central America & Southeast Mexico* (Oxford University Press, New York, 1997).
46. R. A. Pellew, The feeding ecology of a selective browser, the giraffe (*Giraffa camelopardalis tippelskirchi*). *J. Zool.* **202**, 57–81 (1984).
47. M. C. Muhlbachler, N. Solounias, Coevolution of tooth crown height and diet in oreodonts (Merycoidodontidae, Artiodactyla) examined with phylogenetically independent contrasts. *J. Mammal Evol.* **13**, 11–36 (2006).
48. B. Kassa, R. Libois, B. Sinsin, Diet and food preference of the waterbuck (*Kobus ellipsiprymnus defassa*) in the Pendjari National Park, Benin. *Afr. J. Ecol.* **46**, 303–310 (2008).
49. C. Janis, The species richness of Miocene browsers, and implications for habitat type and primary productivity in the North American grassland biome. *Palaeogeog. Palaeoclim. Palaeoecol.* **207**, 371–398 (2004).
50. T. Hofmann, H. Roth, Feeding preferences of duiker (*Cephalophus maxwelli*, *C. rufilatus*, and *C. niger*) in Ivory Coast and Ghana. *Mamm. Biol.* **68**, 65–77 (2003).
51. A. Forsyth, *Mammals of the Canadian Wild* (Firefly Books, Scarborough, Ont., Canada, 1985).
52. S. K. Eltringham, *The Hippos: Natural History and Conservation* (Academic Press, London, 1999).
53. J. J. M. Calede, J. X. Samuels, M. Chen, Locomotory adaptations in entomylachne gophers (Rodentia: Geomyidae) and the mosaic evolution of fossoriality. *J. Morph.* **280**, 879–907 (2019).
54. I. C. R. Barbosa *et al.*, Analysing the isotopic life history of the alpine ungulates *Capra ibex* and *Rupicapra rupicapra rupicapra* through their horns. *Rapid Commun. Mass Spectrom.* **23**, 2347–2356 (2009).
55. C. Blondel, H. Bocherens, A. Mariotti, Stable carbon and oxygen isotope ratios in ungulate teeth from French Eocene and Oligocene localities. *Bull. de la Soc. Géol. de France.* **168**, 775–781 (1997).

56. D. E. Wilson, R. A. Mittermeier, Eds., *Handbook of the Mammals of the World* (Lynx Edicions: Conservation International: IUCN, 2019).
57. S. R. Foss, in *The Evolution of Artiodactyls*, D. R. Prothero, S. E. Foss, Eds. (Johns Hopkins University Press, Baltimore, 2007).
58. P. Myers, R. Espinosa, C. S. Parr, T. Jones, G. S. Hammond, T. A. Dewey, *The Animal Diversity Web* (online) (2021; <https://animaldiversity.org>).
59. *The Paleobiology Database* (2021; www.paleobiodb.org).
60. C. De Muizon, G. Billet, C. Argot, S. Ladevèze, F. Goussard, *Alcidedorbignya inopinata*, a basal pantodont (Placentalia, Mammalia) from the early Palaeocene of Bolivia: anatomy, phylogeny and palaeobiology. *Geodiv.* **37**, 397 (2015).
61. J. R. Wible, G. W. Rougier, M. J. Novacek, R. J. Asher, Cretaceous eutherians and Laurasian origin for placental mammals near the K/T boundary. *Nature.* **447**, 1003–1006 (2007).
62. F. Delsuc *et al.*, The phylogenetic affinities of the extinct glyptodonts. *Curr. Biol.* **26**, R155–R156 (2016).
63. F. Delsuc *et al.*, Ancient mitogenomes reveal the evolutionary history and biogeography of sloths. *Curr. Biol.* **29**, 2031–2042 (2019).
64. A. E. Zurita, M. L. Taglioretti, L. M. de Los Reyes, F. Cuadrelli, D. G. Poire, Regarding the real diversity of Glyptodontidae (Mammalia, Xenarthra) in the late Pliocene (Chapadmalalan Age/Stage) of Argentina. *Anais da Acad. Bras. de Cienc.* **88**, 809–827 (2016).
65. M. S. Springer *et al.*, Interordinal gene capture, the phylogenetic position of Steller's sea cow based on molecular and morphological data, and the macroevolutionary history of Sirenia. *Molec. Phyl. Evol.* **91**, 178–193 (2015).
66. G. Billet, Phylogeny of the Notoungulata (Mammalia) based on cranial and dental characters. *J. Syst. Palaeont.* **9**, 481–497 (2011).

67. F. Welker *et al.*, Ancient proteins resolve the evolutionary history of Darwin’s South American ungulates. *Nature*. **522**, 81–84 (2015).
68. J. A. O’Sullivan, “Evolution of the Proximal Third Phalanx in Oligocene-Miocene Equids, and the Utility of Phalangeal Indices in Phylogeny Reconstruction” in *Mammalian Evolutionary Morphology: A Tribute to Frederick S. Szalay*, E. J. Sargis, M. Dagosto, Eds. (Vertebrate Paleobiology and Paleoanthropology Series, Springer Netherlands, Dordrecht, 2008;), pp. 159–165.
69. J. L. A. Paijmans *et al.*, Evolutionary history of saber-toothed cats based on ancient mitogenomics. *Curr. Biol.* **27**, 3330–3336 (2017).
70. A. Berta, M. Churchill, R. W. Boessenecker, The origin and evolutionary biology of pinnipeds: seals, sea lions, and walruses. *Ann. Rev. Earth Planet. Sci.* **46**, 203–228 (2018).
71. R. Weppe, C. Blondel, M. Vianey-Liaud, T. Pélissié, M. J. Orliac, A new Cainotherioidea (Mammalia, Artiodactyla) from Palembert (Quercy, SW France): Phylogenetic relationships and evolutionary history of the dental pattern of Cainotheriidae. *Palaeontol. Electron.* **23**, 1–20 (2020).
72. M. Spaulding, M. A. O’Leary, J. Gatesy, Relationships of Cetacea (Artiodactyla) Among Mammals: Increased Taxon Sampling Alters Interpretations of Key Fossils and Character Evolution. *PLOS ONE*. **4**, e7062 (2009).
73. M. Spaulding, J. J. Flynn, Phylogeny of the Carnivoramorpha: The impact of postcranial characters. *J. Syst. Palaeont.* **10**, 653–677 (2012).
74. R. S. Feranec, Ecological generalization during adaptive radiation: evidence from Neogene mammals. *Evol. Ecol. Res.* **9**, 555–577 (2007).
75. M. Churchill, J. H. Geisler, B. L. Beatty, A. Goswami, Evolution of cranial telescoping in echolocating whales (Cetacea: Odontoceti). *Evol.* **72**, 1092–1108 (2018).
76. G. T. Lloyd, G. J. Slater, A total-group phylogenetic metatree for Cetacea and the importance of fossil data in diversification analyses. *Syst. Biol.* **70**, 922–939 (2021).

77. J. H. Geisler, M. W. Colbert, J. L. Carew, A new fossil species supports an early origin for toothed whale echolocation. *Nature*. **508**, 383–386 (2014).
78. F. G. Marx, R. E. Fordyce, Baleen boom and bust: a synthesis of mysticete phylogeny, diversity and disparity. *Roy. Soc. Open Sci.* **2**, 140434.
79. G. M. Gasparini, M. Ubilla, *Platygonus* sp. (Mammalia: Tayassuidae) in Uruguay (Raigón? Formation; Pliocene–early Pleistocene), comments about its distribution and palaeoenvironmental significance in South America. *J. Nat. Hist.* **45**, 2855–2870 (2011).
80. N. Rybczynski, M. R. Dawson, R. H. Tedford, A semi-aquatic Arctic mammalian carnivore from the Miocene epoch and origin of Pinnipedia. *Nature*. **458**, 1021–1024 (2009).
81. L. T. Holbrook, J. Lapergola, A new genus of perissodactyl (Mammalia) from the Bridgerian of Wyoming, with comments on basal perissodactyl phylogeny. *J. Vert. Paleont.* **31**, 895–901 (2011).
82. M. C. Muhlbachler, Species taxonomy, phylogeny and biogeography of the Brontotheriidae (Mammalia, Perissodactyla), *Bull. Amer. Mus. Nat. Hist.* **311**, 1–473 (2008).
83. J. Tissier *et al.*, New data on Aynodontidae (Mammalia, Perissodactyla) from Eastern Europe: Phylogenetic and palaeobiogeographic implications around the Eocene-Oligocene transition. *PLOS ONE*. **13**, e0193774 (2018).
84. D. Prothero, *The Evolution of North American Rhinoceroses* (Cambridge University Press, 2005)
85. P.-O. Antoine *et al.*, A revision of *Aceratherium blanfordi* Lydekker, 1884 (Mammalia: Rhinocerotidae) from the Early Miocene of Pakistan: postcranials as a key. *Zool. J. Linn. Soc.* **160**, 139–194 (2010).
86. B. A. Williams, R. F. Kay, E. C. Kirk, New perspectives on anthropoid origins. *Proc. Natl. Acad. Sci. U.S.A.* **107**, 4797–4804 (2010).
87. A. Harrington, M. Silcox, G. Yapuncich, D. Boyer, J. Bloch, First virtual endocasts of adapiform primates. *J. Human Evol.* **99**, 52–78 (2016).

88. J. I. Bloch, M. T. Silcox, D. M. Boyer, E. J. Sargis, New Paleocene skeletons and the relationship of plesiadapiforms to crown-clade primates. *Proc. Natl. Acad. Sci. U.S.A.* **104**, 1159–1164 (2007).
89. S. Hopkins, Phylogeny and evolutionary history of the Aplodontioidea (Mammalia: Rodentia). *Zool. J. Linn. Soc.* **153**, 769–838 (2008).
90. J. J. M. Calede, J. X. Samuels, A new species of *Ceratogaulus* from Nebraska and the evolution of nasal horns in Mylagaulidae (Mammalia, Rodentia, Aplodontioidea). *J. Syst. Palaeont.* **18**, 1395–1414 (2020).
91. P. Virtanen *et al.*, SciPy 1.0: fundamental algorithms for scientific computing in Python. *Nat. Methods.* **17**, 261–272 (2020).
92. E. W. Goolsby, J. Bruggeman, C. Ané, Rphylopar: fast multivariate phylogenetic comparative methods for missing data and within-species variation. *Meth. Ecol. Evol.* **8**, 22–27 (2017).
93. J. Clavel, G. Escarguel, G. Merceron, mvmorph: an r package for fitting multivariate evolutionary models to morphometric data. *Meth. Ecol. Evol.* **6**, 1311–1319 (2015).
94. J. Clavel, H. Morlon, Reliable Phylogenetic Regressions for Multivariate Comparative Data: Illustration with the MANOVA and Application to the Effect of Diet on Mandible Morphology in Phyllostomid Bats. *Syst. Biol.* **69**, 927–943 (2020).
95. L. J. Revell, Phylogenetic signal and linear regression on species data. *Meth. Ecol. Evol.* **1**, 319–329 (2010).
96. E. A. Housworth, E. P. Martins, M. Lynch, The phylogenetic mixed model. *Am. Nat.* **163**, 84–96 (2004).
97. R. P. Freckleton, P. H. Harvey, M. Pagel, Phylogenetic analysis and comparative data: a test and review of evidence. *Am. Nat.* **160**, 712–726 (2002).

Acknowledgments: We are indebted to the numerous colleagues, curators, and collections staff at international museums that provided access to specimens for this project, in particular Roberto Portela Míguez, Roula Pappa, Pip Brewer, Richard Sabin, and Louise Tomsett (NHM), Pierre-Henri Fabre (Université de Montpellier), Judy Galkin, Ruth O’Leary, and Alana Gishlick (AMNH), Gertrud Rößner (BSP), S. and R. Boessenecker (CCNHM), Bill Simpson (FMNH), Desui Miao (KU), Judith Chupasko (MCZ), Sam McLeod,

Xiaoming Wang, and Jorge Velez-Juarbe (LACM), Jack Ashby and Paolo Viscardi (LDUCZ), Marcelo Reguero (MLP), Guillaume Billet, Jacques Cuisin, and Geraldine Veron (MNHN), Pat Holroyd, Mark Goodwin, and Jack Tseng (UCMP), Bill Sanders (UMMP), Amanda Millhouse and Suzanne Peurach (USNM), Chris Norris and Dan Brinkman (YPM), Ross Secord and George Carter (UNSM), and Loic Costeur (NMB). We are grateful to Vincent Fernandez and Brett Clark (NHM) and Jonathan Keller (UMN) for support in microCT scanning and to the ‘plate-forme de morphometrie’ of the UMS 2700 (CNRS, MNHN) for access to the surface scanner. We thank Emily Watt (NHM/UCL) for uploading scans to online repositories. We are grateful to the two anonymous reviewers and the editor for their thoughtful comments. We thank V. Herridge for putting a name to this phenomenon.

Funding: European Research Council grant STG-2014-637171 (AG)

National Science Foundation SF-EAR 1349607 (JG, BB, AG, MC)

Gerstner Scholar Postdoctoral Research Fellowship (AC, NS)

Natural Environment Research Council Doctoral Training Partnership training grant
NE/L002485/1 (EC)

Horizon 2020 MCSA Fellowship IF 797373-EVOTOOLS (JC)

National Science Foundation EAR 1338262 (DLF)

Labex BCDiv 10-LABX-0003 (ACF)

Author contributions:

Conceptualization: AG

Methodology: AG, RNF, JC, ACF, AW

Software: AG, RNF, JC, AW, ACF

Investigation: AG, RNF, EN, JC, EC, ACF, TJDH, AC, MC, BB, JG, NS, DLF

Visualization: AG, RNF

Funding acquisition: AG, EC, JG, BB, AC, NS

Writing – original draft: AG

Writing – review & editing: AG, RNF, EN, JC, EC, ACF, TJDH, AC, MC, BB, JG, NS,
DLF, AW

Competing interests: Authors declare that they have no competing interests.

Data and materials availability: Morphometric data and novel code are provided on Github

(https://github.com/anjoswami/Goswami_et_al_Placental_evolution_2022). 3D meshes

for all specimens are available for free download on Phenome10k.org or

Morphosource.org, as detailed in data S1, unless specifically restricted by specimen

repositories. All specimen and species details, including physical and online repository

information and trait data, are provided in data S1.

Supplementary Materials:

Supplementary Materials and Methods

Figures S1 to S8

Tables S1 to S2

Data S1

References (23–97)

Figure captions

Figure 1. Cranial variation across placental mammals is highly concentrated. A) Cranial morphospace for placental mammals showing PC1-3, with density contours reflecting three concentrations of placental mammal skull shapes, two dominated by single clades, and highlighting specimens along the edges of each of the high-density regions. B) Detailed morphospace of PC1-2, showing superordinal and ordinal affiliations of specimens and wireframe models of the variation along each axis. Symbols and colours in the morphospace indicate clade affiliation, as described on the legend (version with color-blind palette provided in figure S2). Colours on skull wireframes denote different cranial elements (see table S1 for details).

Figure 2. Rapid evolutionary rates are observed near the base of several placental mammal clades. Estimated branch-specific rates of cranial evolution using a variable-rates Brownian motion model with a lambda tree transformation, shown here for one example tree (Topology 2, root age 80-85Ma, tree 85 of 100). Warmer and cooler colors indicate faster and slower rates of evolution, respectively, with yellow indicating moderate rates. Fast branches are concentrated within Cetacea, indicated with a whale icon, as well as more basal branches for several orders. A subset of the sampled skulls is positioned proximal to their terminal branches to demonstrate the immense cranial diversity of living and extinct placentals. Geological age is indicated by alternating shading of circles, from innermost outwards: Cretaceous, Paleogene, Neogene, Quaternary.

Figure 3. Rates of evolution peak early in placental mammal evolution and attenuate through time. A) Rates of evolution through time are shown for one sample tree per root age for

topology 2, colored by root age, while clade-specific tip rates and ancestral estimates are shown for topology 2, root age 80-85, tree 85, as in Fig. 2. The Cretaceous-Paleogene (K/Pg) boundary and the Paleocene-Eocene Thermal Maximum (PETM) are indicated with red and green lines, respectively. B) Subsetting terminal branch rates by each order demonstrates the slow pace of evolution in stem placental mammals and euarchontoglires, in contrast to Afrotheria and several laurasiatherian clades. * indicates wholly extinct orders. Estimated ancestral cranial shapes (excluding teeth and bullae) for C) Placentalia and D) each superorder, using *Vulpes pallida* for the reference mesh, suggest remarkable similarity among the estimated MRCAs for placental mammal superorders.

Figure 4. Aquatic, herbivorous, precocial, and social placental mammals evolve at the fastest rates. Rates of evolution based on ecological and life history traits for placentals, with diet and locomotion estimated for all living and extinct taxa sampled, while the other four categories are limited to extant taxa. Distributions represent results from 100 sampled trees for topology 2, root age 80-85.

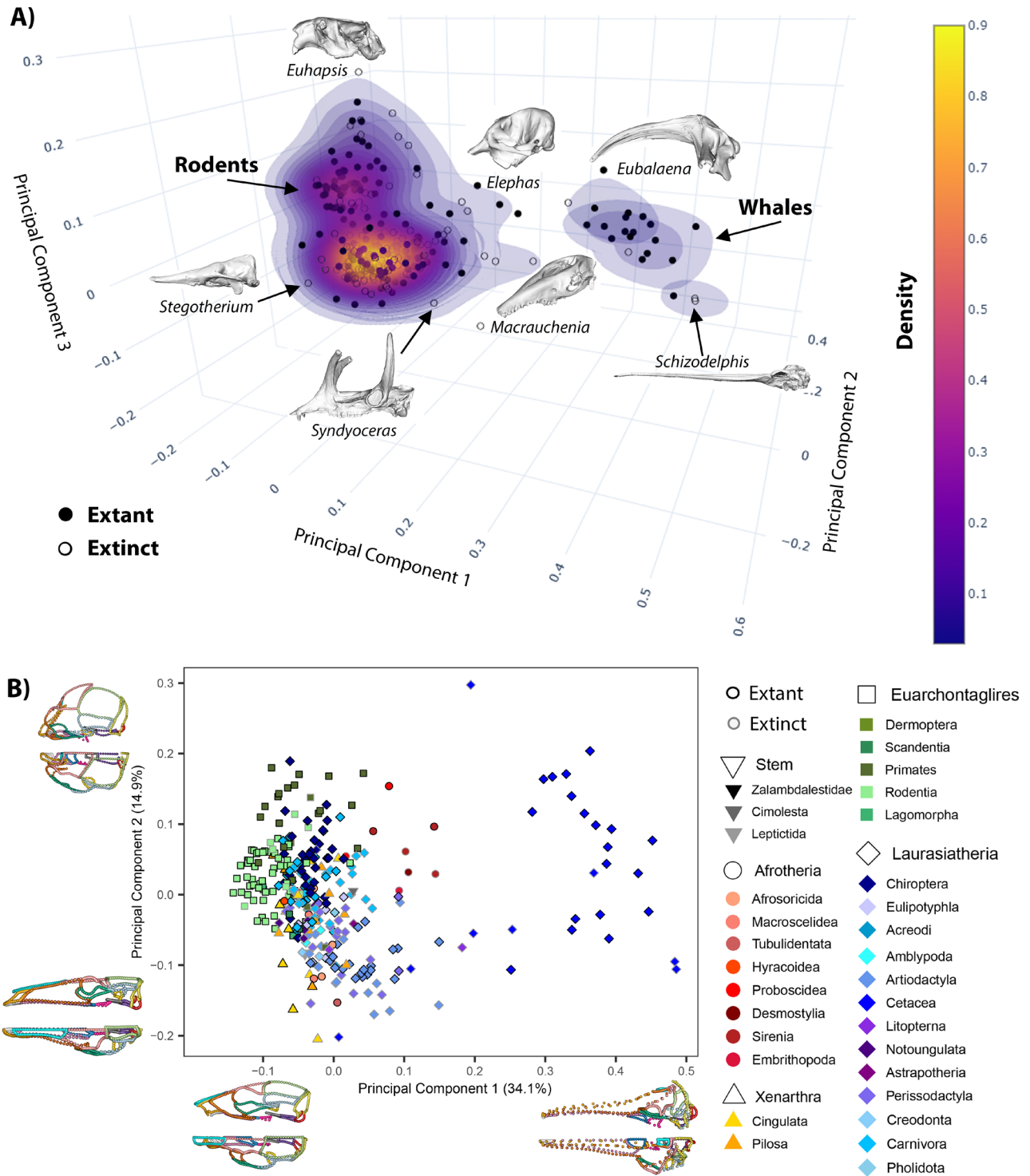


Figure 1. Cranial variation across placental mammals is highly concentrated.

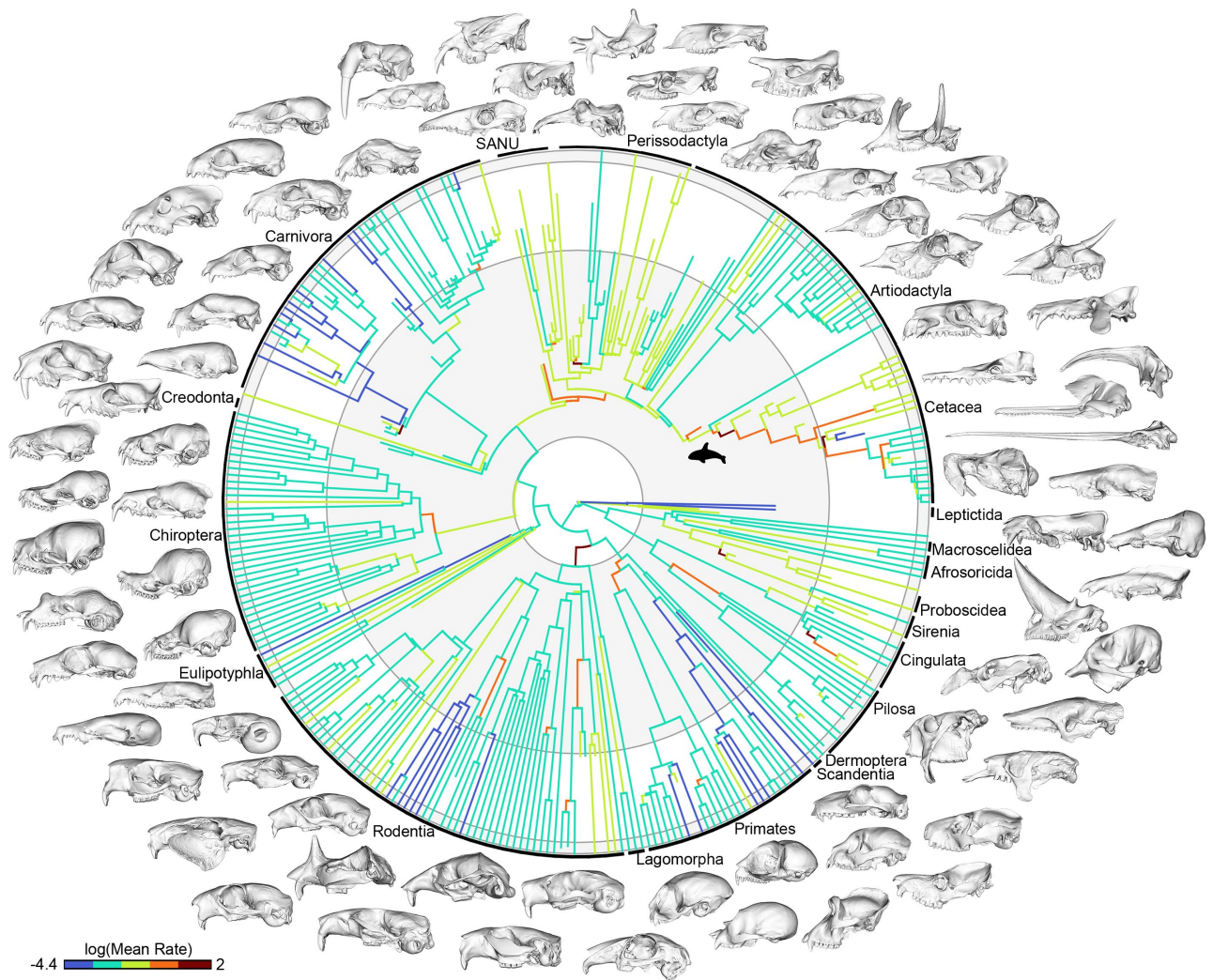


Figure 2. Rapid evolutionary rates are observed near the base of several placental mammal clades.

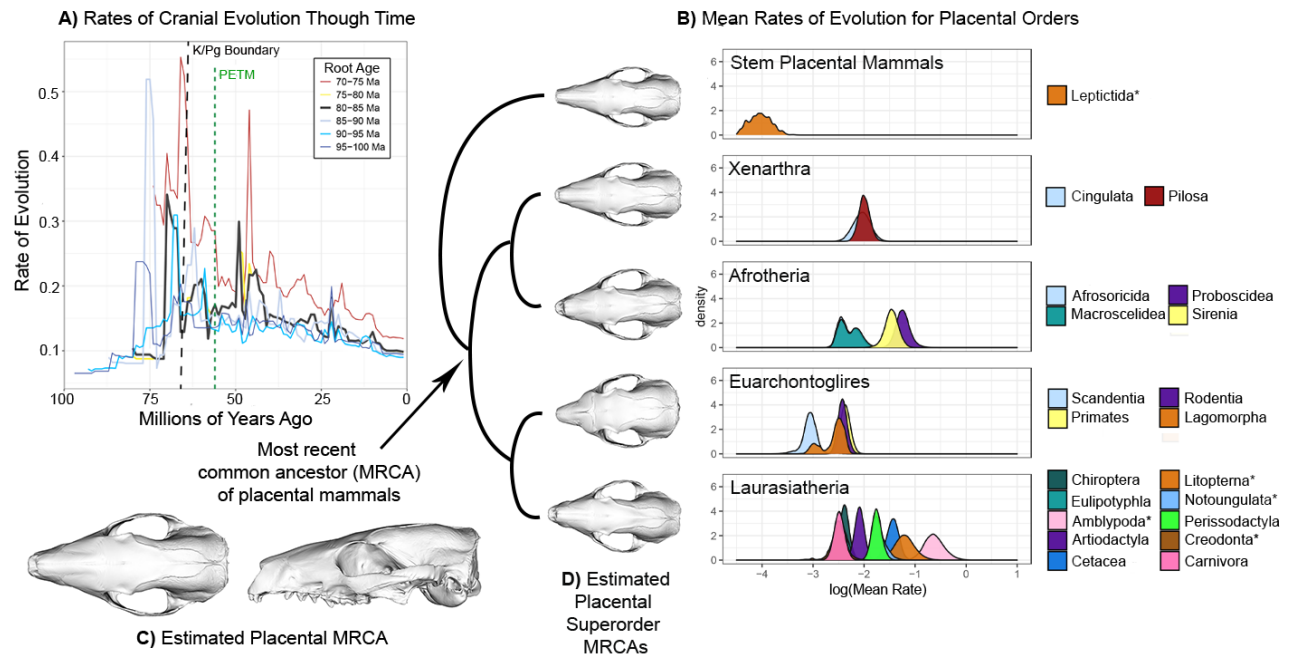


Figure 3. Rates of evolution peak early in placental mammal evolution and attenuate through time.

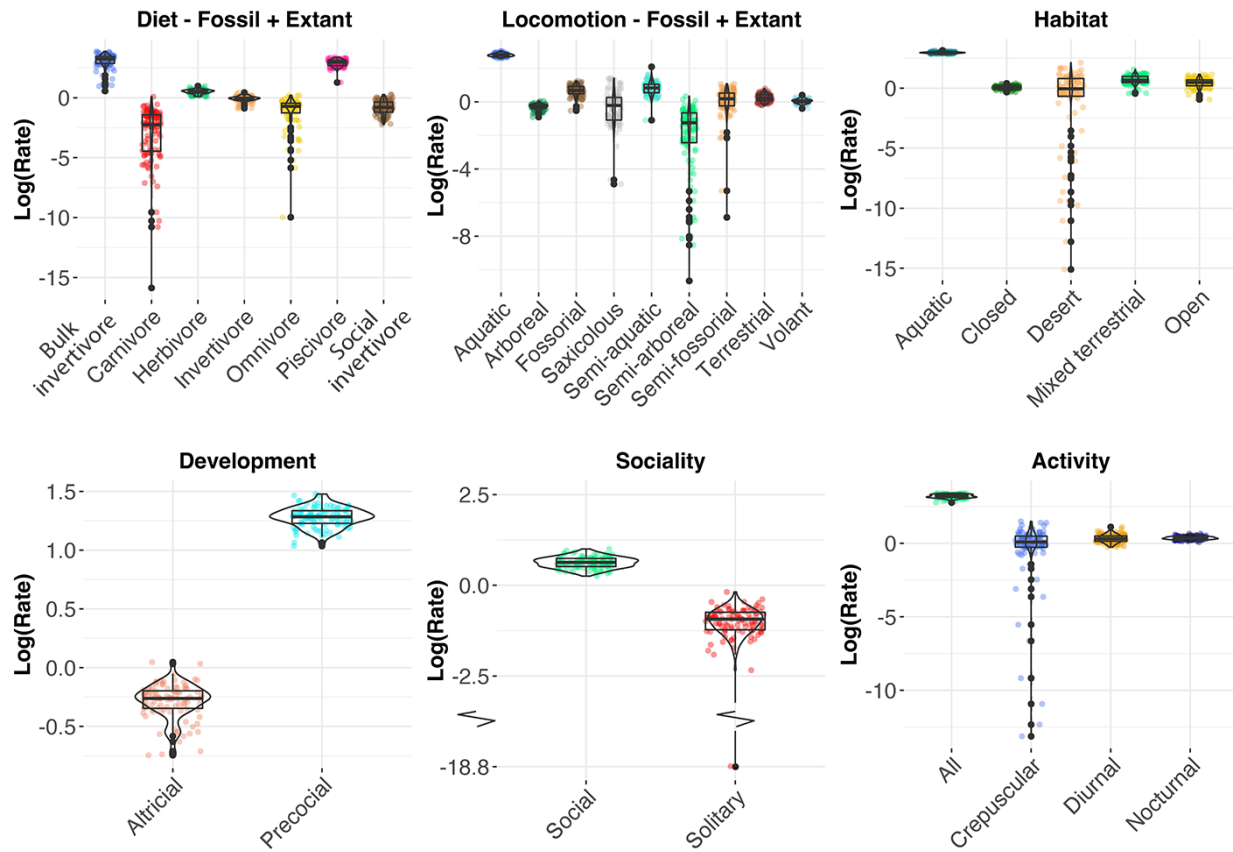


Figure 4. Aquatic, herbivorous, precocial, and social placental mammals evolve at the fastest rates.



Supplementary Materials for

Title: Attenuated evolution of mammals through the Cenozoic

Authors: Anjali Goswami, Eve Noirault, Ellen J. Coombs, Julien Clavel, Anne-Claire Fabre, Thomas J.D. Halliday, Morgan Churchill, Abigail Curtis, Akinobu Watanabe, Nancy B. Simmons, David L. Fox, Brian L. Beatty, Jonathan H. Geisler, Ryan N. Felice

Correspondence to: a.goswami@nhm.ac.uk

This PDF file includes:

Materials and Methods
Figs. S1 to S8
Tables S1 to S2

Other Supplementary Materials for this manuscript include the following:

Data S1

Materials and Methods

Specimens

Our dataset samples 322 crown and stem placental mammals, including 207 extant and 115 extinct species (data S1). Sampling includes 123 (of ~127) extant placental families and an additional 58 wholly extinct families, with multiple subfamilies sampled for most large clades. Sampling was selected to cover the full phylogenetic, ecological, and morphological breadth of living and extinct placentals, with sampling of fossil specimens limited to those that are known from well-preserved complete crania. Because of the requirement for skulls that are undeformed in 3D, we were only able to sample Cenozoic representatives of “Cretaceous lineages”, i.e. wholly extinct, likely stem lineages that the fossil record supports unambiguously as having diverged in the Cretaceous, such as leptictids and cimolestids (23). Within these limitations of requiring undeformed 3D specimens, we made great efforts to sample the full breadth of extinct placental lineages, particularly those that appear proximal to the K/Pg mass extinction. Full details of specimens are included in data S1. 3D scans of specimens were obtained from micro-CT and surface scanning at 25 international institutions. Surface scans were obtained with a FARO Edge Arm and Laser Line Probe, a Creaform Go!SCAN 20, a Creaform Go!SCAN 50, or a Breuckmann StereoSCAN3D white light fringed surface scanner. A minimum of 0.2mm resolution was used for all but the largest specimens, i.e., those with crania over a metre in length, which were scanned with 0.5mm resolution with the Creaform GoScan 50. Additional specimen scans were sourced from public repositories, including Phenome10k, Digimorph, and Morphosource. Specimen locations and, if applicable, scan sources, are provided in data S1. Micro-CT scans were processed with Avizo Lite 8.0 (FEI Visualisation), and all surface and micro-CT scans were processed in Geomagic Wrap 2017 (3D Systems) prior to collection of morphometric data. All scans are available for download on Phenome10k (subject to institutional permissions).

Morphometric data

3D landmark and semi-landmark data were collected for the left side of the skull using Stratovan Checkpoint. 66 landmarks were selected to represent points of unambiguous Type I and Type II homology. 69 semi-landmark curves were then placed that connected landmarks and largely follow the sutures of cranial bones (Fig. S1, Table S1). The lacrimal, which variably has a facial aspect, was included with the maxilla when present on the facial surface. Variably present bones, including the premaxilla, nasal, and jugal, were treated as zero-area structures when absent, following the protocol in (24). Landmarks and semi-landmarks were imported into R for analysis using the `SURGE` package (github.com/rnfelice/SURGE), where curves were resampled to a common number of semi-landmarks and slid to minimize bending energy with the `Morpho` v. 2.8 package (25). A full description of landmarks and curves is provided in Table S1 and Fig. S1. Following sliding, morphometric data were mirrored using midline landmarks with the `paleomorph` package and then subjected to Generalized Procrustes Analysis in the `geomorph` package v. 4.0 (26). Mirrored landmarks were then removed, leaving a total of 757 3D landmarks and sliding semi-landmarks. Centroid size output from the Procrustes superimposition was used as a proxy for body size in further analyses. Shape data are available at https://github.com/anjoswami/Goswami_et_al_Placental_evolution_2022.

Ecological and life history traits

Ecological and life history data were collected from the published literature for the following categories: Diet, Locomotion, Habitat, Development, Social Structure, and Activity Pattern (27–59). Published reconstructions were used to score diet and locomotion for extinct taxa, while all six traits were scored for extant taxa. Given the taxonomic breadth of this dataset, inevitable uncertainties on ecology and life history for rare species, and the need for a minimum of five species in each bin for statistical analyses, we used relatively broad categories for diet, locomotion, and habitat. Development and social structure were treated as binary traits, while activity pattern used four distinct states. Details of traits and references are provided in data S1.

Phylogeny

While molecular data has largely resolved the higher-level topology of placental mammals and there are detailed morphological phylogenies available for many extinct placental clades, there is continuing debate over the positions of some entirely extinct clades within Placentalia. There is also extensive debate over the root age of the crown group, with persistent gaps between paleontological and molecular data. For example, the most recent molecular analyses of placental phylogeny (15) provide a distribution of trees that vary in root age from 70 Ma to over 100 Ma, whereas no unambiguous crown placental fossils predate the end-Cretaceous mass extinction that occurred 66 million years ago (9, 13, 23). The timing of origin for Placentalia and the positions of the earliest post-Cretaceous lineages are clearly critical for placing the radiation in the appropriate environmental and evolutionary context, and the lack of resolution in this area is a key factor in the exclusion of fossil taxa from most analyses of mammal diversification.

In the absence of a well-resolved phylogenetic hypothesis that samples all living and extinct taxa in our dataset and constrained to a reasonably narrow range of root ages, we constructed an extensive range of alternative phylogenies that capture the impact of this phylogenetic uncertainty on our results. To do so, we started with the maximum credibility consensus tree from the most recent species-level molecular analysis of placental relationship, which samples all of our extant sample, as well as some recently extinct species (15). We then used a suite of recent morphological phylogenetic analyses (13, 23, 60–90) that include our fossil sample to place the extinct taxa within the molecular tree, generating three alternative composite topologies that capture the major points of uncertainty in the relationships of early placentals, particularly the potentially paraphyletic cimolestids and amblyopods. We focused the alternative topologies on these problematic branches near the base of Placentalia, as they encompass contentious members of the wastebasket taxon “Condylarthra” or are variably considered to be stem or early crown placentals. Most of the other fossil taxa in our sample are better resolved in terms of phylogenetic affiliations, with remaining uncertainty largely involving within-group relationships that should have little impact on rate estimations at this level of sampling.

A notable large group with considerable ongoing debate in their phylogenetic affinities are the South American Native Ungulates (SANUs), here represented by three of the five large orders: Notoungulata, Litopterna, and Astrapotheria. Recent analyses support Notoungulata and Litopterna as allied with Perissodactyla (67), and Astrapotheria has also been supported in a close relationship with Notoungulata (66). Other SANU clades have been supported outside of Laurasiatheria, meaning that SANUs is potentially polyphyletic [see discussion in (60)]. Treating this group as monophyletic could exaggerate evolutionary rates from the (incorrectly

reconstructed) ancestral node to the base of each SANU clade. Because the sample of 8 SANU taxa here don't include some of the more enigmatic taxa and are better supported in an affiliation with Perissodactyla, this effect is unlikely to have impacted our results. Nonetheless, it is important to remember that uncertainty in the phylogenetic positions of extinct mammals remains a continuing hindrance to the integration of fossil data into macroevolutionary analyses, despite the quality of the Cenozoic mammal fossil record, and that this issue will only be resolved through continuing dedicated systematic analysis.

As noted above, uncertainty in the topology of the placental tree is matched by uncertainty in estimating the timing of placental divergences. We first attempted to date the trees generated as described above using a fossilized birth-death approach, but this approach consistently generated trees with unambiguously incorrect divergence estimates. To circumvent this issue and capture the uncertainty in the root age of the placental tree, we first drew a set of node-dated trees from the posterior distribution of (15) that had the same topology as the MCC tree. We then binned these trees into six 5-million year bins (70-75Ma, 75-80Ma, 80-85Ma, 85-90Ma, 90-95Ma, and 95-100Ma). We then took our three composite topologies and grafted the extinct taxa onto all of the trees across six bins, with the node age for fossil branch divergences randomly selected from within each third of the parent branch (resulting in three alternative divergence estimates for each node leading to an extinct branch for each topology). This process generated 419,400 alternative trees, which we subsampled to 1800 trees, 100 for each of the six 5-million-year root age bin for each of the three topologies. These 1800 trees form the basis of the following analyses and cover broadly much of the immense range of continued uncertainty in the placental tree. Code for grafting trees is available at <https://github.com/rnfelice>.

Cranial shape variation

To examine the overall pattern of cranial variation across placentals, we conducted a principal components analysis using Procrustes-aligned 3D landmarks data in `geomorph`. We reconstructed wireframe models for the minimum and maximum shapes on the first four principal components, which together account for 64.5% of the total variation in the dataset. We projected the first three components into a morphospace (Fig. 1) and generated density contours to identify concentrations of cranial morphology by estimating 3D Gaussian kernel density using the `gaussian_kde` function in SciPy (91). We further generated plots of PC1 and 2 (Fig. 1) and PC3 and 4 (Fig. S2) to highlight the distributions of ordinal and superordinal level clades and extinct and extant taxa. We also conducted a phylogenetic PCA in `geomorph` and extracted the pPC scores for the components which combined explain 95% of the total variation in the dataset (67 components for the tree figured in Fig. 2). Finally, we estimated the ancestral shape for the placental MRCA and each superordinal MRCA by maximum likelihood in the R package `Rphylopars` v0.2.11 (92) and warped a reference mesh (*Vulpes pallida*) to the target shape to produce 3d models of the ancestral estimates in `Morpho`. Using alternative reference meshes, including unusual forms such as the armadillo (*Oryzomys azer*) had no impact on results.

Macroevolutionary modelling

We assessed 10 alternative evolutionary models (variable- and single-rate models for Brownian motion, Ornstein-Uhlenbeck, and BM with lambda, kappa, or delta tree transformations) for cranial evolution with a reversible-jump Markov Chain Monte Carlo (MCMC) algorithm implemented in BayesTraits v. 3 (<http://www.evolution.rdg.ac.uk/>) (5), using phylogenetic PC

scores as input data. Because initial tests demonstrated that a run of 1,000,000,000 iterations were required to achieve convergence in parameter value estimates, we ran analyses on a subset of one randomly sampled tree from each topology and root age bin, for a total of 18 alternative trees. We used a burn-in of 500,000,000 and sampled every 5,000 trees, resulting in a posterior distribution of 100,000 trees from 1,000,000,000 iterations. Trace plots were examined to ensure that the chains reached stationarity after burn-in. Convergence of the chains was assessed using Gelman and Rubin's convergence diagnostic implemented in the R package 'coda' v.0.19-3.

Bayes Factor supported the variable rates Brownian Motion model with a lambda tree transformation as the best fit model for all 18 phylogenetic frameworks (Fig. S3). The lambda transformation effectively lengthens terminal branches, thereby accommodating error due to within-species variation and artefacts such as measurement error, which can be important factors in evolutionary modelling (26). Lambda values range from 0.629 to 0.741 across all phylogenetic frameworks, with the lowest values for those trees with the youngest root ages (70-75 Mya) and the highest values for those with the oldest root ages (95-100 Mya). We plotted mean per-branch rates on each tree and summarized by the branch-specific average rate and the posterior probability of rate shifts estimated from the posterior samples using the 'BTRTools' R package v.0.0.0.9000 (<https://github.com/hferg/btrtools/tree/master/R>). Rate shifts with a probability greater than 0.5 are indicated on Fig. S4. We binned rates by geological time and plotted their pattern through time for the 18 alternative trees (results for the six trees for Topology 2 shown in Fig. 3). We then extracted rates for the terminal branches and plotted them by clade to assess differences in mean rate across clades (Fig. 3, Fig. S5), with the distributions representing the variation in rates across branches within each tree for the mean tree of the posterior distribution of 100,000 trees.

Ecological and life history associations with cranial evolution

We assessed the association of life history and ecological traits on cranial variation and evolutionary rates using the 'mvMORPH' package v 1.1.4 (93). We conducted Type II phylogenetic MANOVAs (phylogenetic regressions) on the Procrustes coordinates with log centroid size and each of the six factors as predictors. We conducted one analysis of size, diet, and locomotion for the full dataset of living and extinct species ($n = 322$) and a second one of all six factors for just the extant taxa ($n = 207$). Multivariate phylogenetic linear models with Pagel's lambda by penalized likelihood were fit using "mvgl", with significance assessed using the "manova.gls" function with Pillai's statistic and 1000 permutations. Using Pagel's lambda corresponds to fitting a phylogenetic mixed model which allows accounting for departure from Brownian motion and usually provides increased flexibility in estimating the error structure (94–97). Some of these factors may interact, e.g. social structure and development, or locomotion and habitat, but because many, possibly the majority, of intersecting bins do not have any representatives (e.g., there are no volant bulk invertivores, or aquatic social insectivores), we limited analyses of factor interactions to size with all other factors. Because the MANOVAs and permutation tests took multiple weeks for each analysis to run on a dataset of this size, even on the Crop Diversity Bioinformatics High Performance Computing cluster, we performed analyses on the same subset of 18 trees as used in the BayesTraits analyses above, allowing us to assess the effect of phylogenetic uncertainties on our results (Table S2).

Finally, we used the state-specific Brownian motion (BMM) model in the ‘mvglsl’ function in *mvMORPH* to estimate rates of evolution for each ecological and life history state. The reconstructed histories for each category were estimated with stochastic character mapping across the full sample of 1800 trees using an ‘ARD’ model in the R package *phytools* v. 0.7-70. We performed model fitting by jointly estimating the contribution of measurement error and intra-specific variation, which is flexible to departures from Brownian motion. Results were binned by tree topology and root age estimate to again assess the impact of phylogenetic uncertainty on results (Fig. 4, Fig. S6).

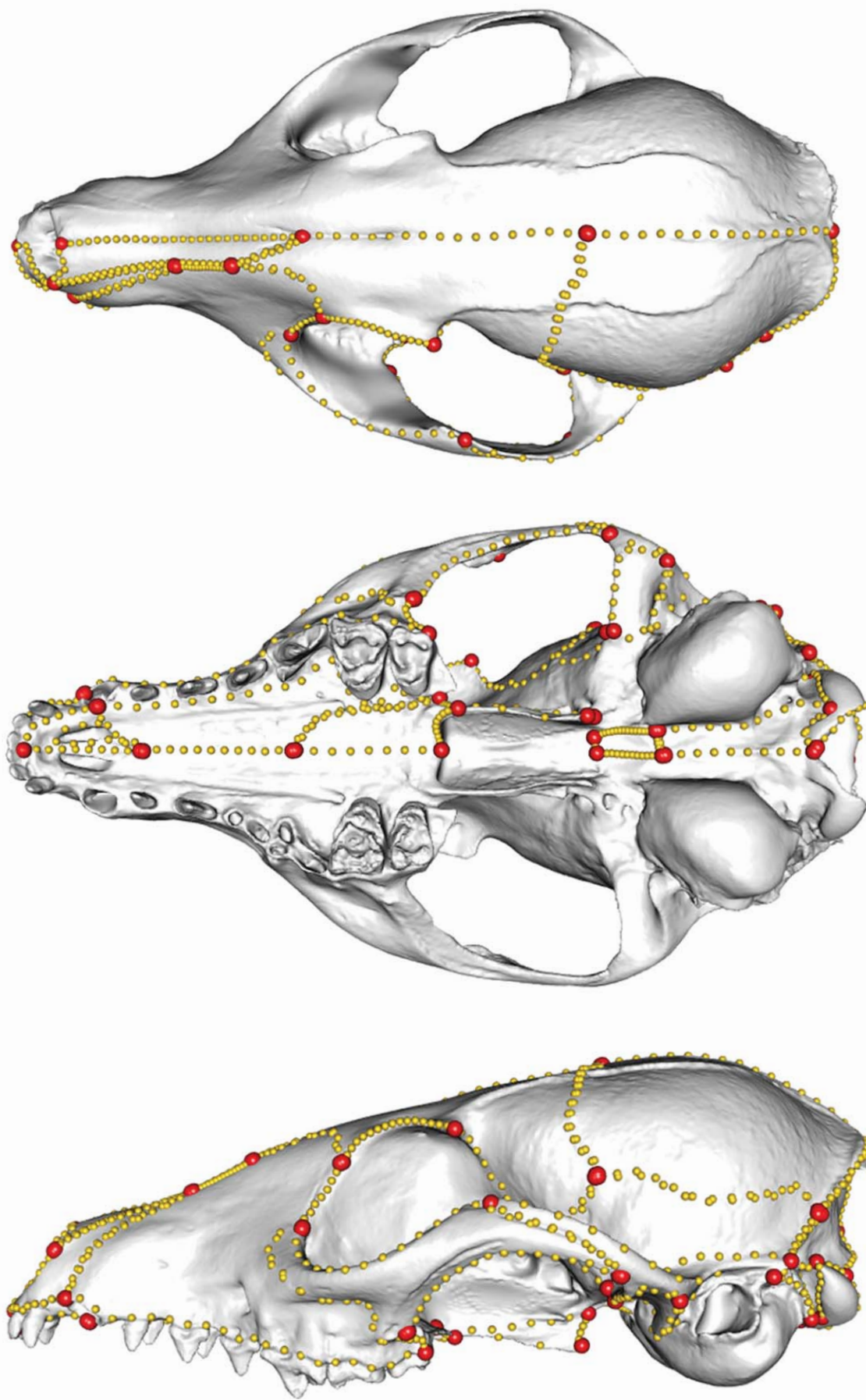


Fig. S1. Landmarks (red) and sliding semi-landmarks (gold) shown on *Vulpes pallida* in dorsal, ventral, and lateral views (top to bottom)

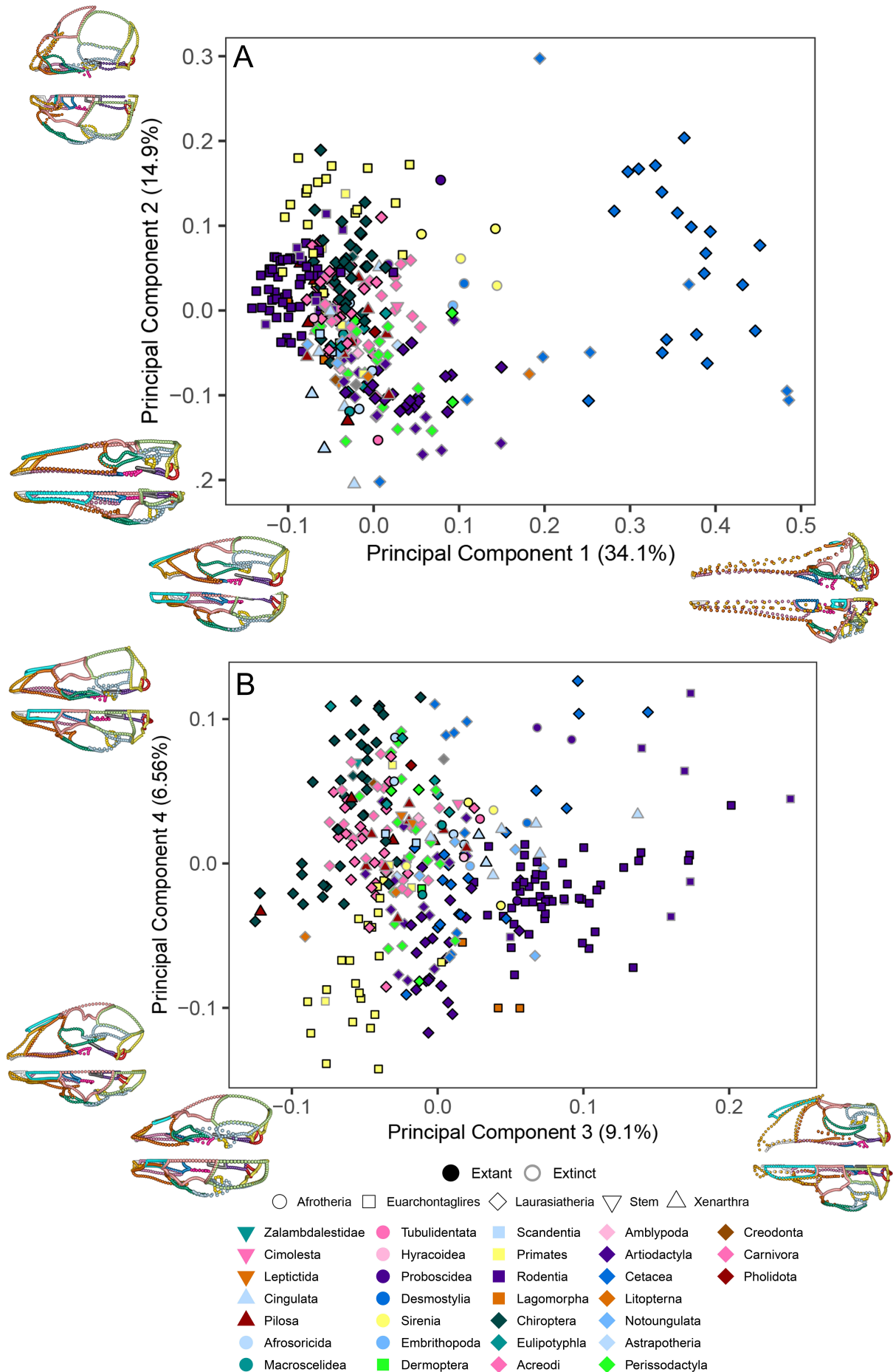


Fig. S2. Morphospace and wireframes for A) PC1 and 2 and B) PC3 and 4, using a color-blind palette for taxon symbols. Interactive morphospaces produced with Plotly (Montreal, Quebec) are available at https://github.com/anjgoswami/Goswami_et_al_Placental_evolution_2022.

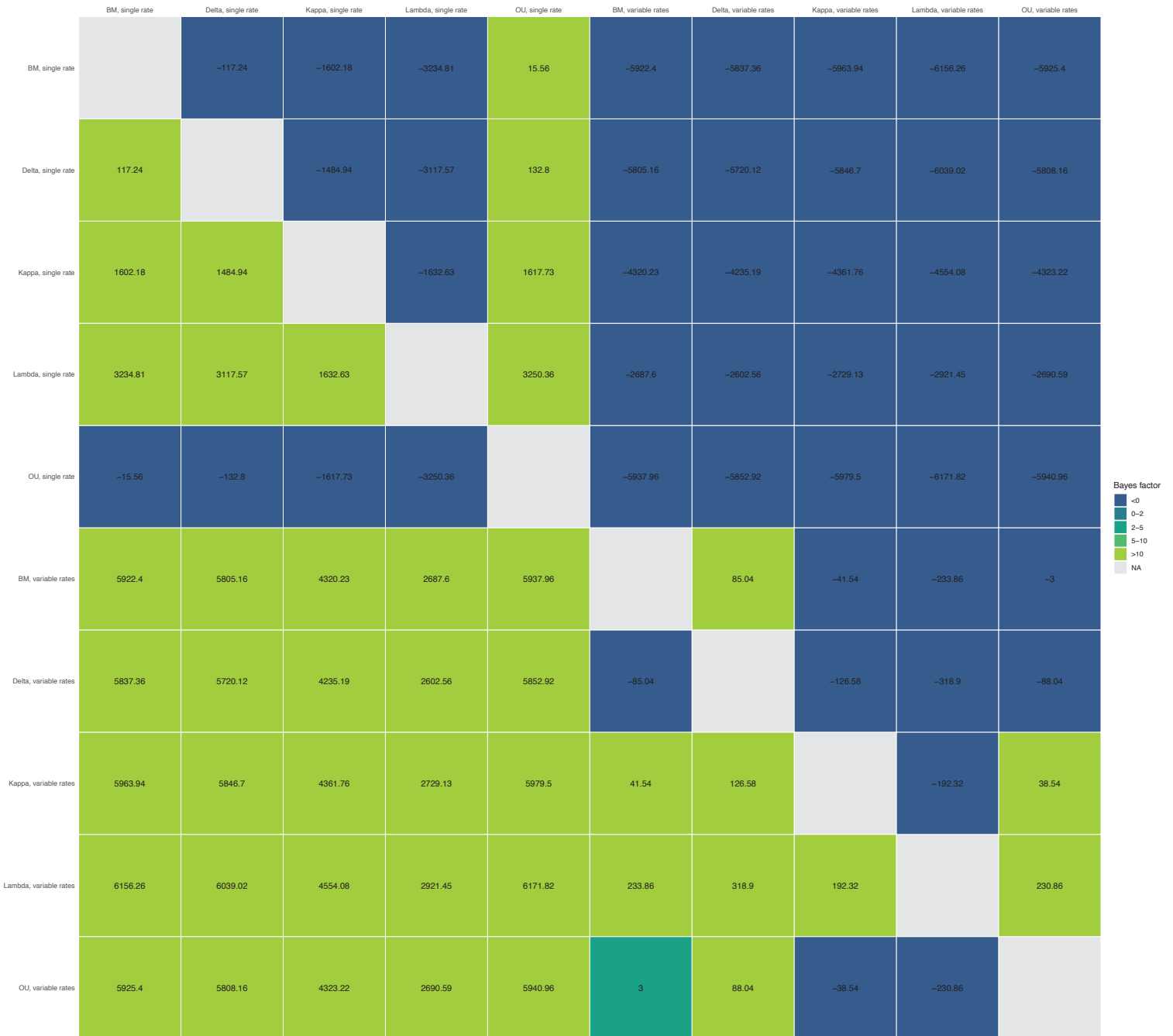


Fig. S3. A) Bayes Factor comparisons for 10 alternative evolutionary models for Tree Topology 1, Root Age = 70-75Ma.

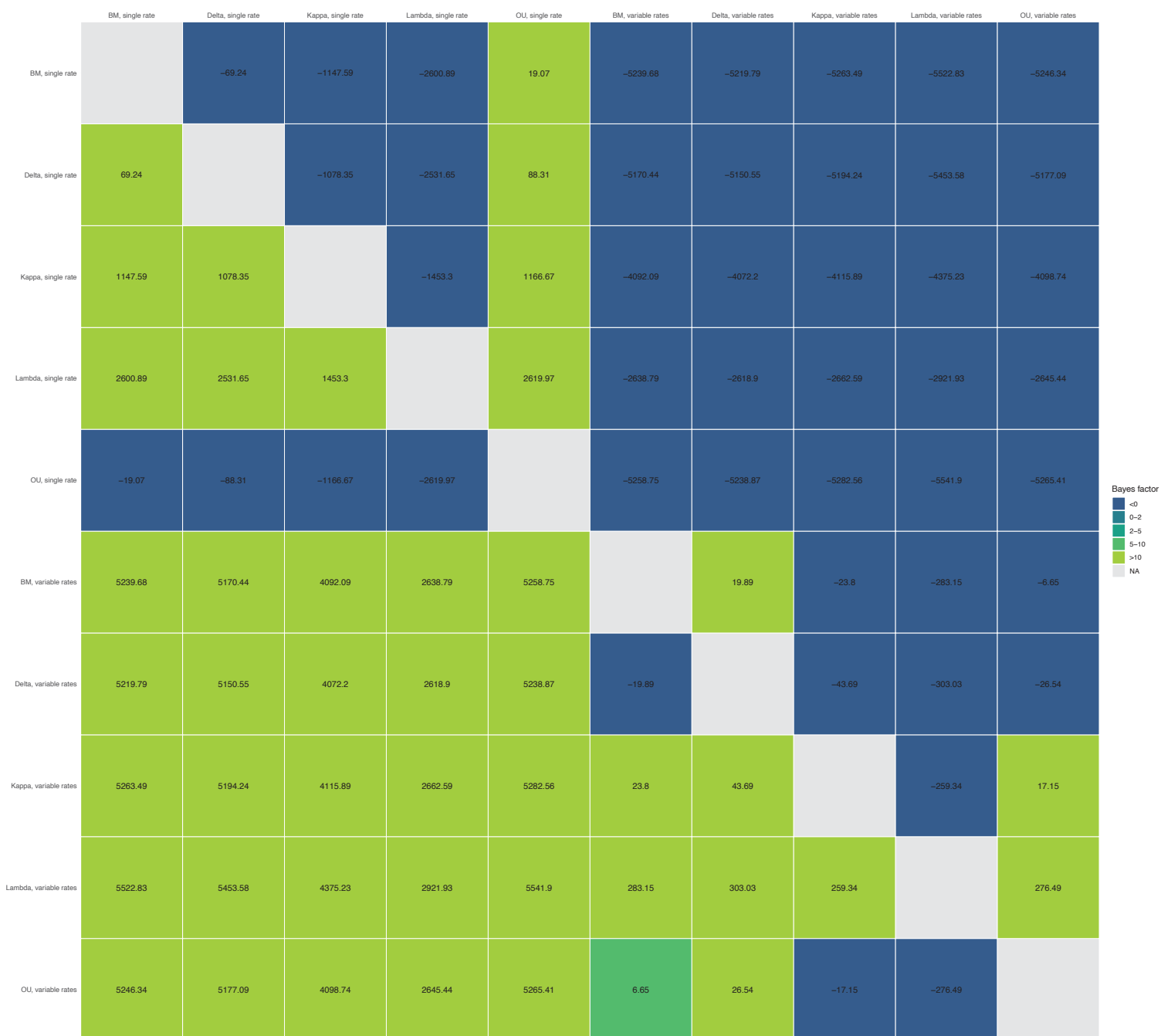


Fig. S3. B) Bayes Factor comparisons for 10 alternative evolutionary models for Tree Topology 1, Root Age = 75-80Ma.

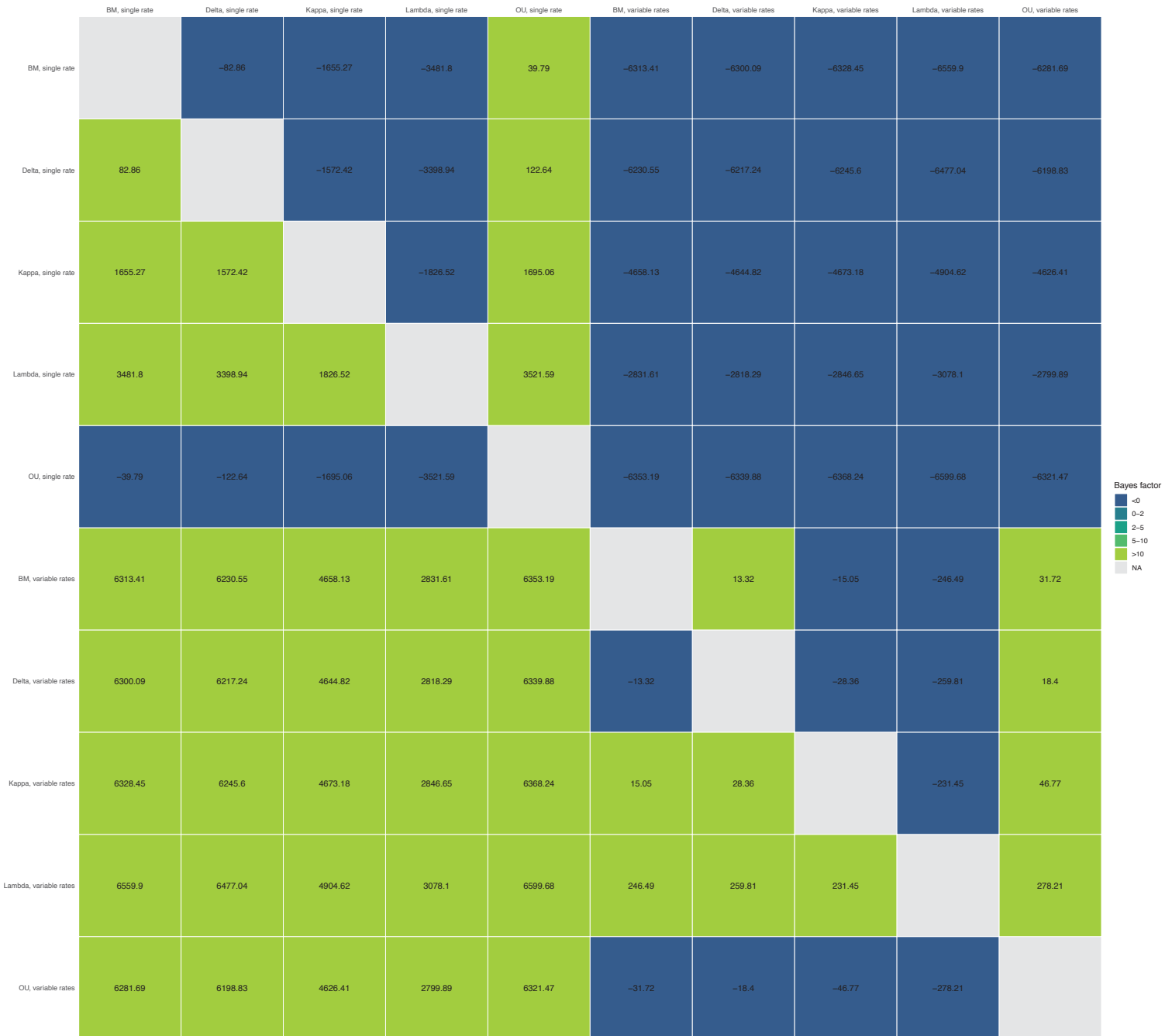


Fig. S3. C) Bayes Factor comparisons for 10 alternative evolutionary models for Tree Topology 1, Root Age = 80-85Ma.

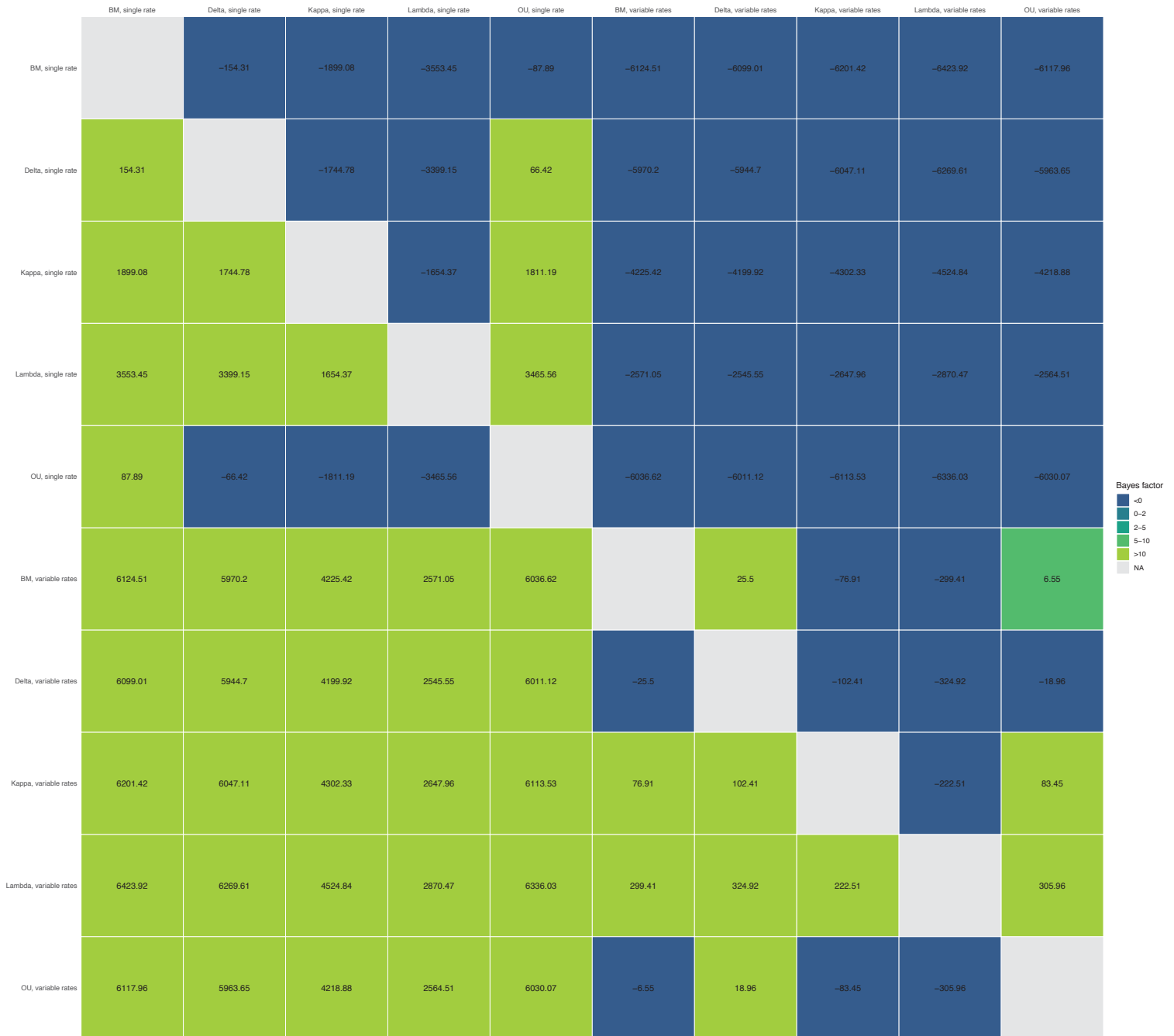


Fig. S3. D) Bayes Factor comparisons for 10 alternative evolutionary models for Tree Topology 1, Root Age = 85-90Ma.

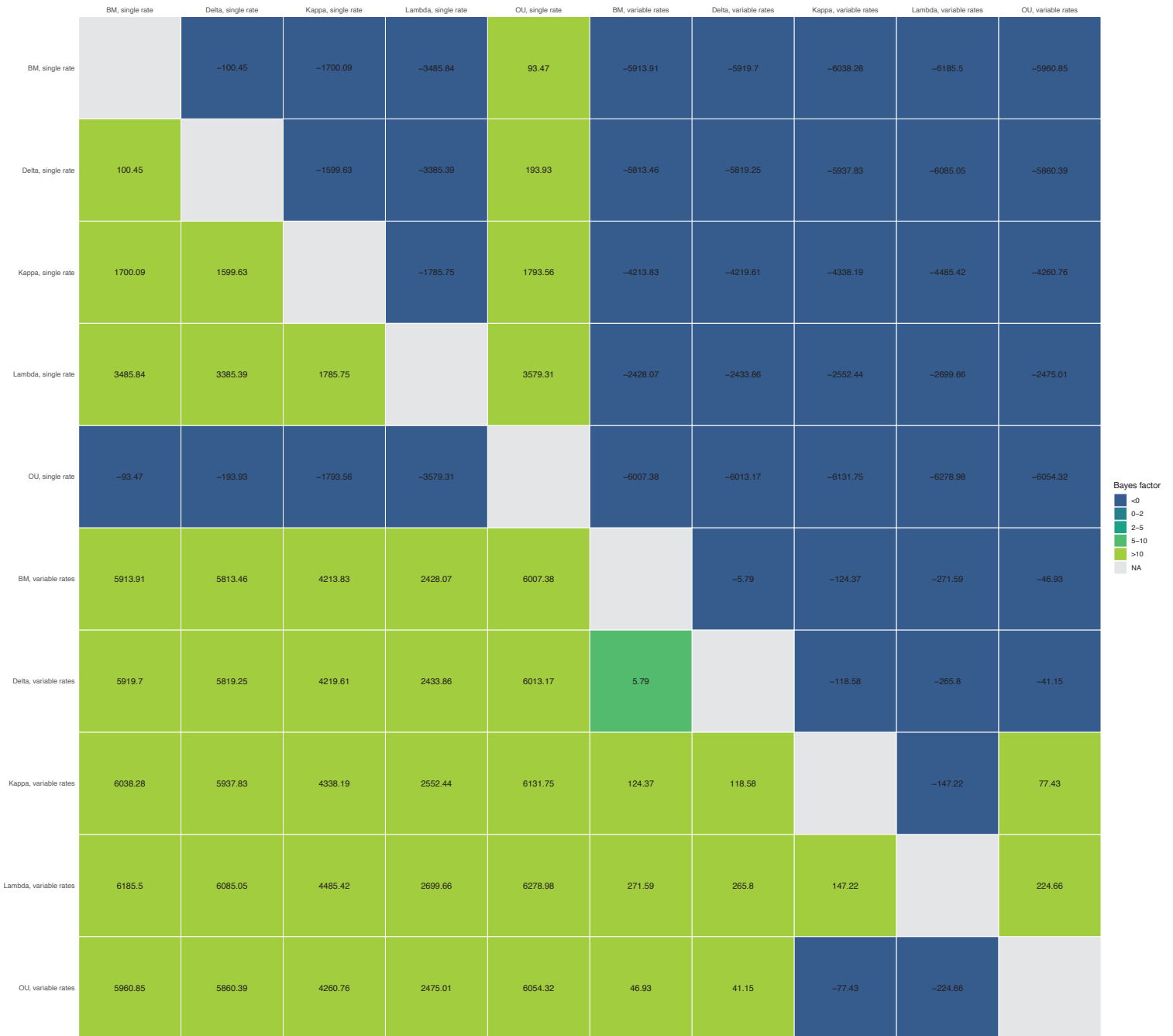


Fig. S3. E) Bayes Factor comparisons for 10 alternative evolutionary models for Tree Topology 1, Root Age = 90-95Ma.

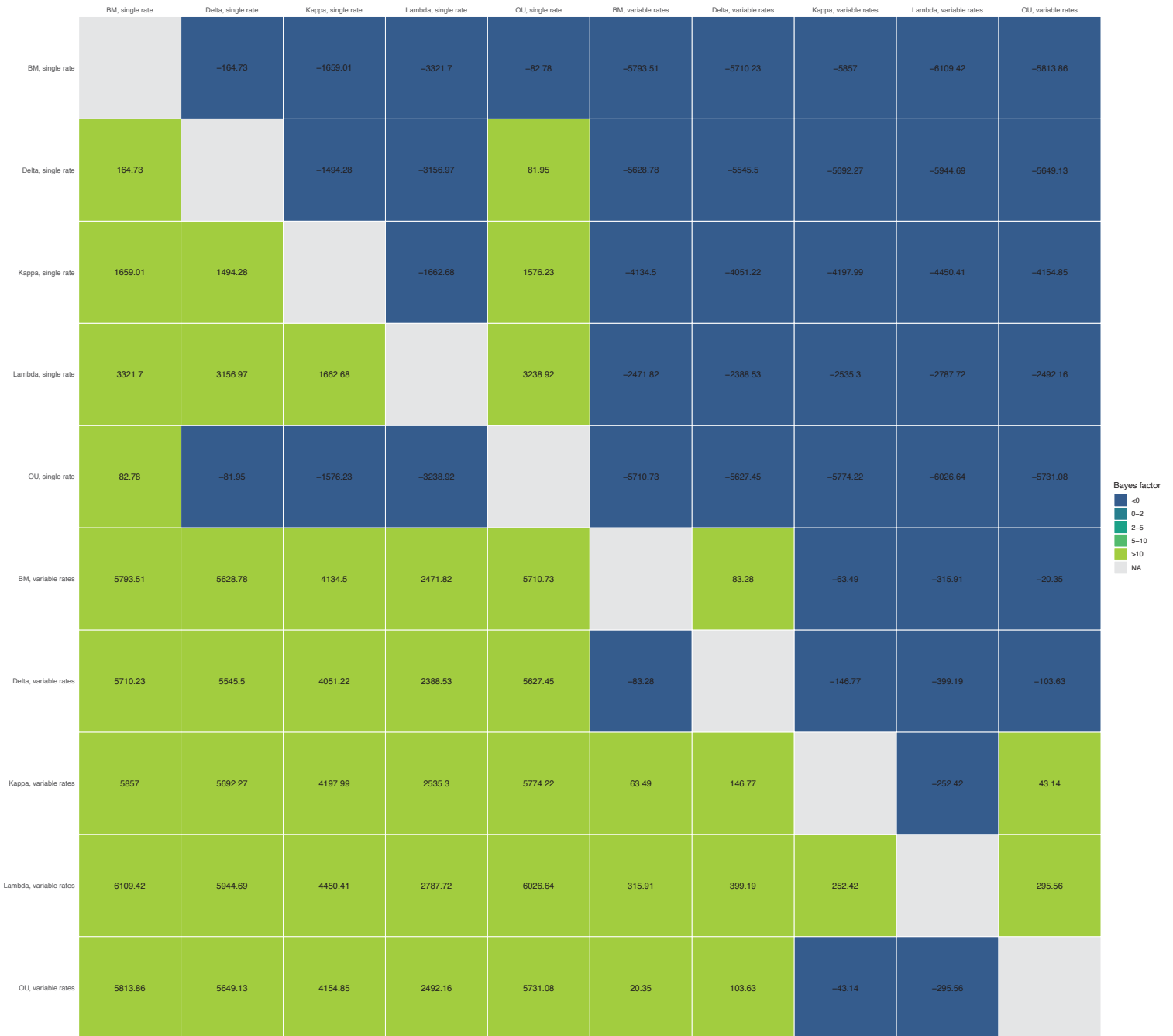


Fig. S3. F) Bayes Factor comparisons for 10 alternative evolutionary models for Tree Topology 1, Root Age = 95-100Ma.

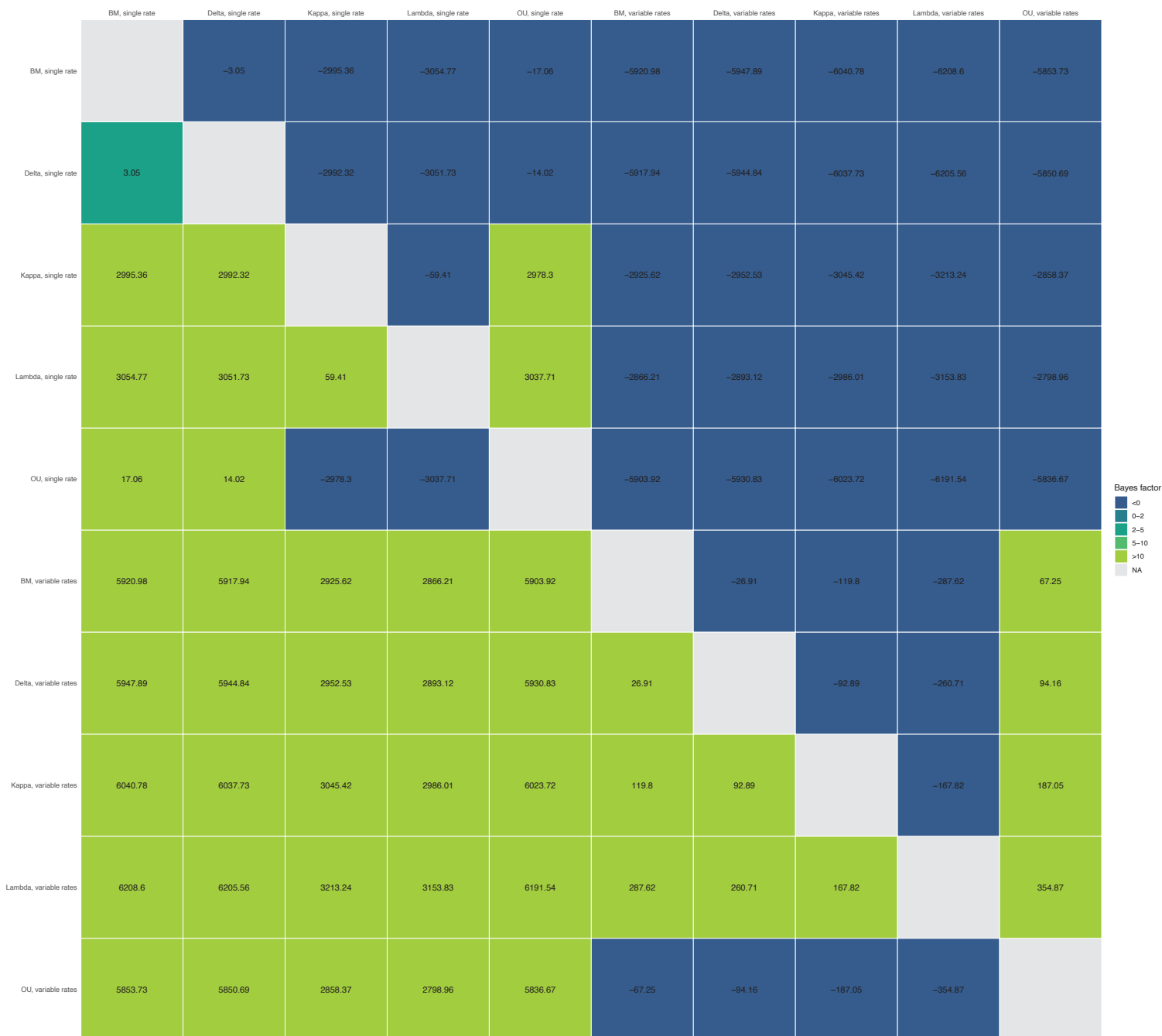


Fig. S3. G) Bayes Factor comparisons for 10 alternative evolutionary models for Tree Topology 2, Root Age = 70-75Ma.

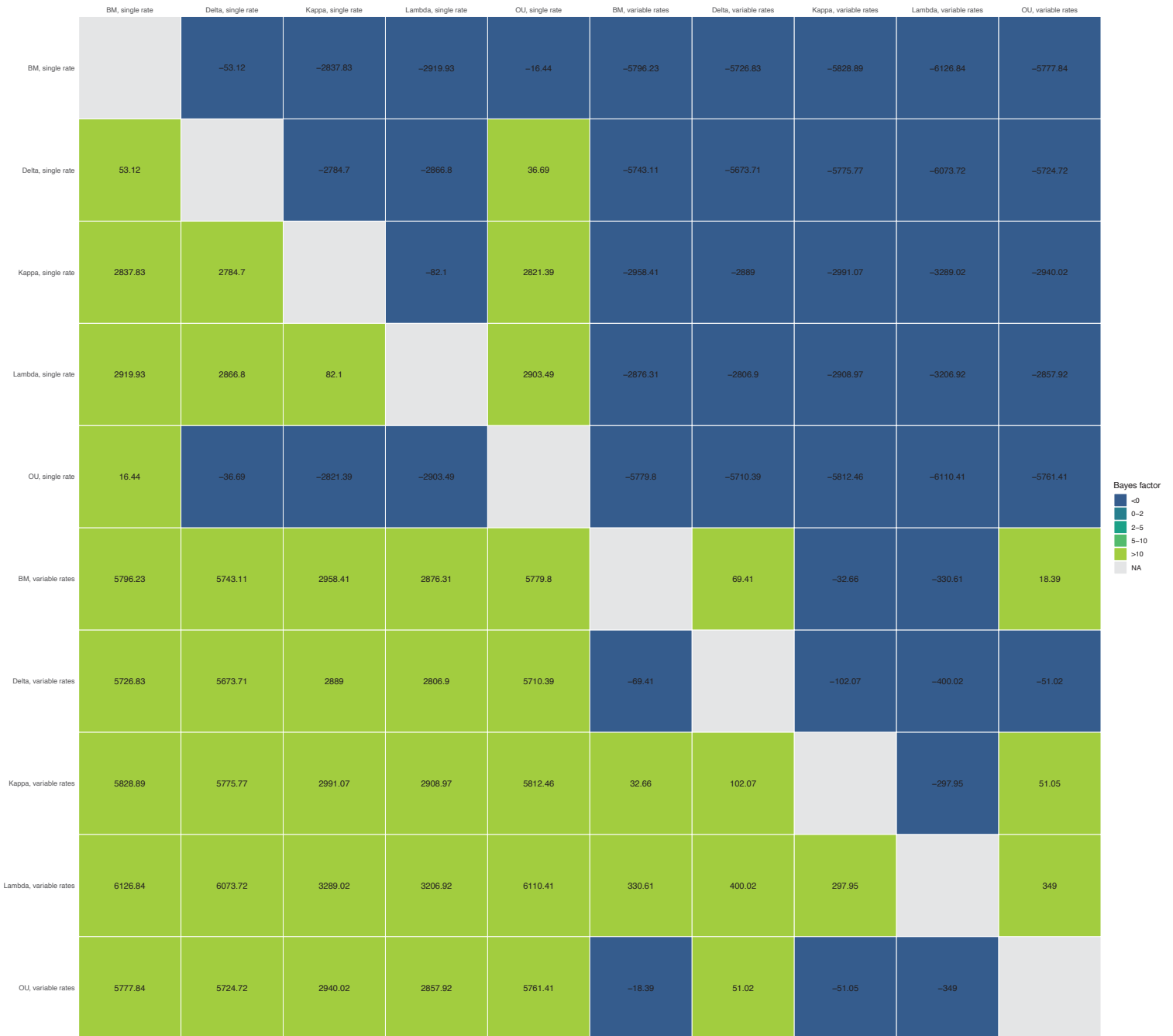


Fig. S3. H) Bayes Factor comparisons for 10 alternative evolutionary models for Tree Topology 2, Root Age = 75-80Ma.

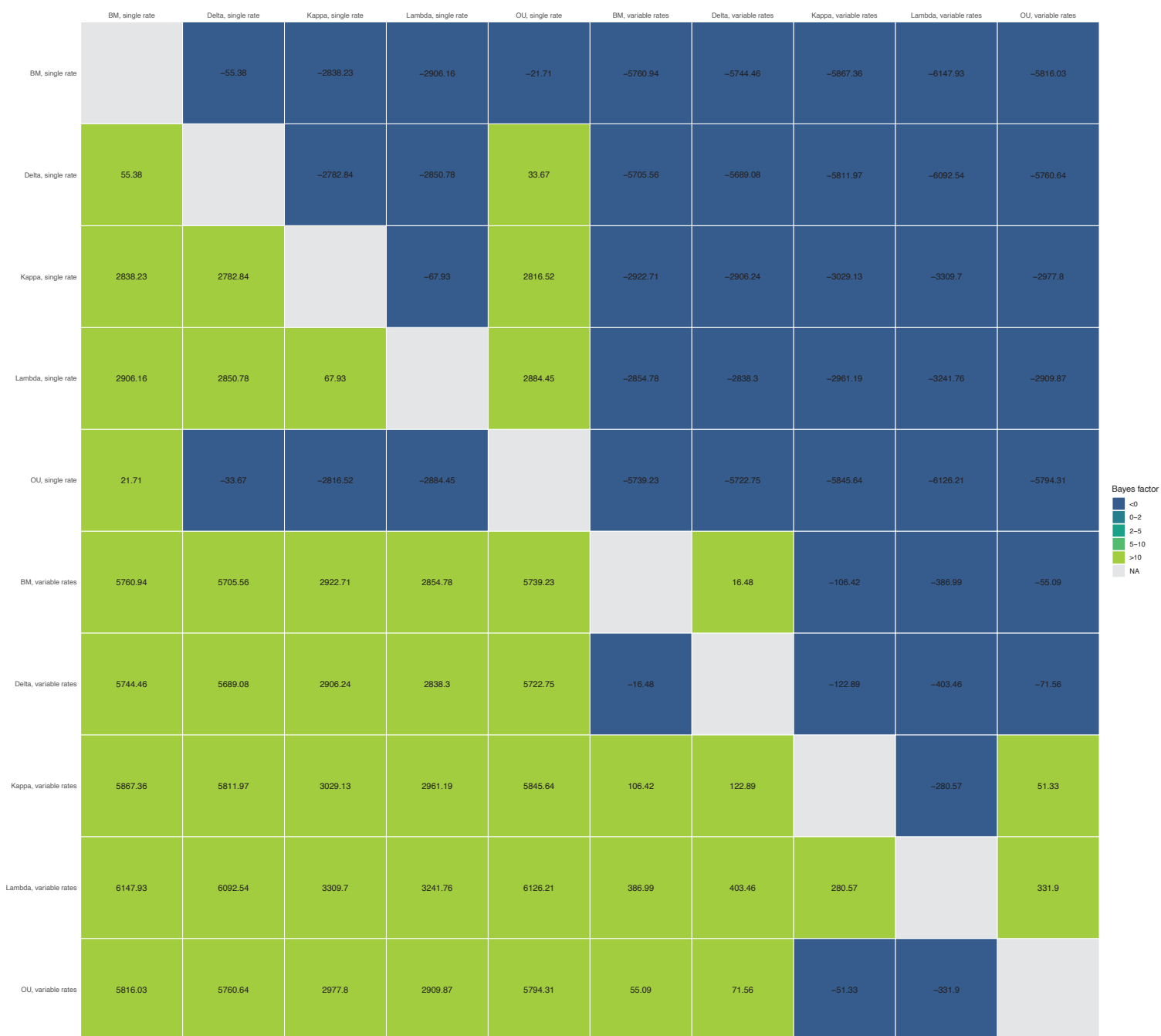


Fig. S3. I) Bayes Factor comparisons for 10 alternative evolutionary models for Tree Topology 2, Root Age = 80-85Ma.

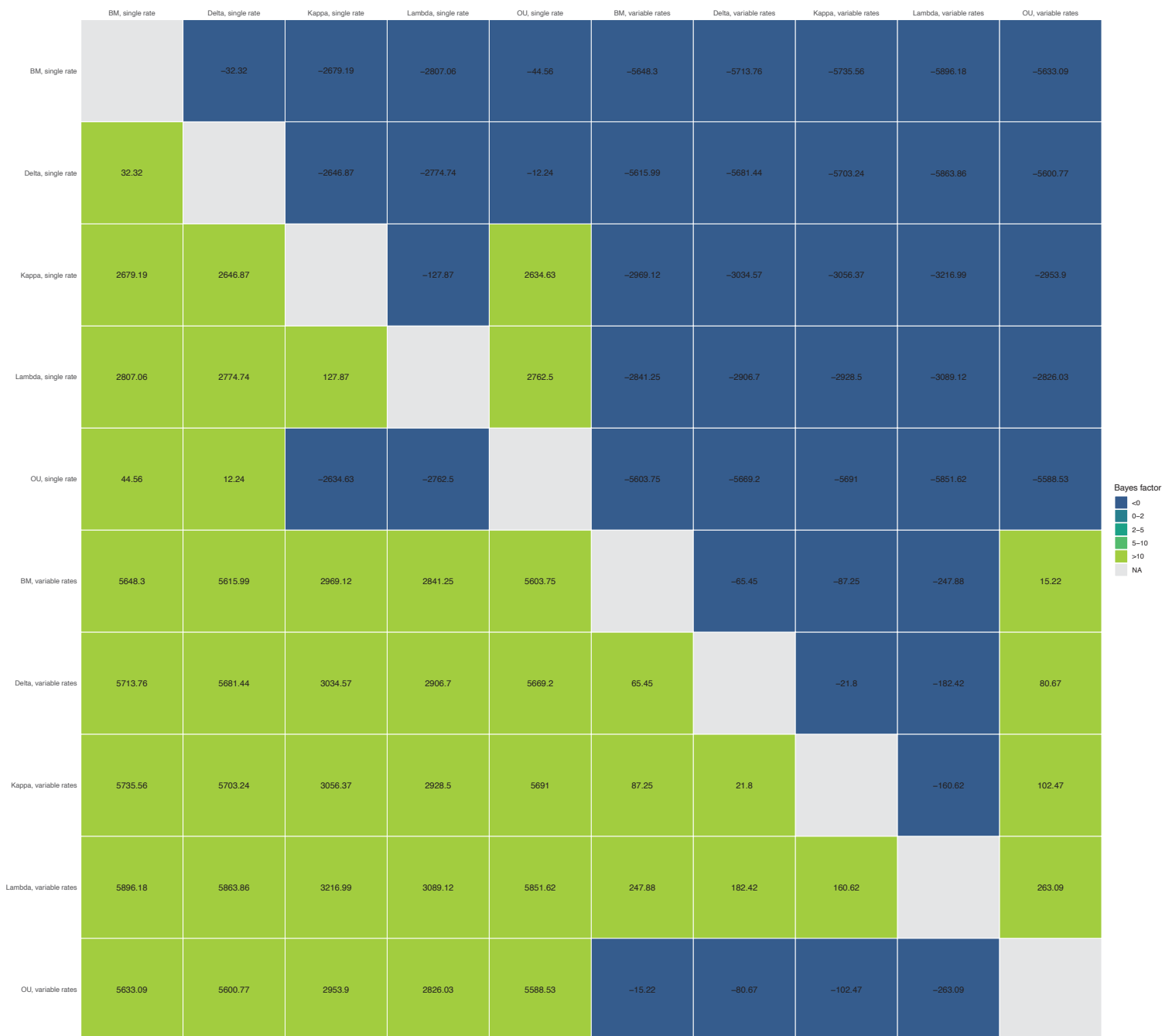


Fig. S3. J) Bayes Factor comparisons for 10 alternative evolutionary models for Tree Topology 2, Root Age = 85-90Ma.

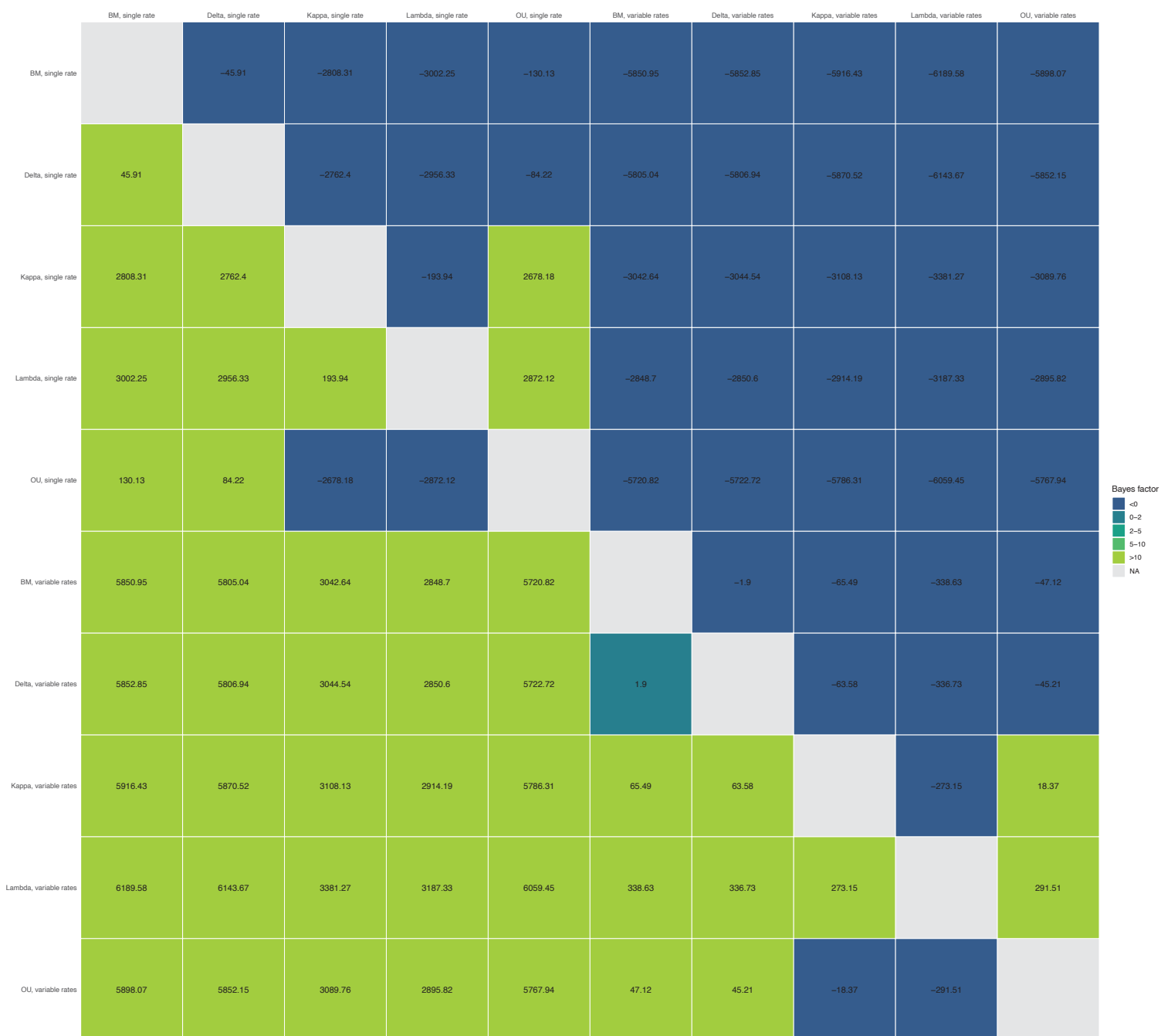


Fig. S3. K) Bayes Factor comparisons for 10 alternative evolutionary models for Tree Topology 2, Root Age = 90-95Ma.

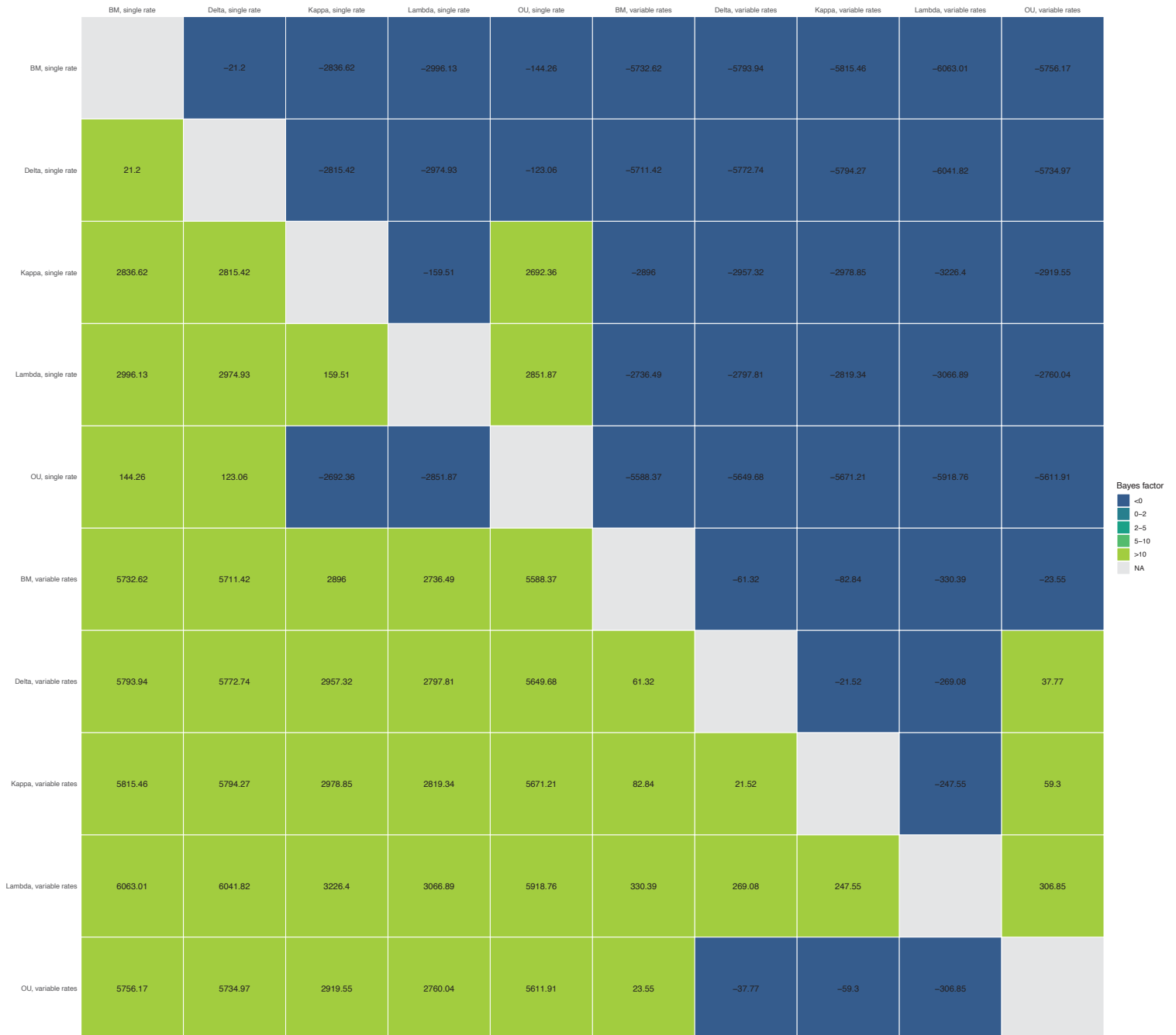


Fig. S3. L) Bayes Factor comparisons for 10 alternative evolutionary models for Tree Topology 2, Root Age = 95-100Ma.

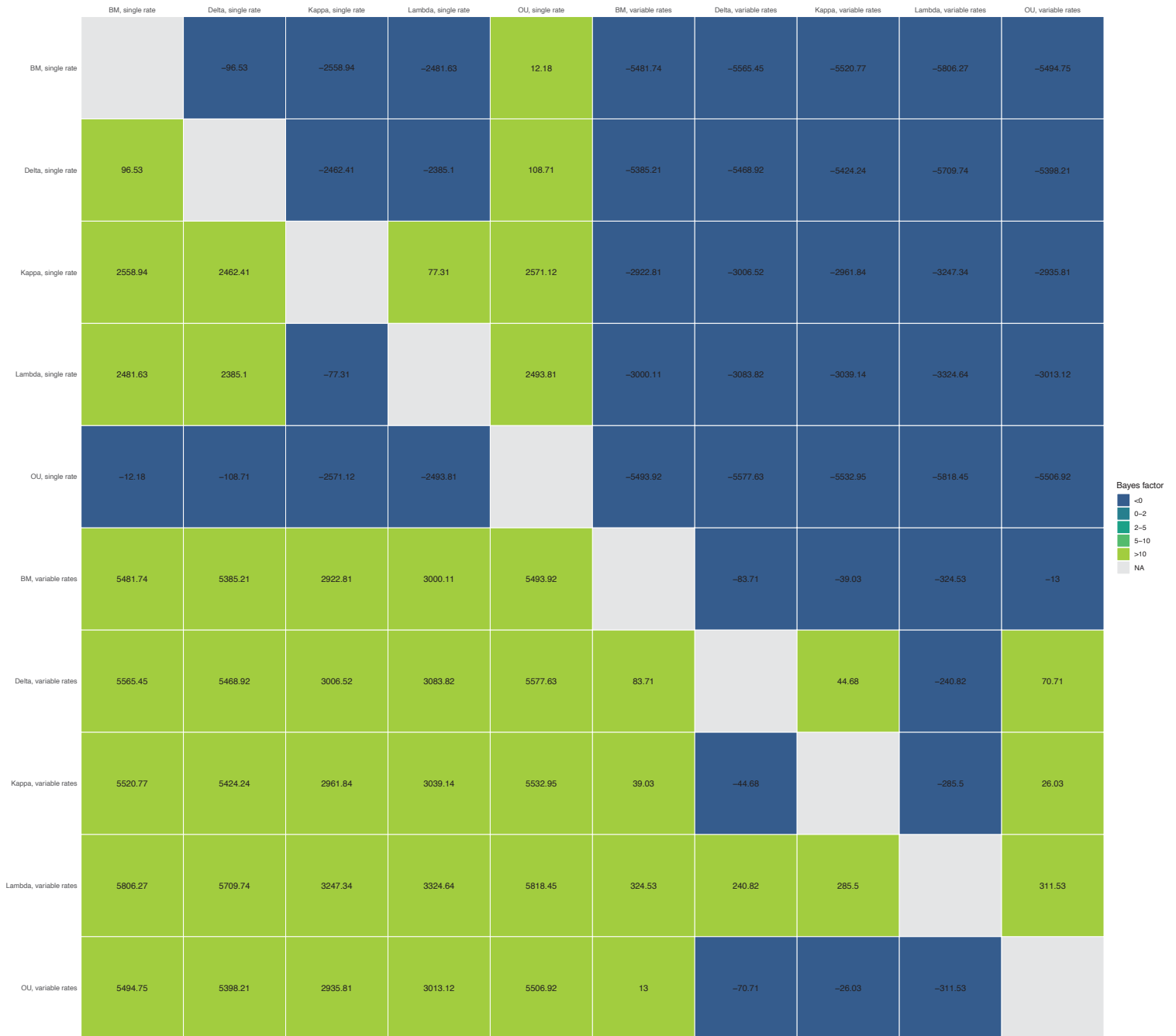


Fig. S3. M) Bayes Factor comparisons for 10 alternative evolutionary models for Tree Topology 3, Root Age = 70-75Ma.

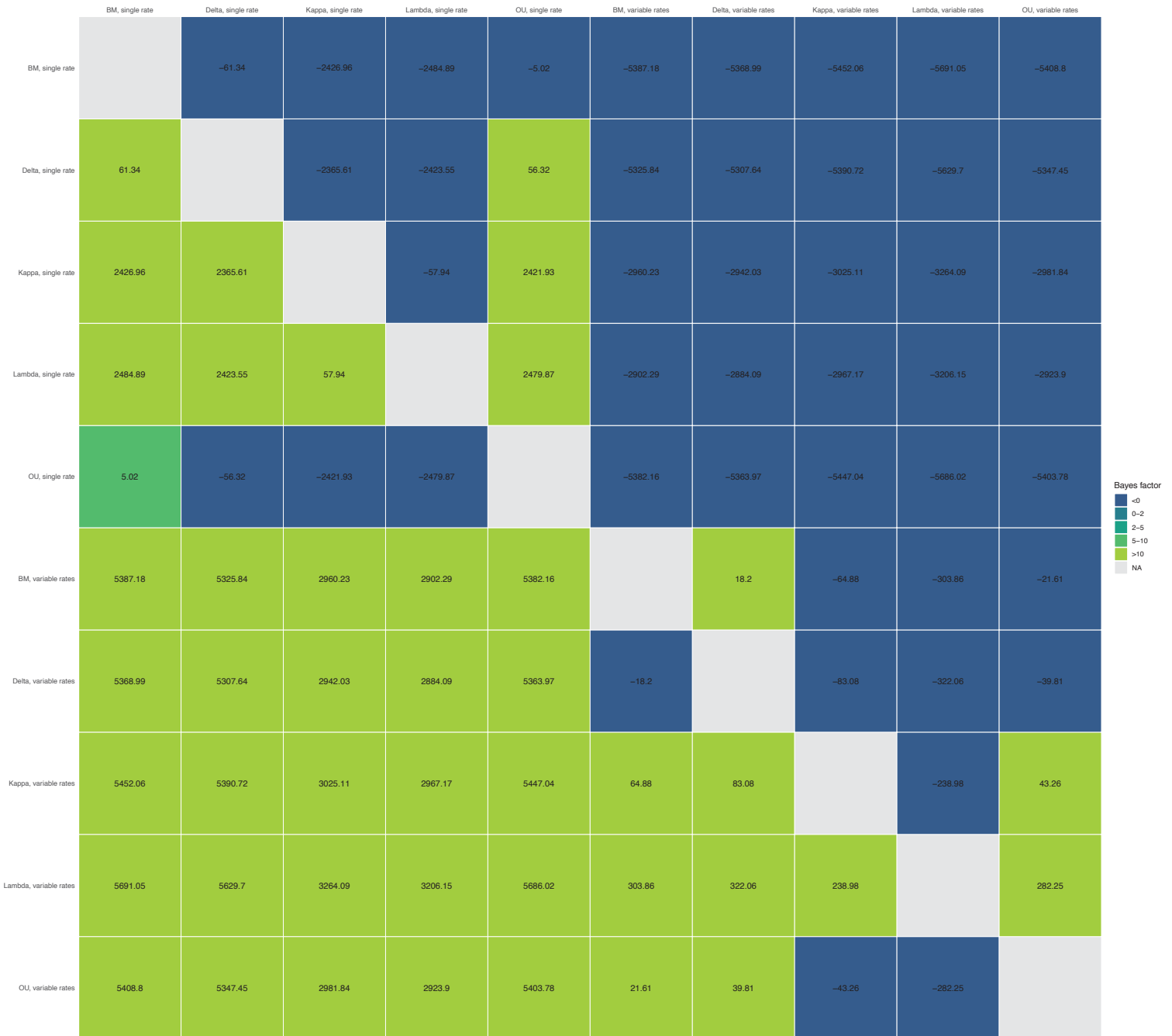


Fig. S3. N) Bayes Factor comparisons for 10 alternative evolutionary models for Tree Topology 3 Root Age = 75-80Ma.

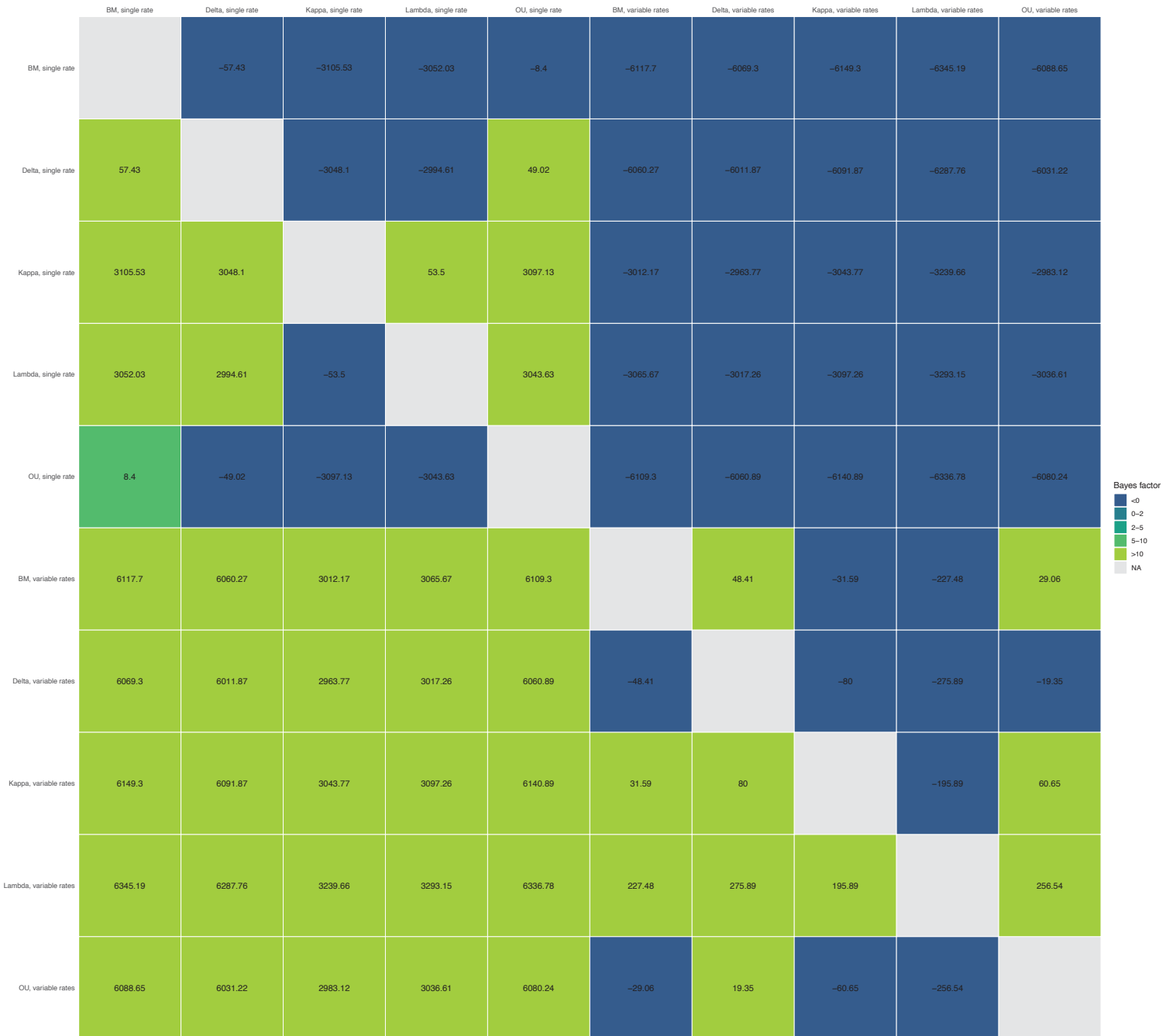


Fig. S3. O) Bayes Factor comparisons for 10 alternative evolutionary models for Tree Topology 3, Root Age = 80-85Ma.

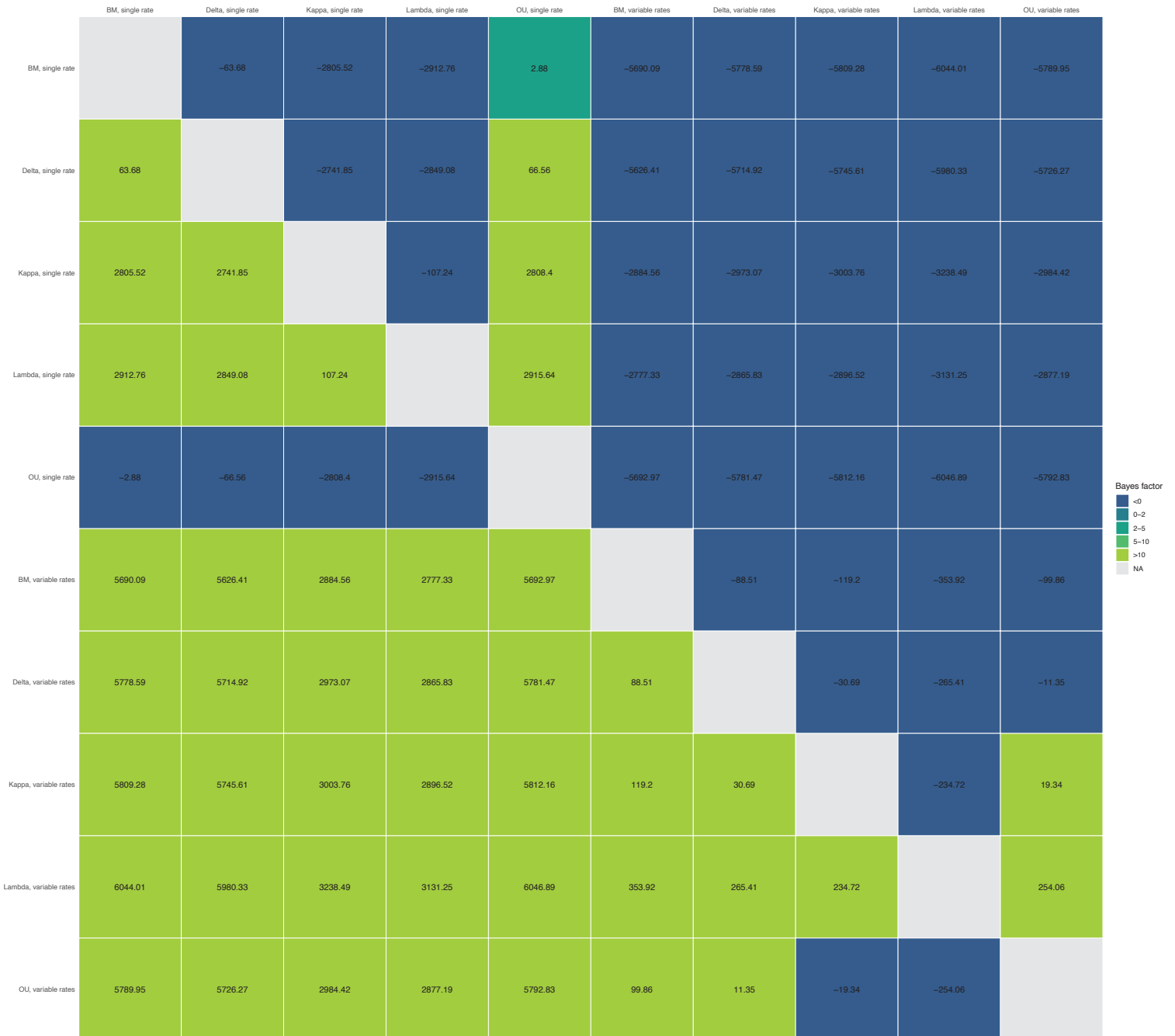


Fig. S3. P) Bayes Factor comparisons for 10 alternative evolutionary models for Tree Topology 3, Root Age = 85-90Ma.

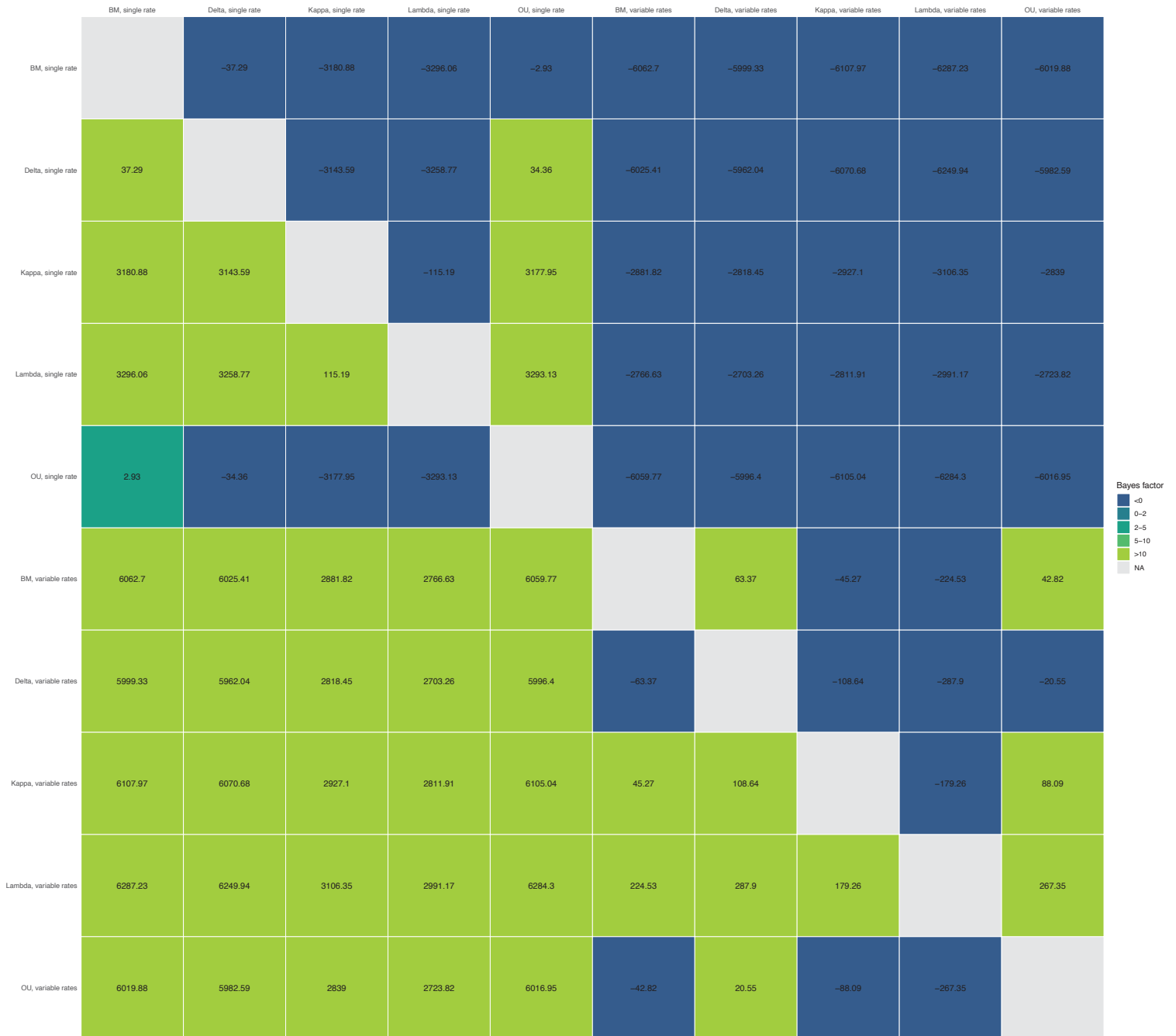


Fig. S3. Q) Bayes Factor comparisons for 10 alternative evolutionary models for Tree Topology 3, Root Age = 90-95Ma.

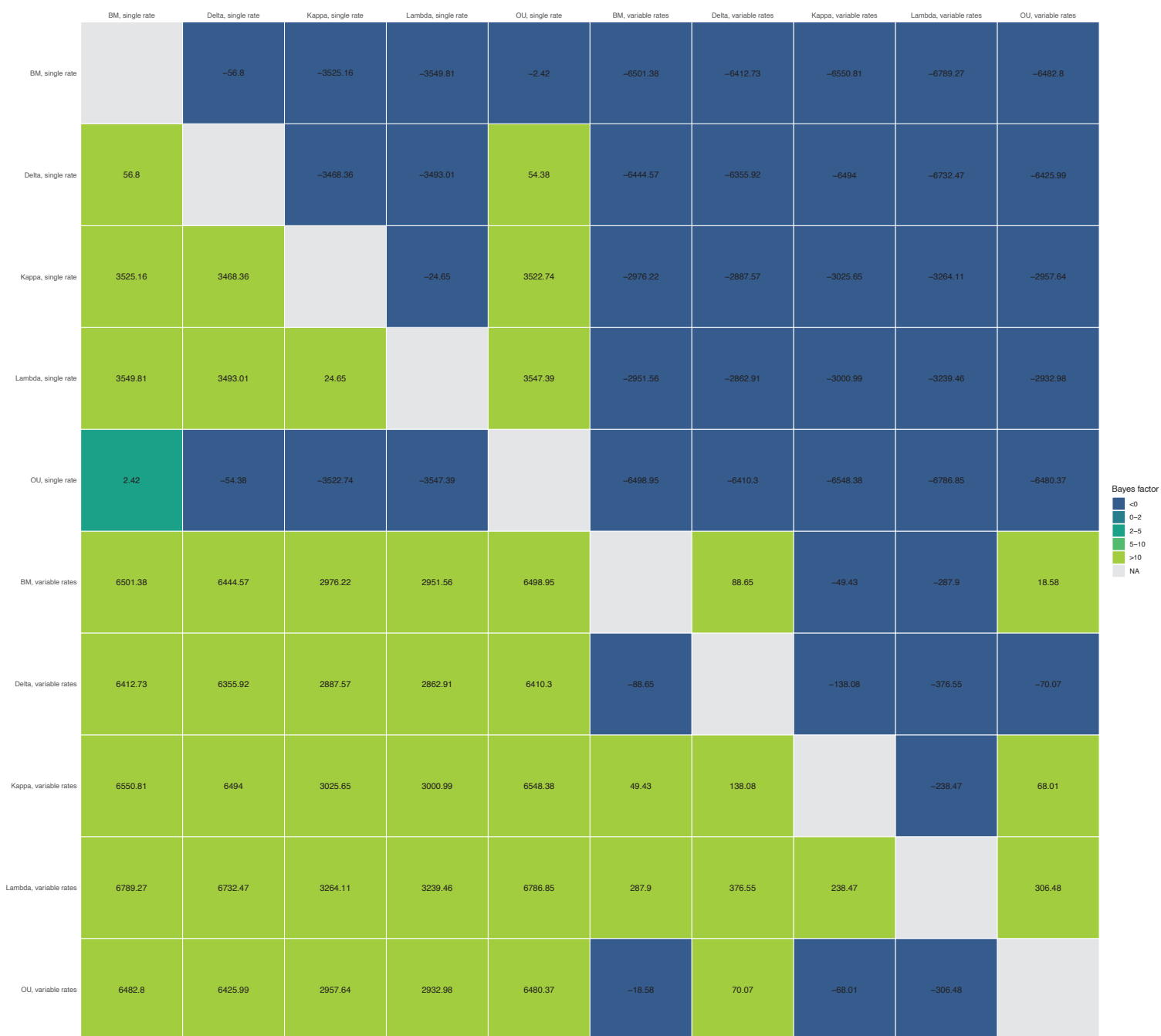


Fig. S3. R) Bayes Factor comparisons for 10 alternative evolutionary models for Tree Topology 3, Root Age = 95-100Ma.

Tree Topology 1: Root Age = 80 - 85 Ma

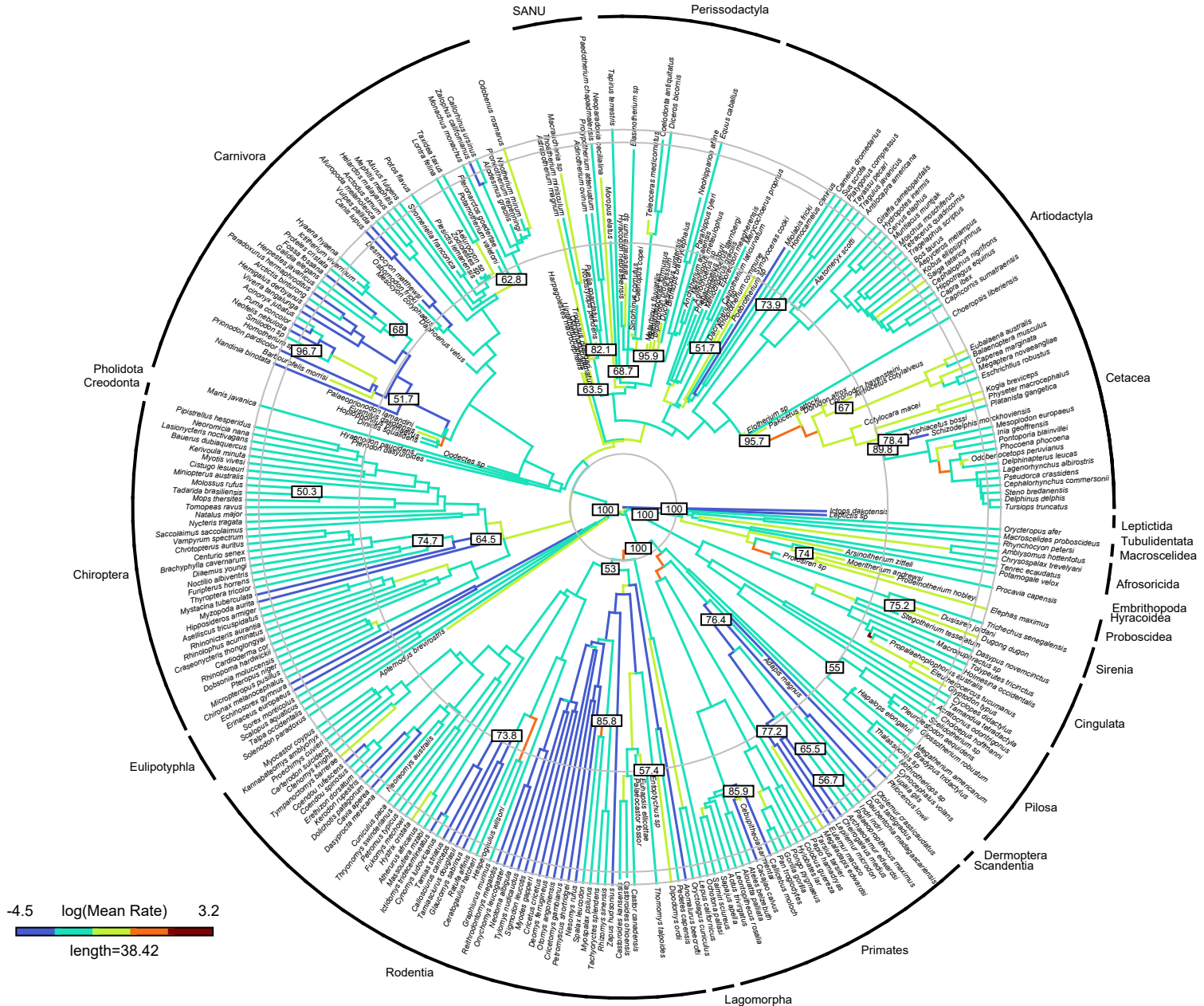


Fig. S4. C) Estimated branch-specific rates of cranial evolution using a variable-rates Brownian motion model with a lambda tree transformation for Tree Topology 1, Root Age = 80-85Ma.

Tree Topology 1: Root Age = 85 - 90 Ma

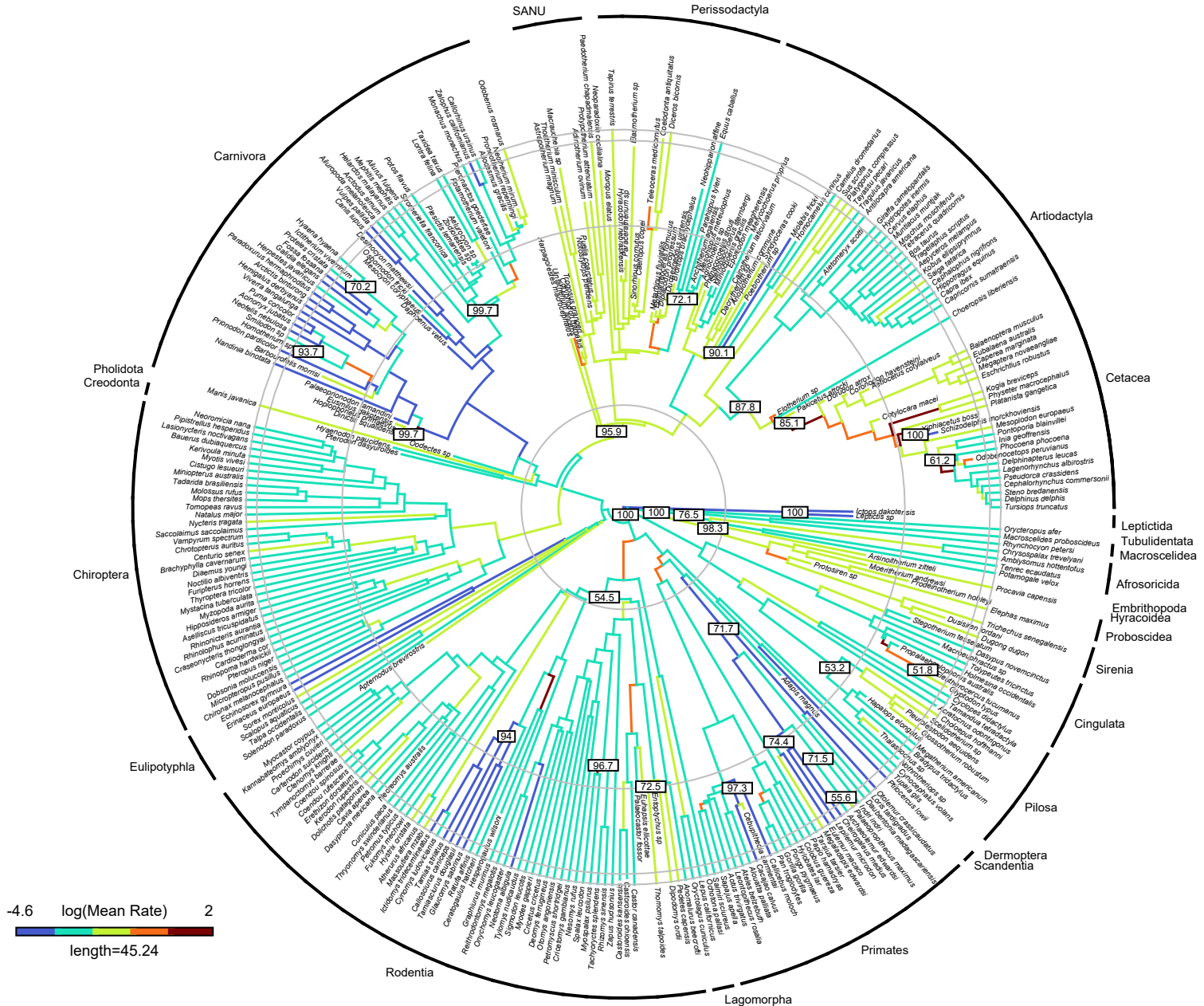


Fig. S4. D) Estimated branch-specific rates of cranial evolution using a variable-rates Brownian motion model with a lambda tree transformation for Tree Topology 1, Root Age = 85-90Ma.

Tree Topology 1: Root Age = 90 - 95 Ma

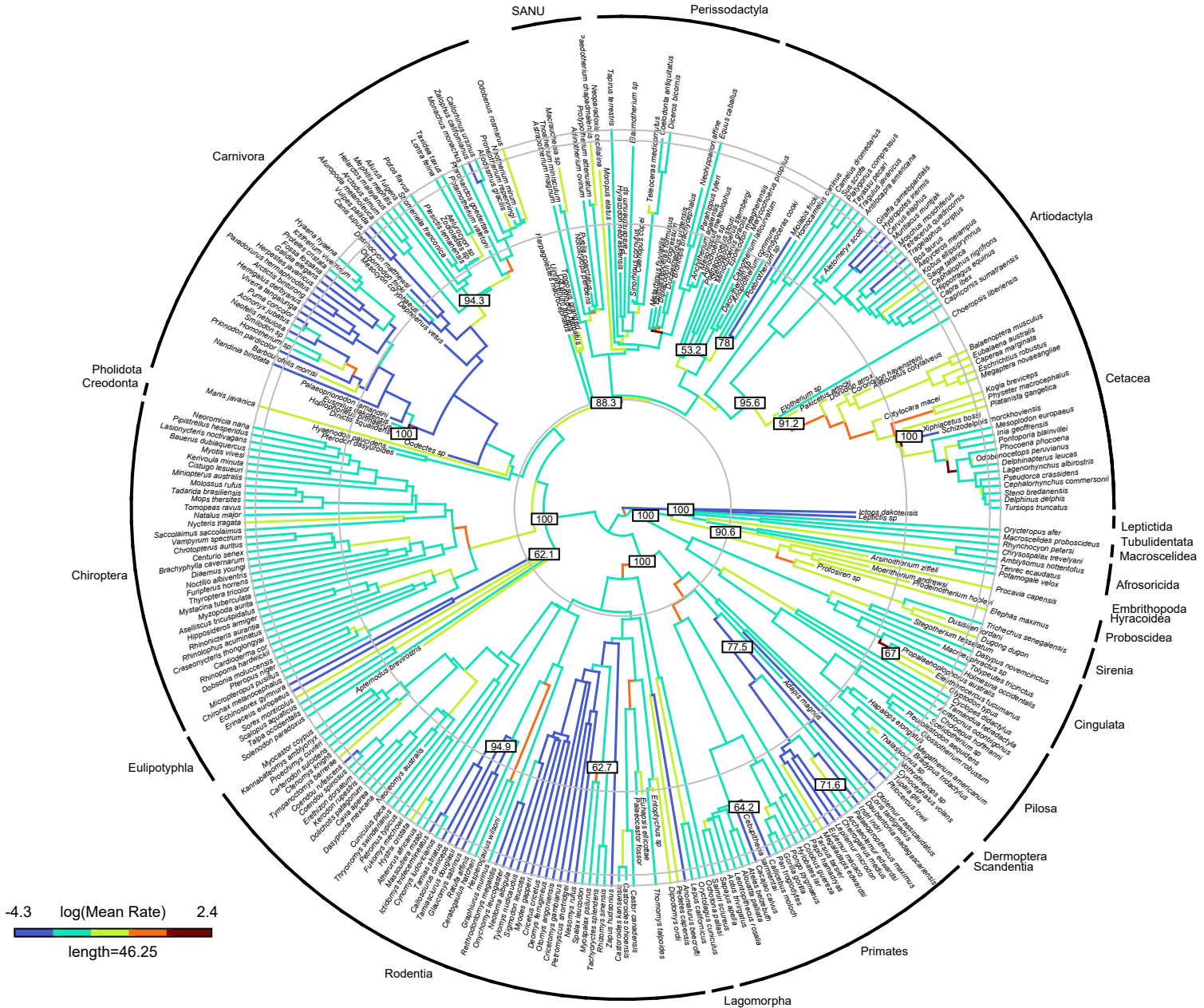


Fig. S4. E) Estimated branch-specific rates of cranial evolution using a variable-rates Brownian motion model with a lambda tree transformation for Tree Topology 1, Root Age = 90-95Ma.

Tree Topology 1: Root Age = 95 - 100 Ma

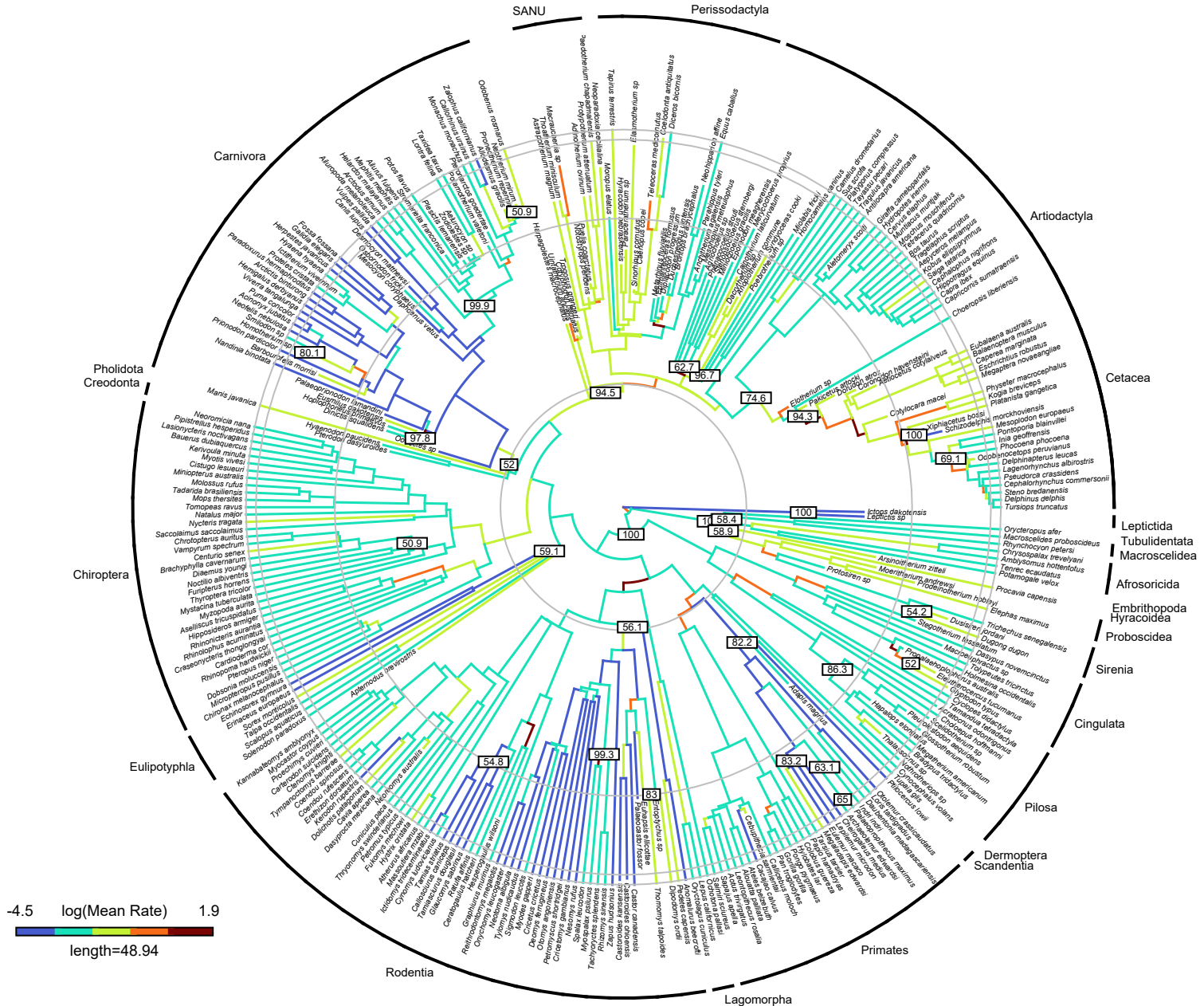


Fig. S4. F) Estimated branch-specific rates of cranial evolution using a variable-rates Brownian motion model with a lambda tree transformation for Tree Topology 1, Root Age = 95-100Ma.

Tree Topology 2: Root Age = 70 - 75 Ma

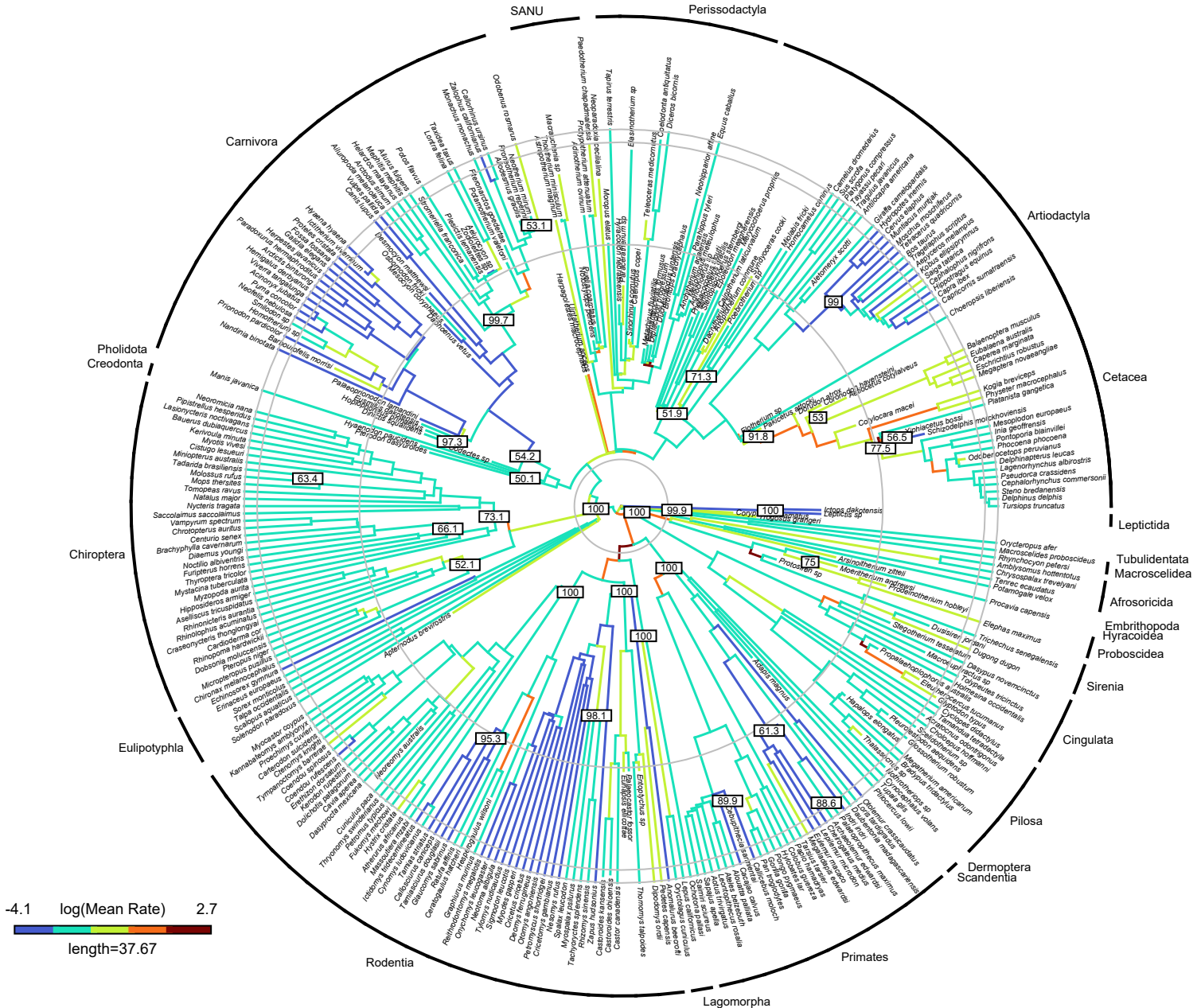


Fig. S4. G) Estimated branch-specific rates of cranial evolution using a variable-rates Brownian motion model with a lambda tree transformation for Tree Topology 2, Root Age = 70-75Ma.

Tree Topology 2: Root Age = 75 - 80 Ma

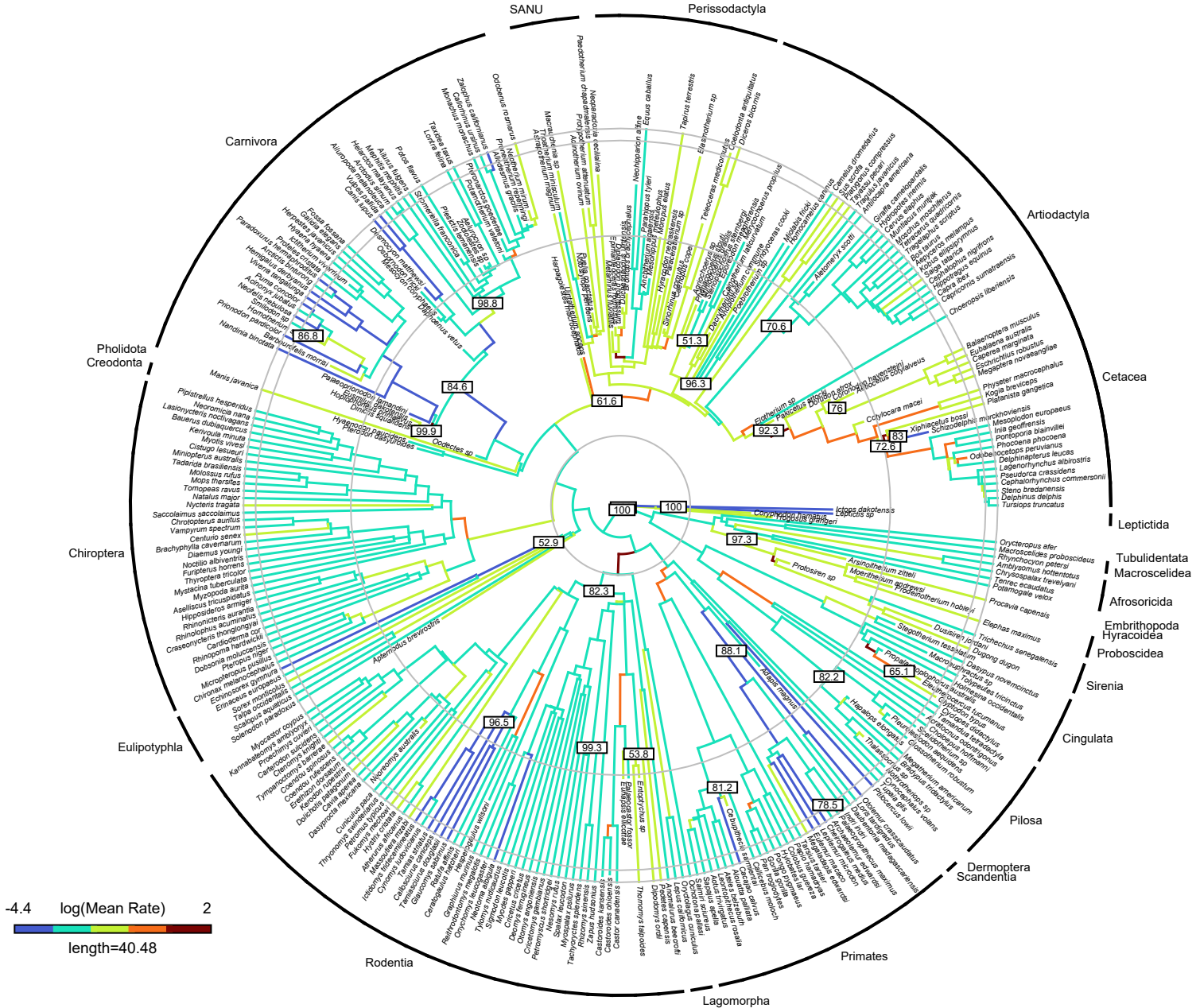


Fig. S4. H) Estimated branch-specific rates of cranial evolution using a variable-rates Brownian motion model with a lambda tree transformation for Tree Topology 2, Root Age = 75-80Ma.

Tree Topology 2: Root Age = 85 - 90 Ma

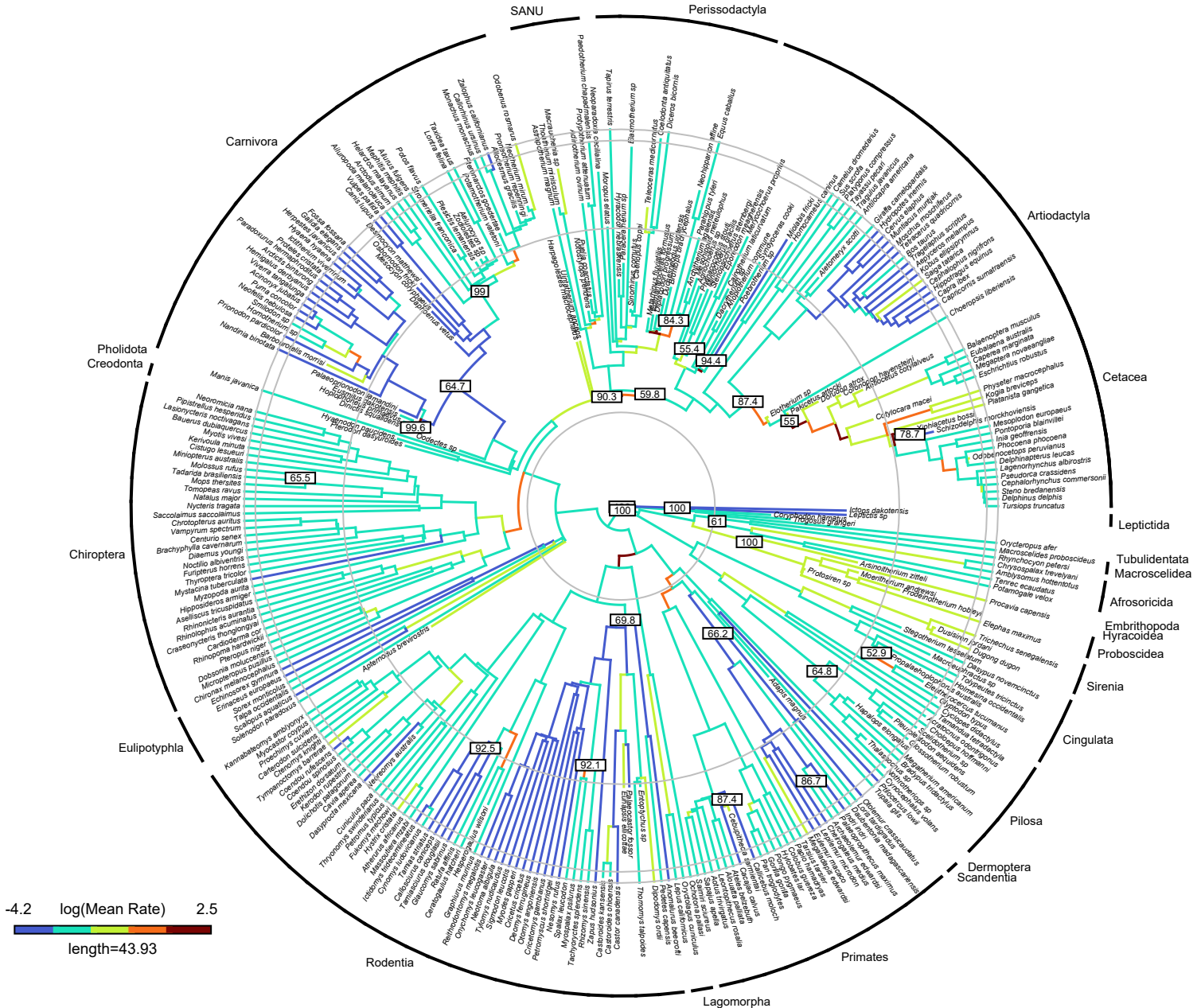


Fig. S4. J) Estimated branch-specific rates of cranial evolution using a variable-rates Brownian motion model with a lambda tree transformation for Tree Topology 2, Root Age = 85-90Ma.

Tree Topology 2: Root Age = 90 - 95 Ma

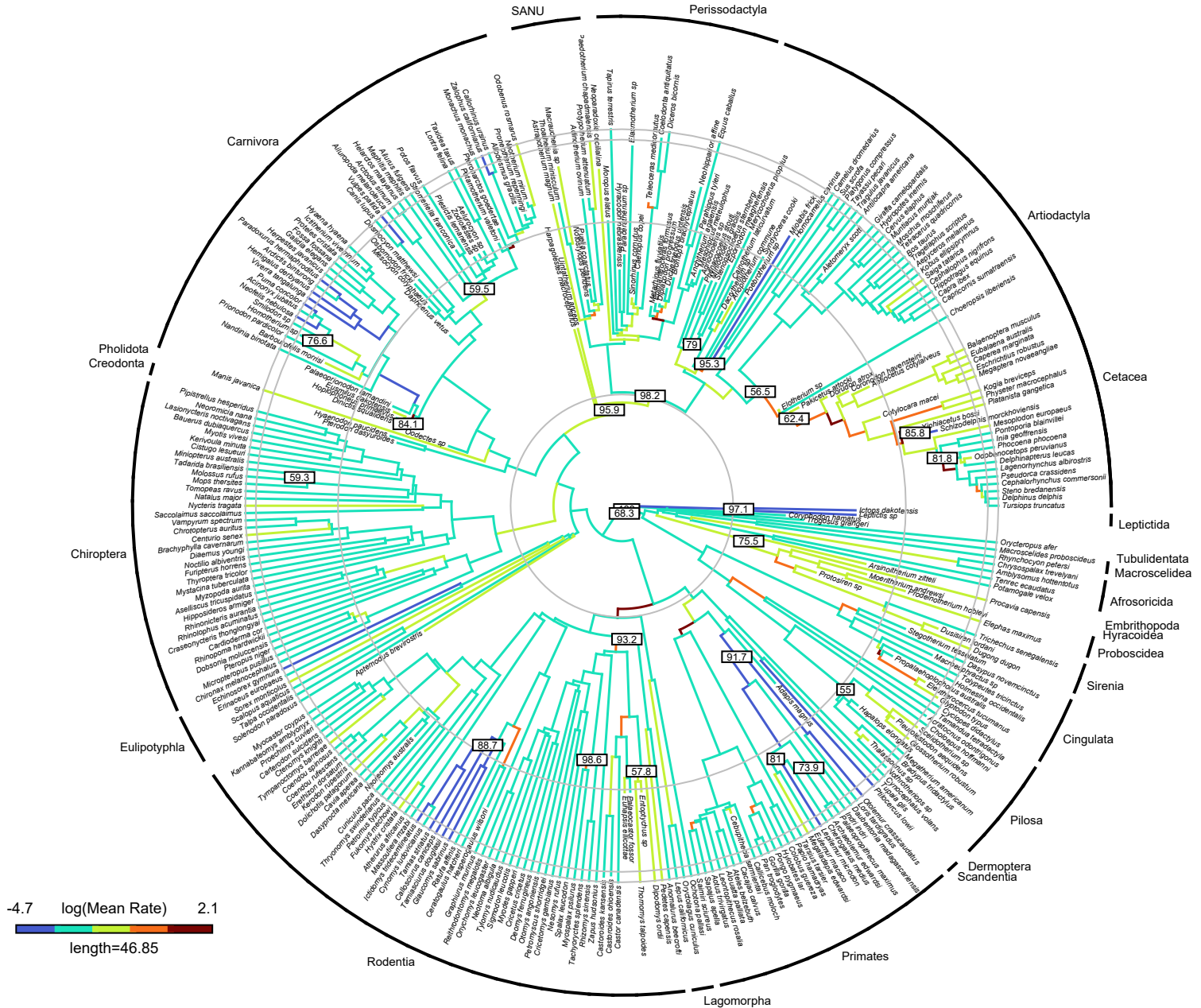


Fig. S4. K) Estimated branch-specific rates of cranial evolution using a variable-rates Brownian motion model with a lambda tree transformation for Tree Topology 2, Root Age = 90-95Ma.

Tree Topology 2: Root Age = 95 - 100 Ma

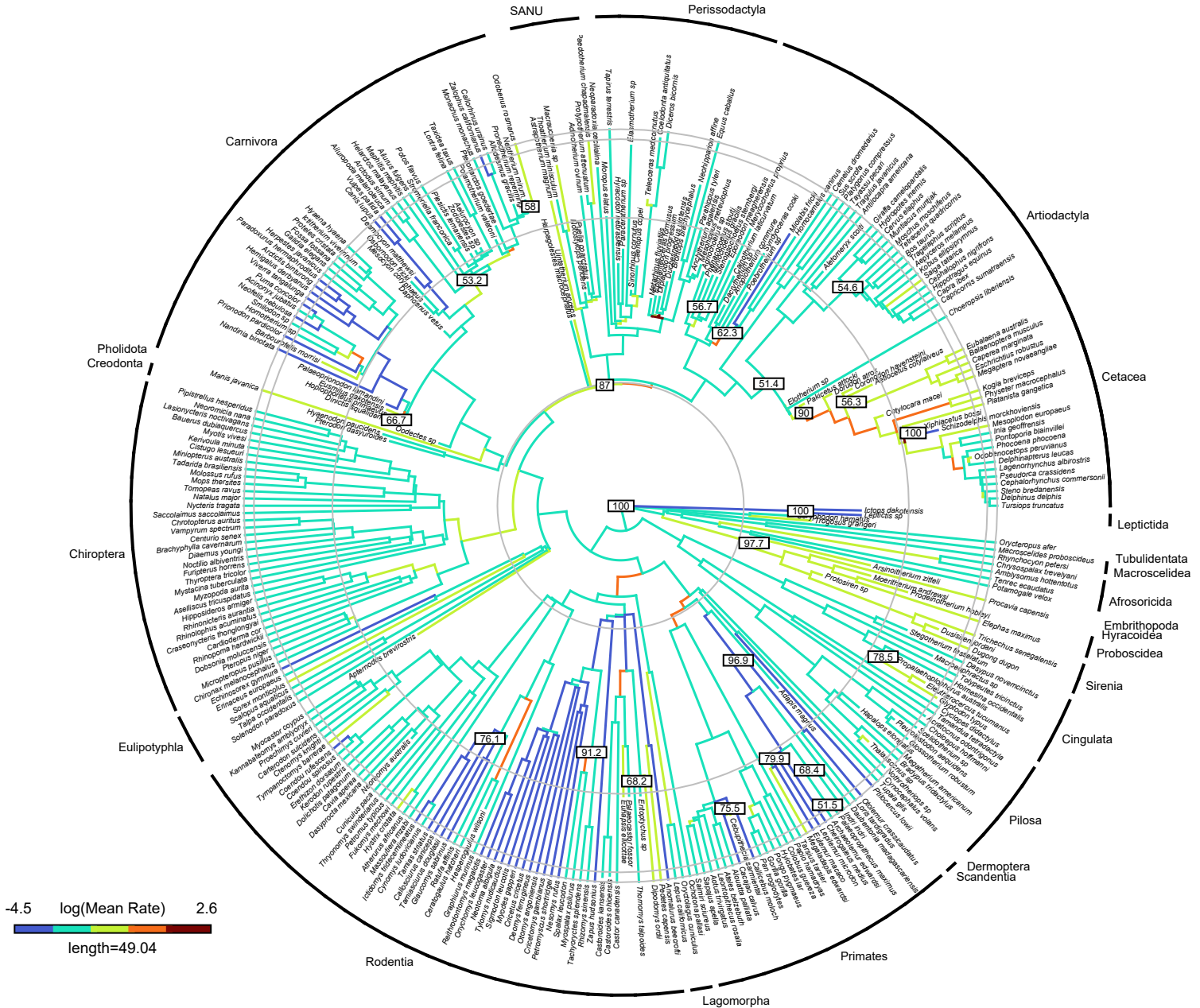


Fig. S4. L) Estimated branch-specific rates of cranial evolution using a variable-rates Brownian motion model with a lambda tree transformation for Tree Topology 2, Root Age = 95-100Ma.

Tree Topology 3: Root Age = 80 - 85 Ma

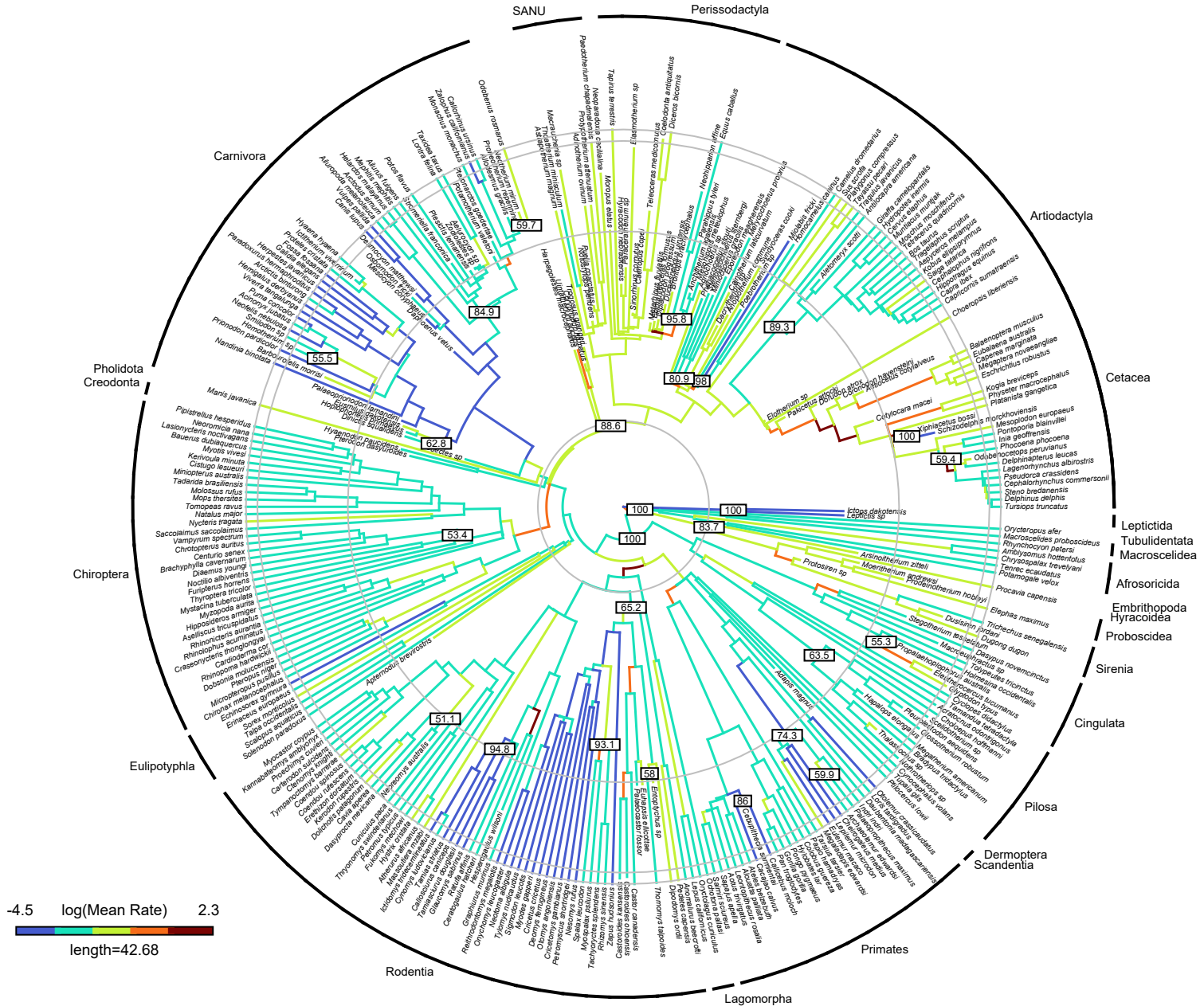


Fig. S4. O) Estimated branch-specific rates of cranial evolution using a variable-rates Brownian motion model with a lambda tree transformation for Tree Topology 3, Root Age = 80-85Ma.

Tree Topology 3: Root Age = 85 - 90 Ma

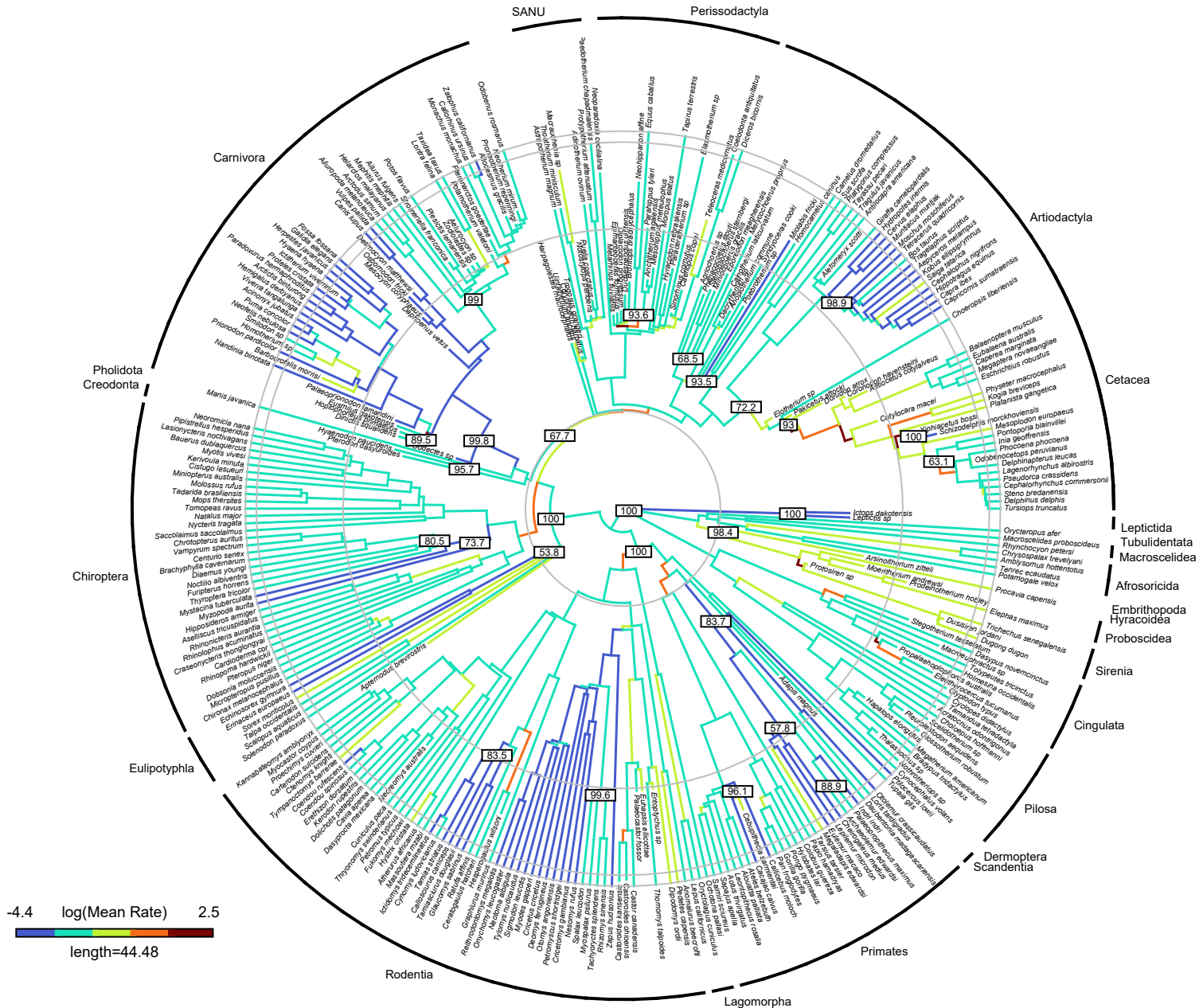


Fig. S4. P) Estimated branch-specific rates of cranial evolution using a variable-rates Brownian motion model with a lambda tree transformation for Tree Topology 3, Root Age = 85-90Ma.

Tree Topology 3: Root Age = 95 - 100 Ma

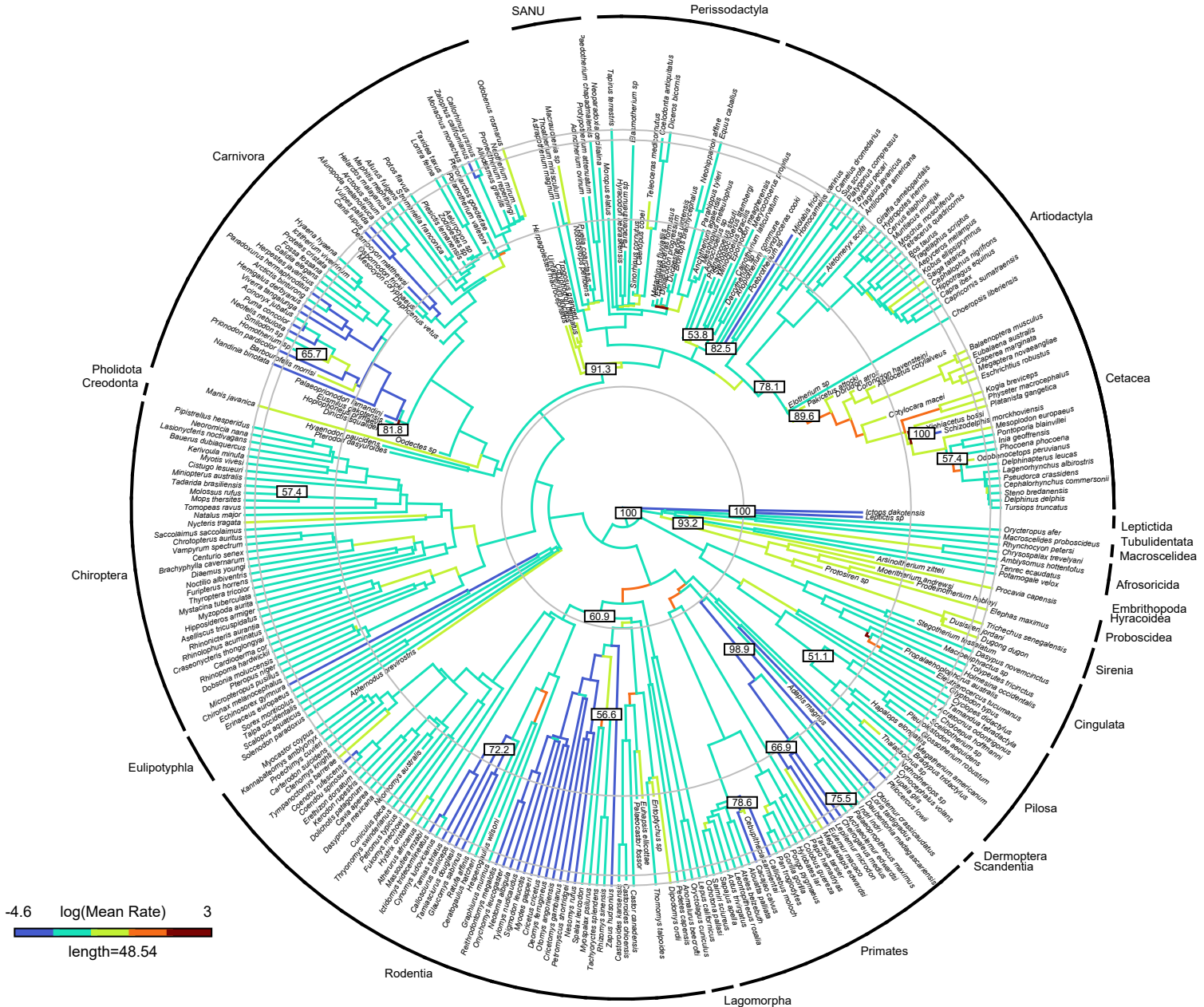


Fig. S4. R) Estimated branch-specific rates of cranial evolution using a variable-rates Brownian motion model with a lambda tree transformation for Tree Topology 3, Root Age = 95-100Ma.

Tree Topology 1: Root Age 70–75 Ma

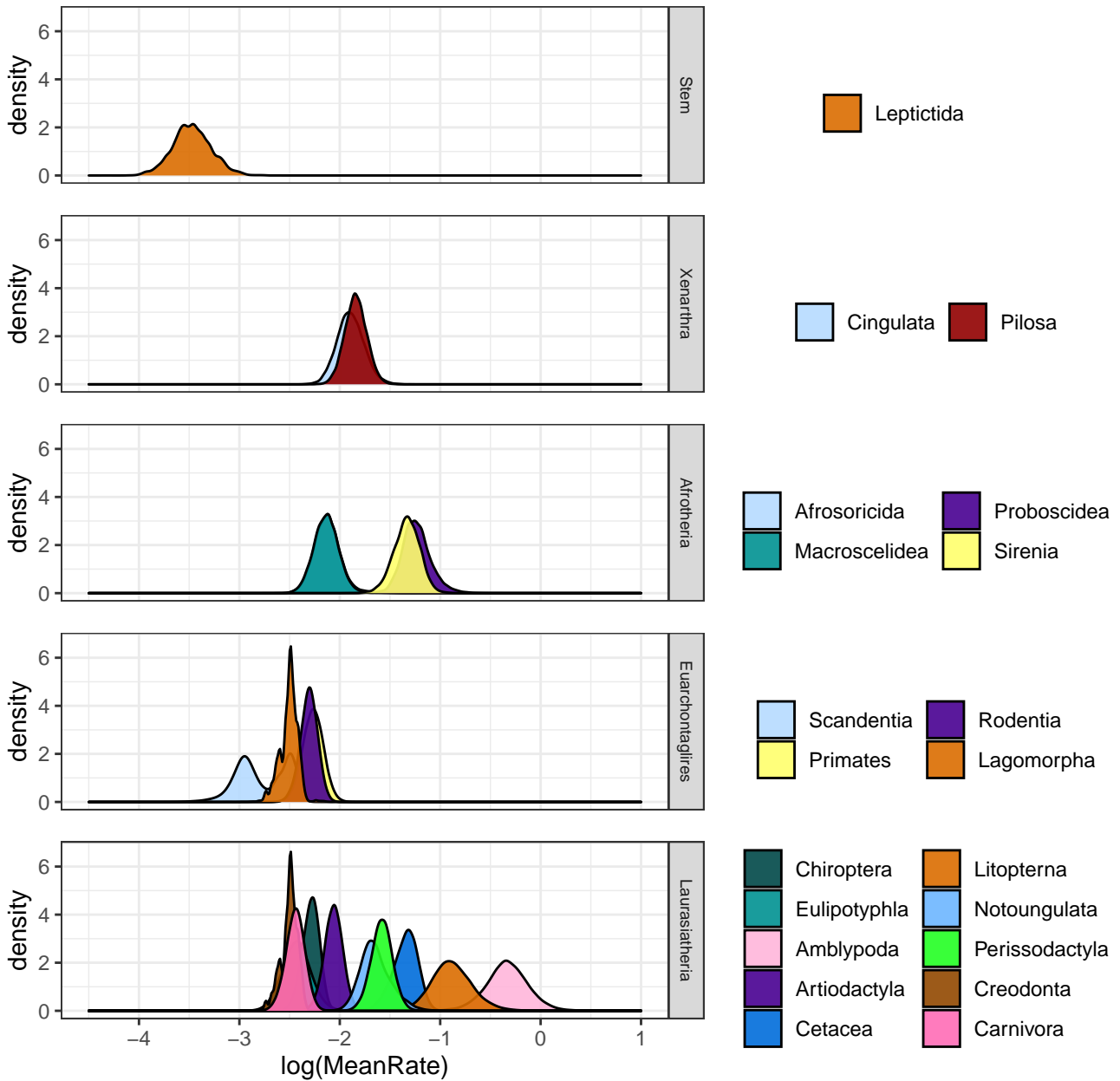


Fig. S5. A) Rates of evolution for terminal branches, subsetted into placental orders, for Tree Topology 1, Root Age = 70-75Ma.

Tree Topology 1: Root Age 75–80 Ma

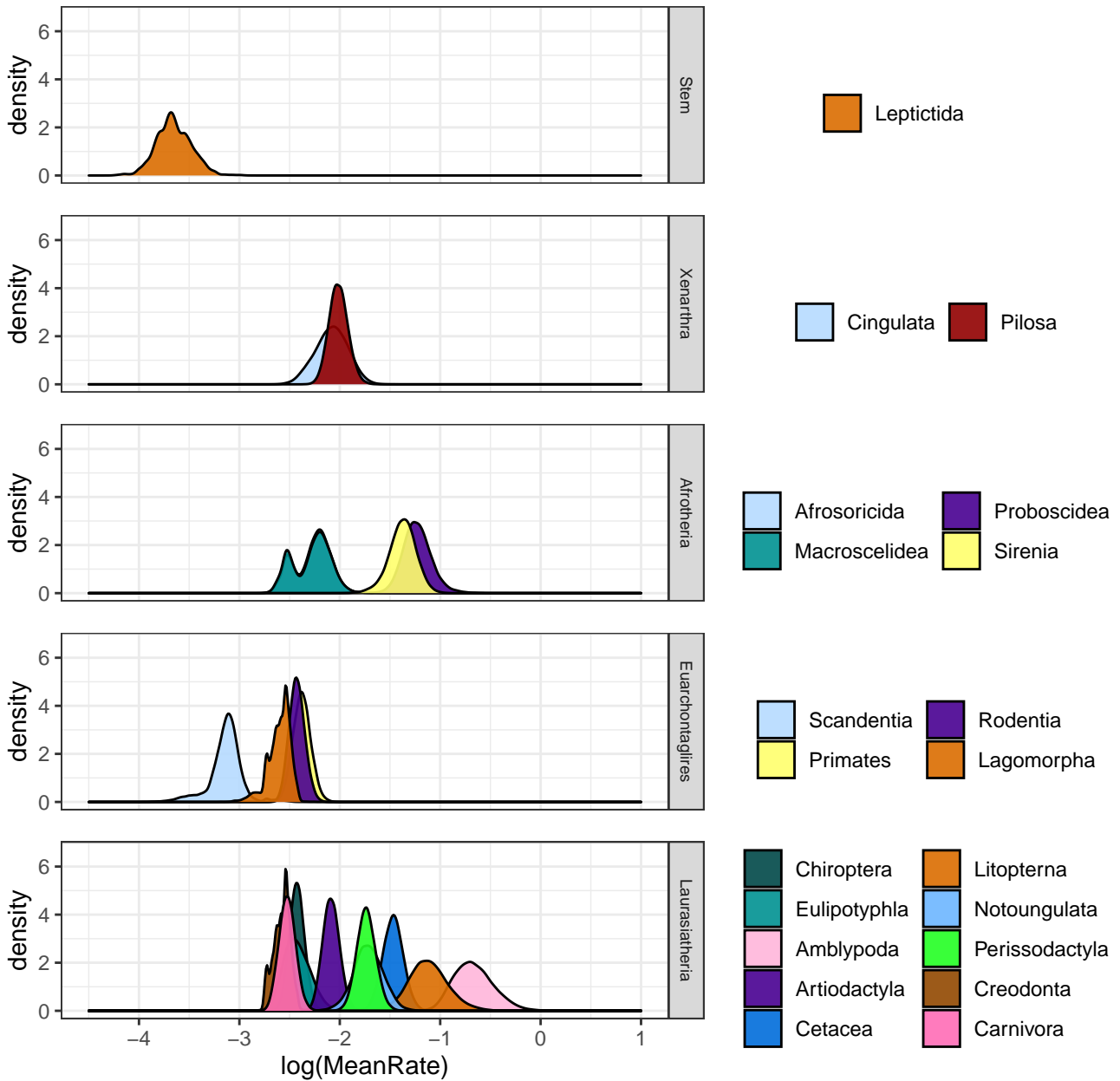


Fig. S5. B) Rates of evolution for terminal branches, subsetted into placental orders, for Tree Topology 1, Root Age = 75-80Ma.

Tree Topology 1: Root Age 80–85 Ma

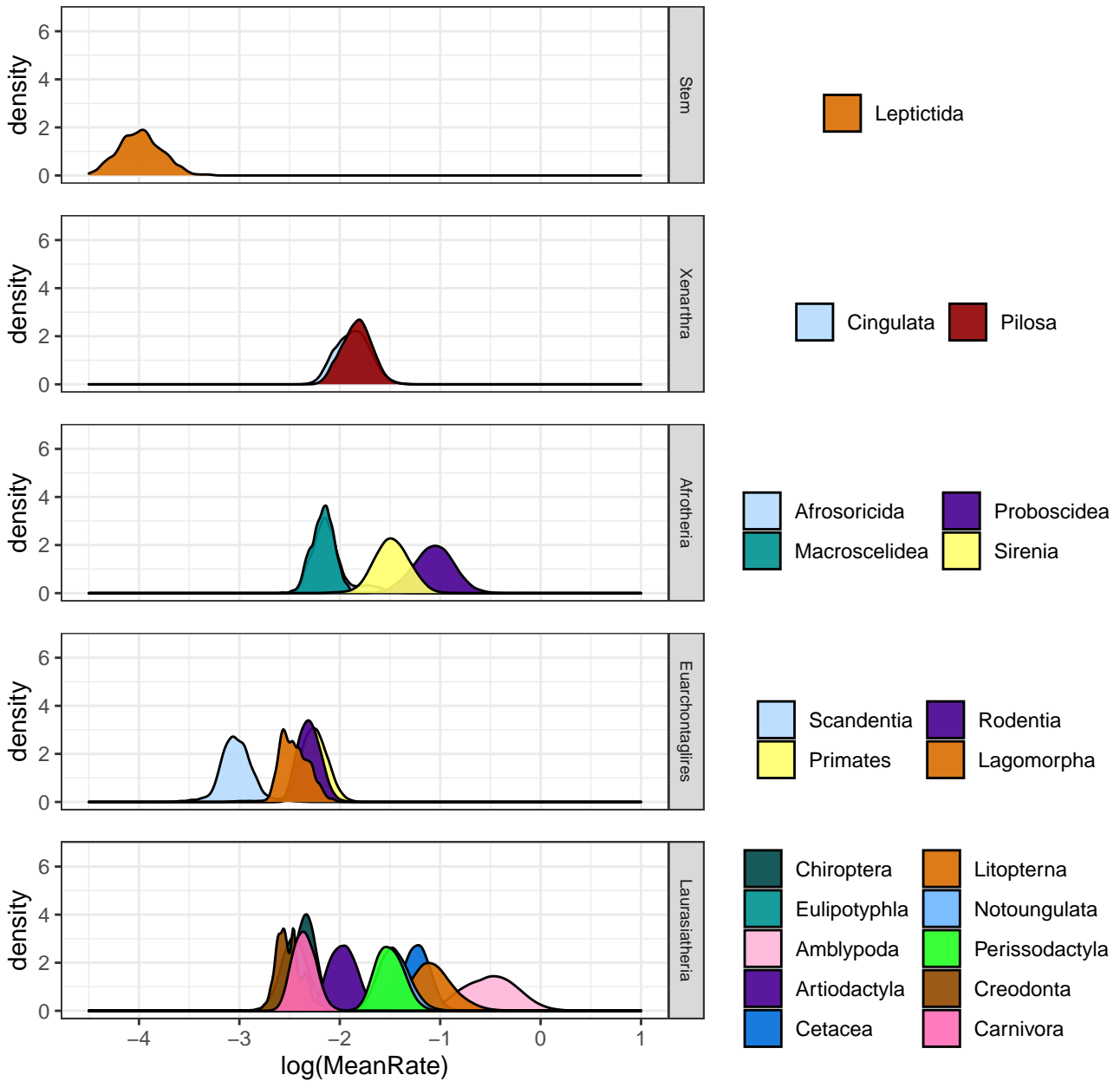


Fig. S5. C) Rates of evolution for terminal branches, subsetted into placental orders, for Tree Topology 1, Root Age = 80-85Ma.

Tree Topology 1: Root Age 85–90 Ma

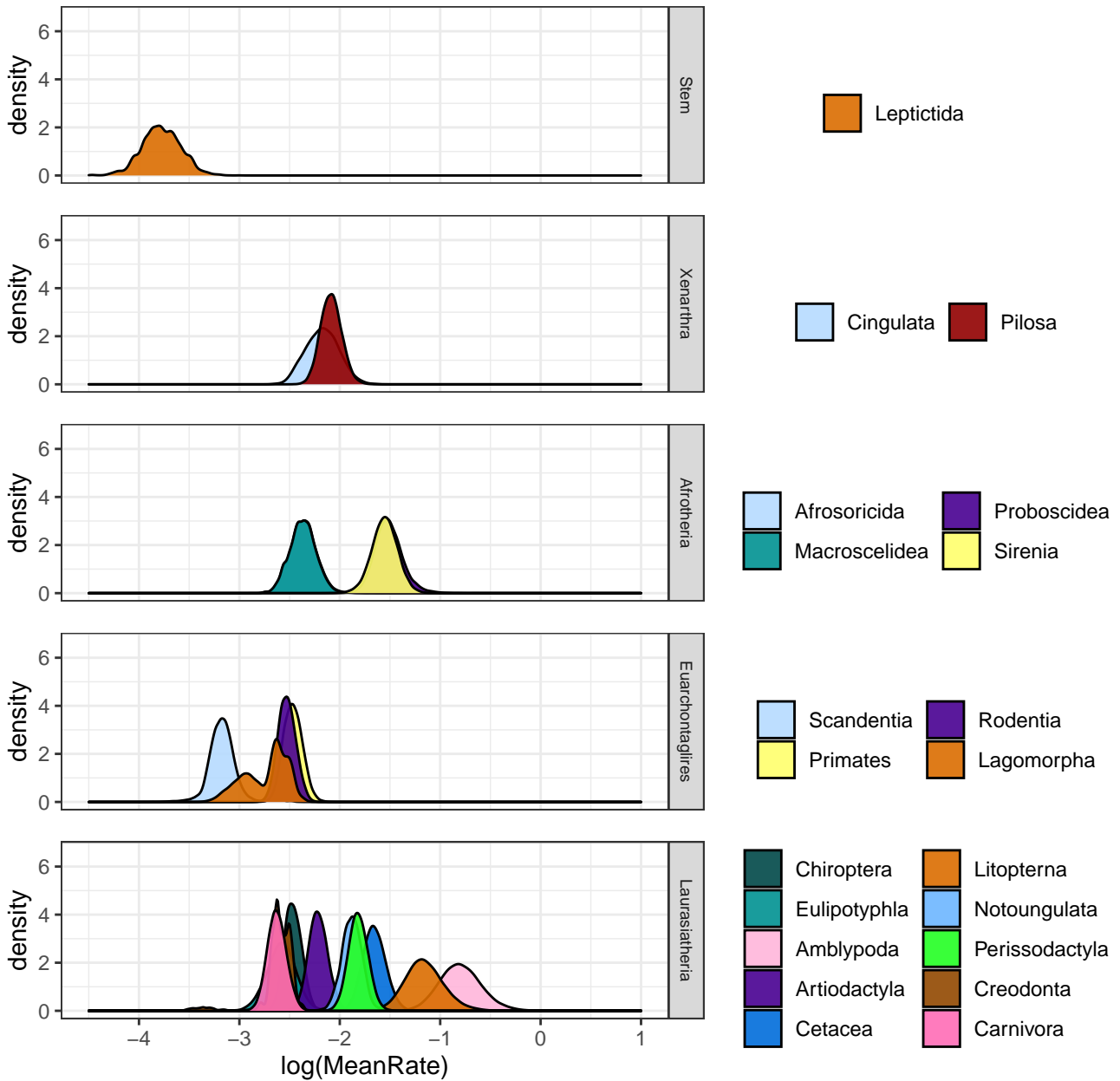


Fig. S5. D) Rates of evolution for terminal branches, subsetted into placental orders, for Tree Topology 1, Root Age = 85-90Ma.

Tree Topology 1: Root Age 90–95 Ma

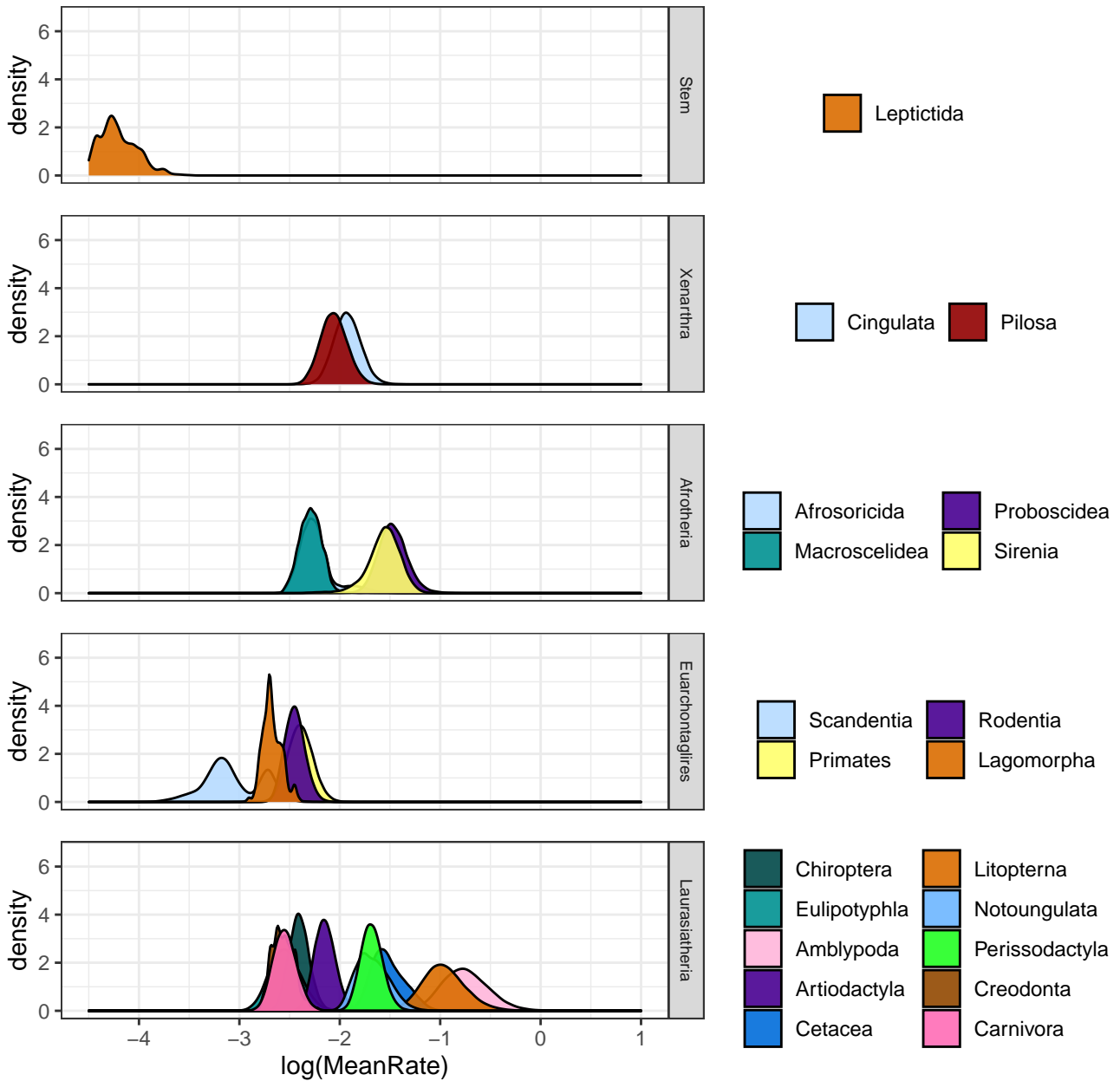


Fig. S5. E) Rates of evolution for terminal branches, subsetted into placental orders, for Tree Topology 1, Root Age = 90-95Ma.

Tree Topology 1: Root Age 95–100 Ma

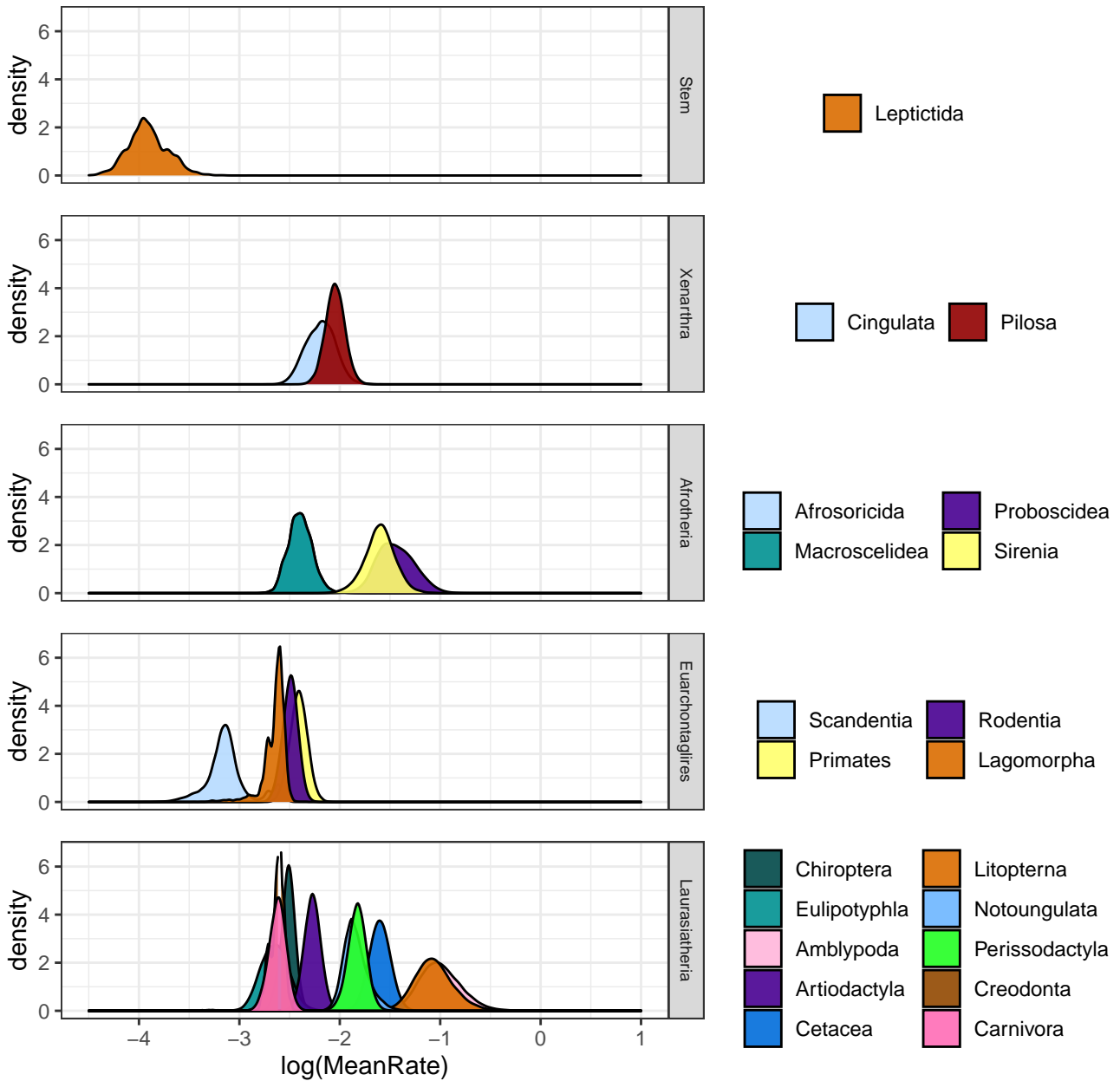


Fig. S5. F) Rates of evolution for terminal branches, subsetted into placental orders, for Tree Topology 1, Root Age = 95-100Ma.

Tree Topology 2: Root Age 70–75 Ma

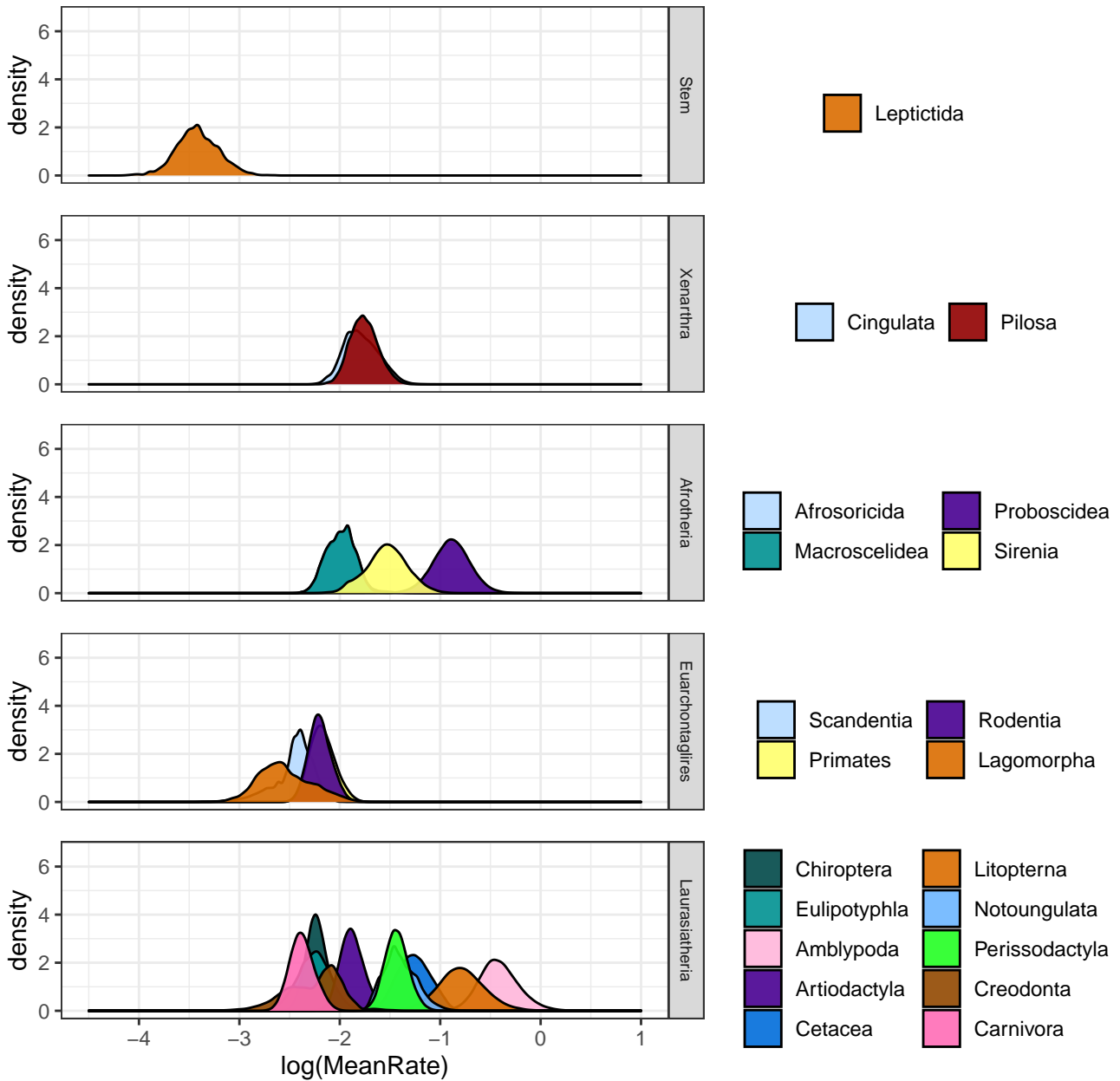


Fig. S5. G) Rates of evolution for terminal branches, subsetted into placental orders, for Tree Topology 2, Root Age = 70-75Ma.

Tree Topology 2: Root Age 75–80 Ma

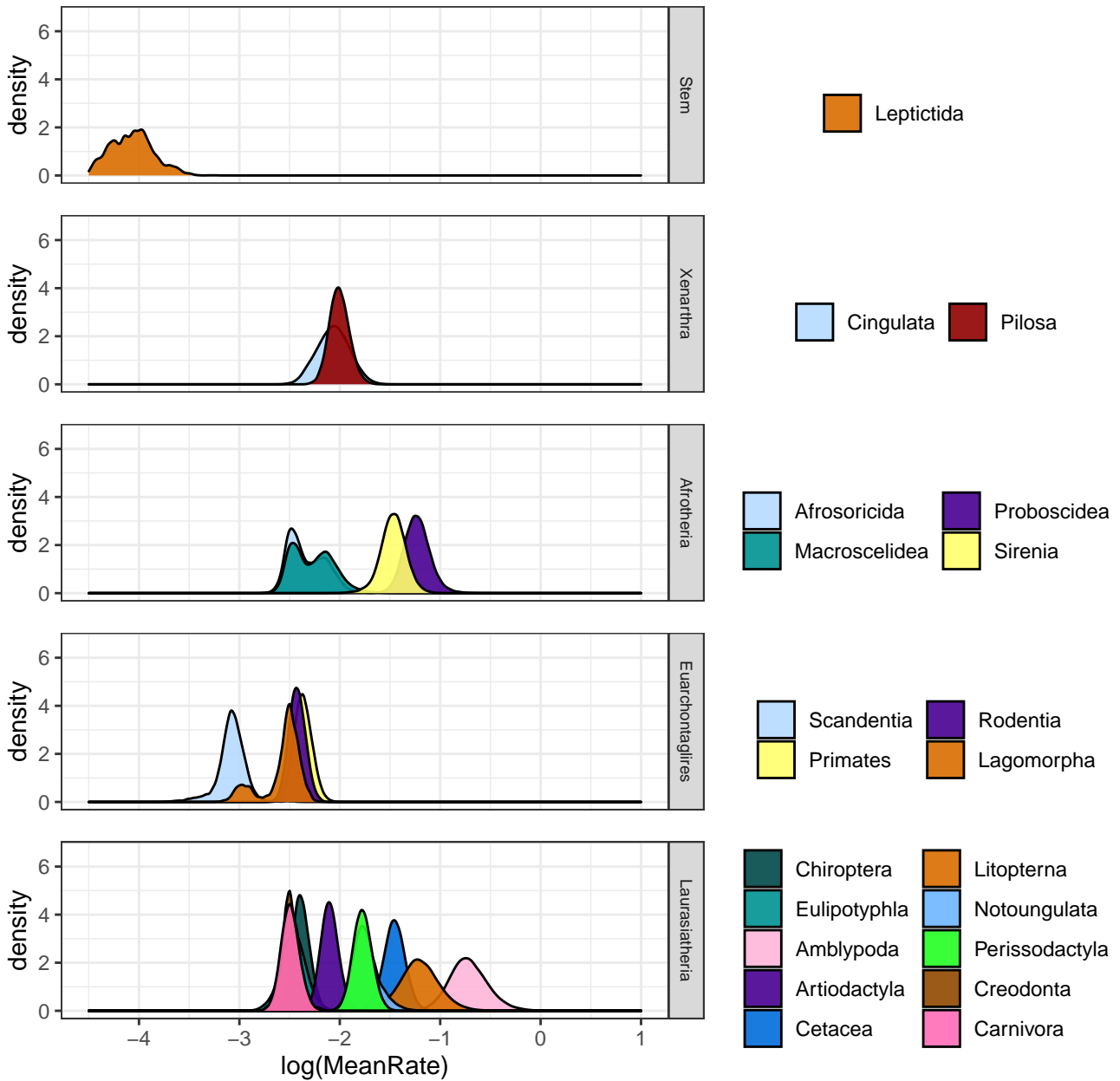


Fig. S5. H) Rates of evolution for terminal branches, subsetted into placental orders, for Tree Topology 2, Root Age = 75-80Ma.

Tree Topology 2: Root Age 80–85 Ma

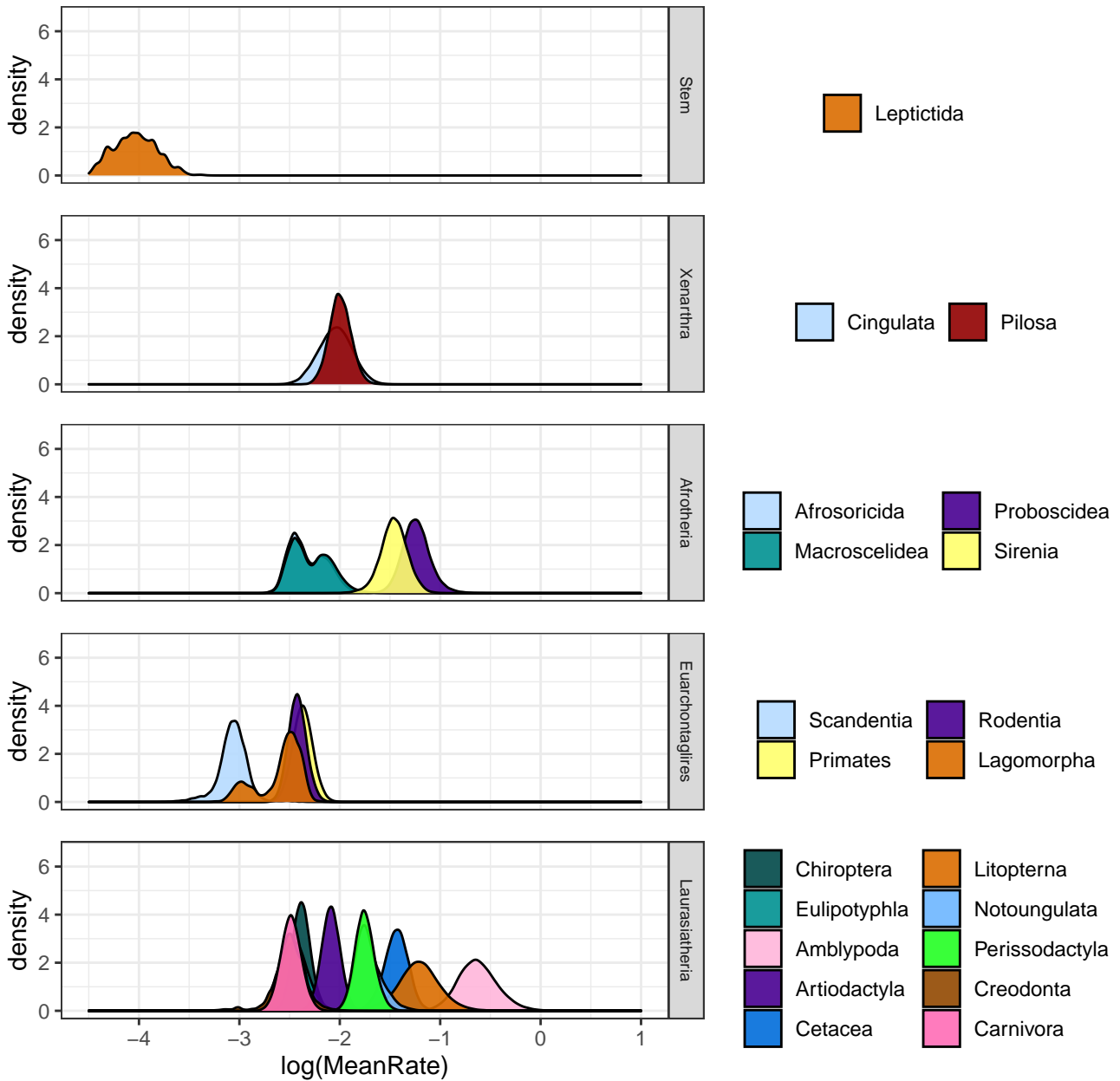


Fig. S5. i) Rates of evolution for terminal branches, subsetted into placental orders, for Tree Topology 2, Root Age = 80-85Ma.

Tree Topology 2: Root Age 85–90 Ma

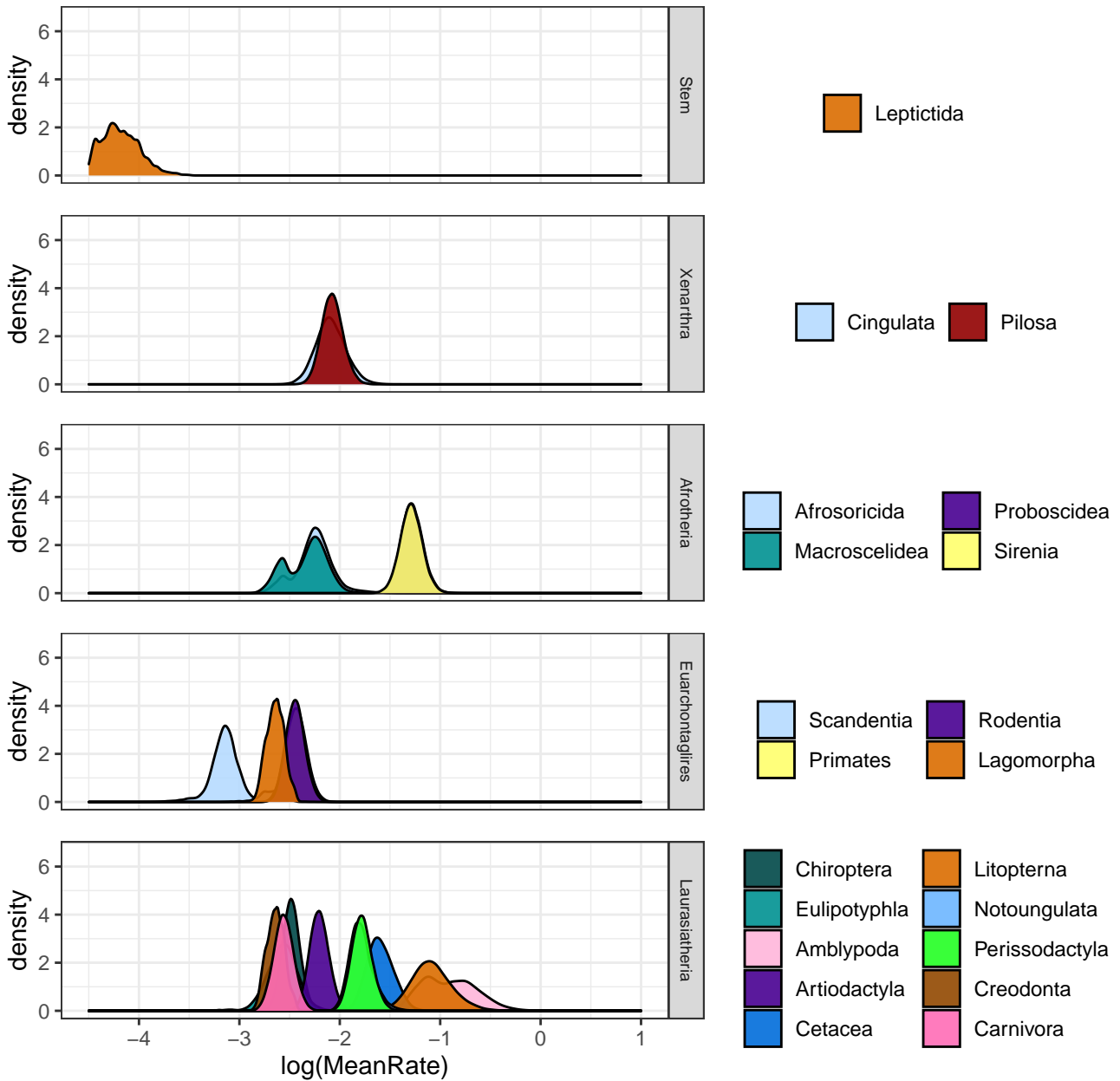


Fig. S5. J) Rates of evolution for terminal branches, subsetted into placental orders, for Tree Topology 2, Root Age = 85-90Ma.

Tree Topology 2: Root Age 90–95 Ma

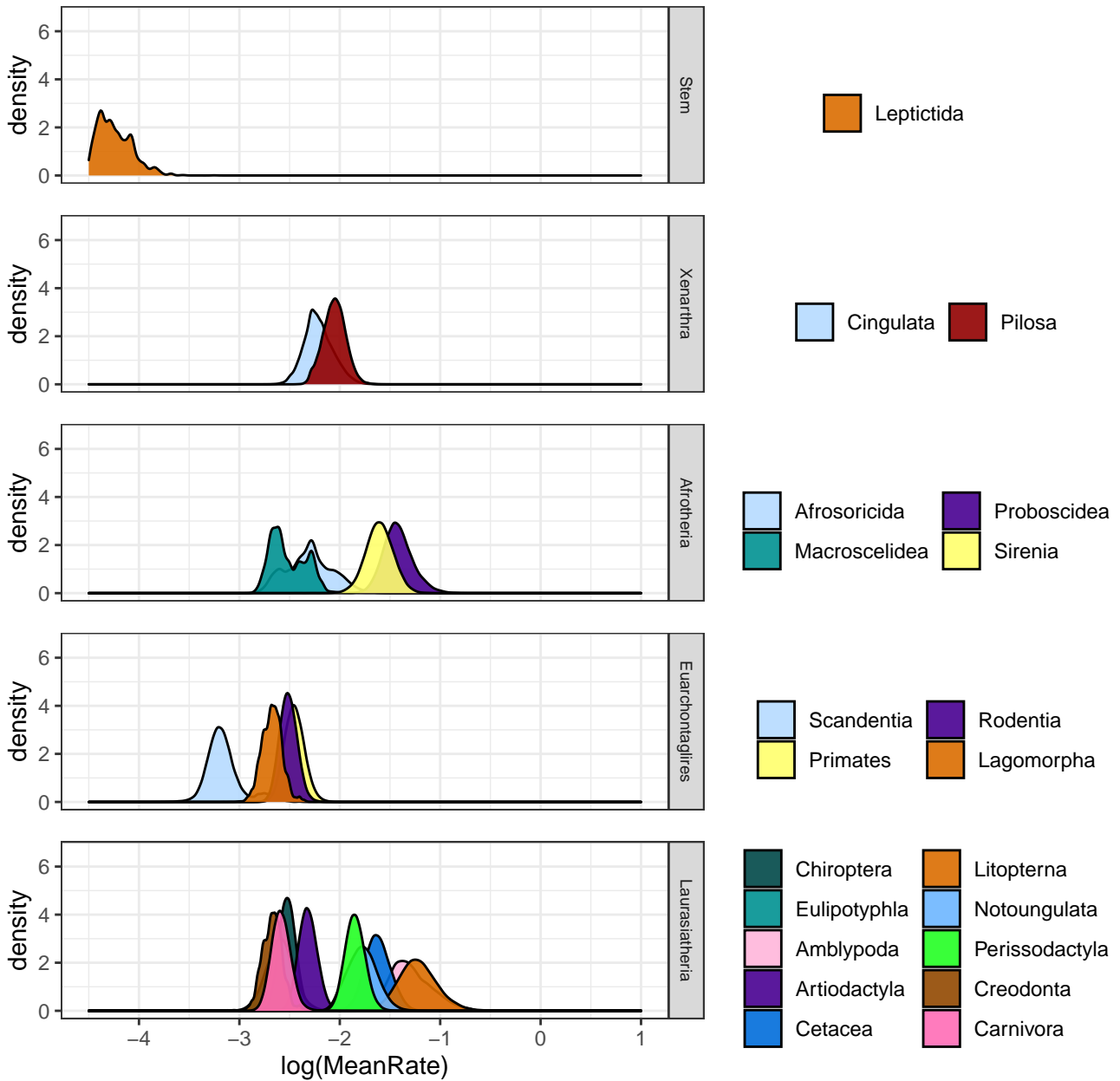


Fig. S5. K) Rates of evolution for terminal branches, subsetted into placental orders, for Tree Topology 2, Root Age = 90-95Ma.

Tree Topology 2: Root Age 95–100 Ma

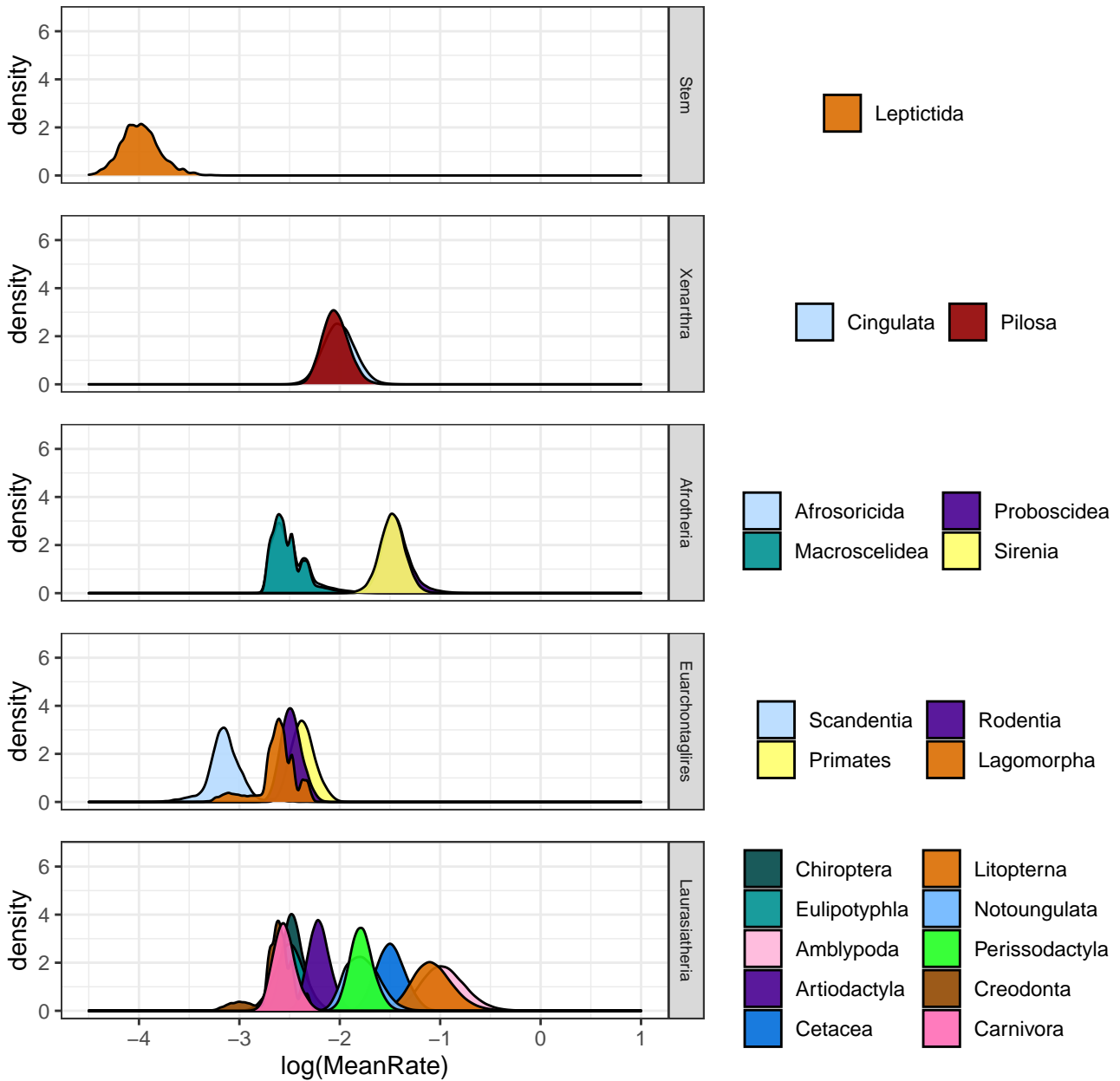


Fig. S5. L) Rates of evolution for terminal branches, subsetted into placental orders, for Tree Topology 2, Root Age = 95-100Ma.

Tree Topology 3: Root Age 70–75 Ma

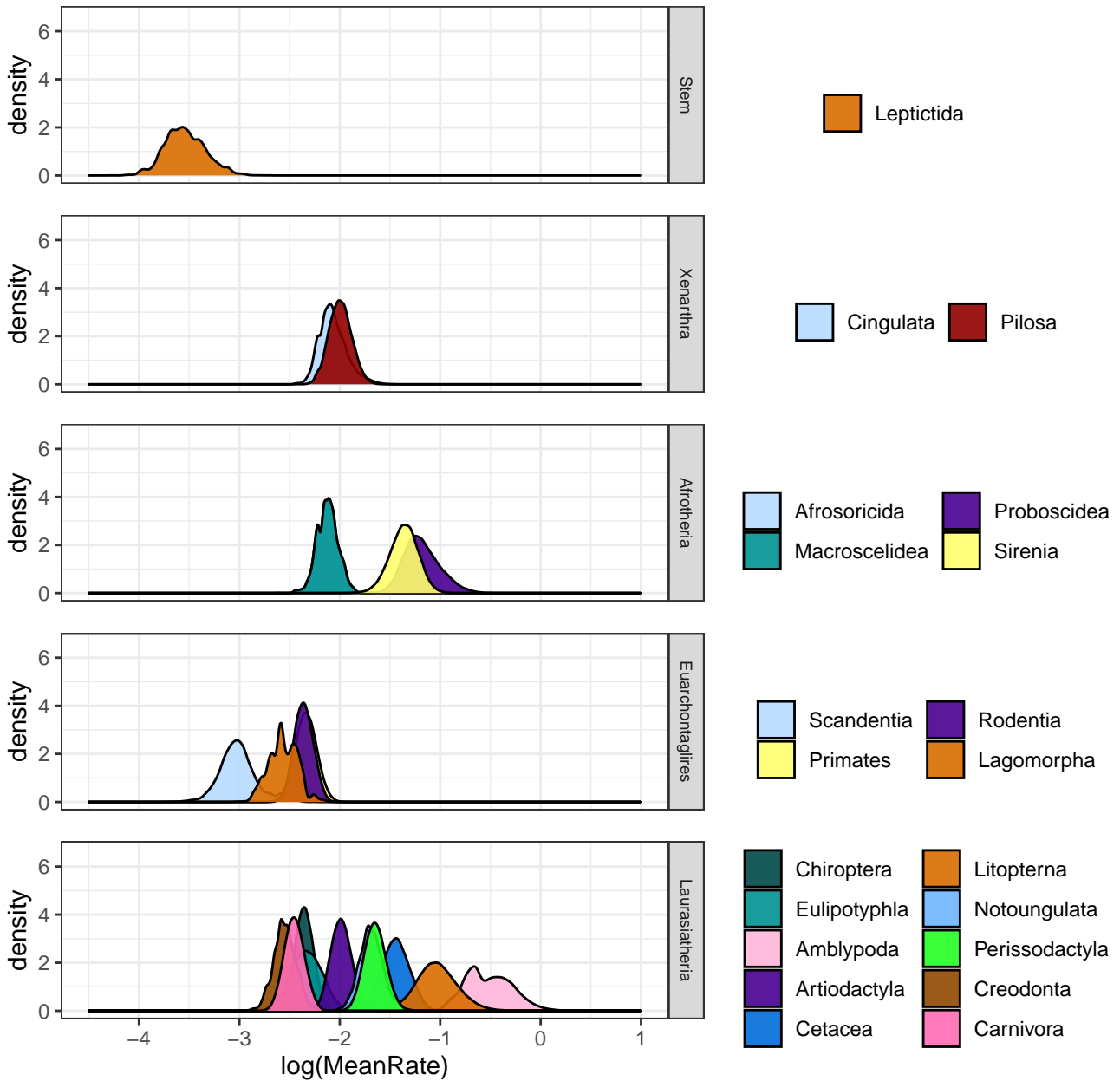


Fig. S5. M) Rates of evolution for terminal branches, subsetted into placental orders, for Tree Topology 3, Root Age = 70-75Ma.

Tree Topology 3: Root Age 75–80 Ma

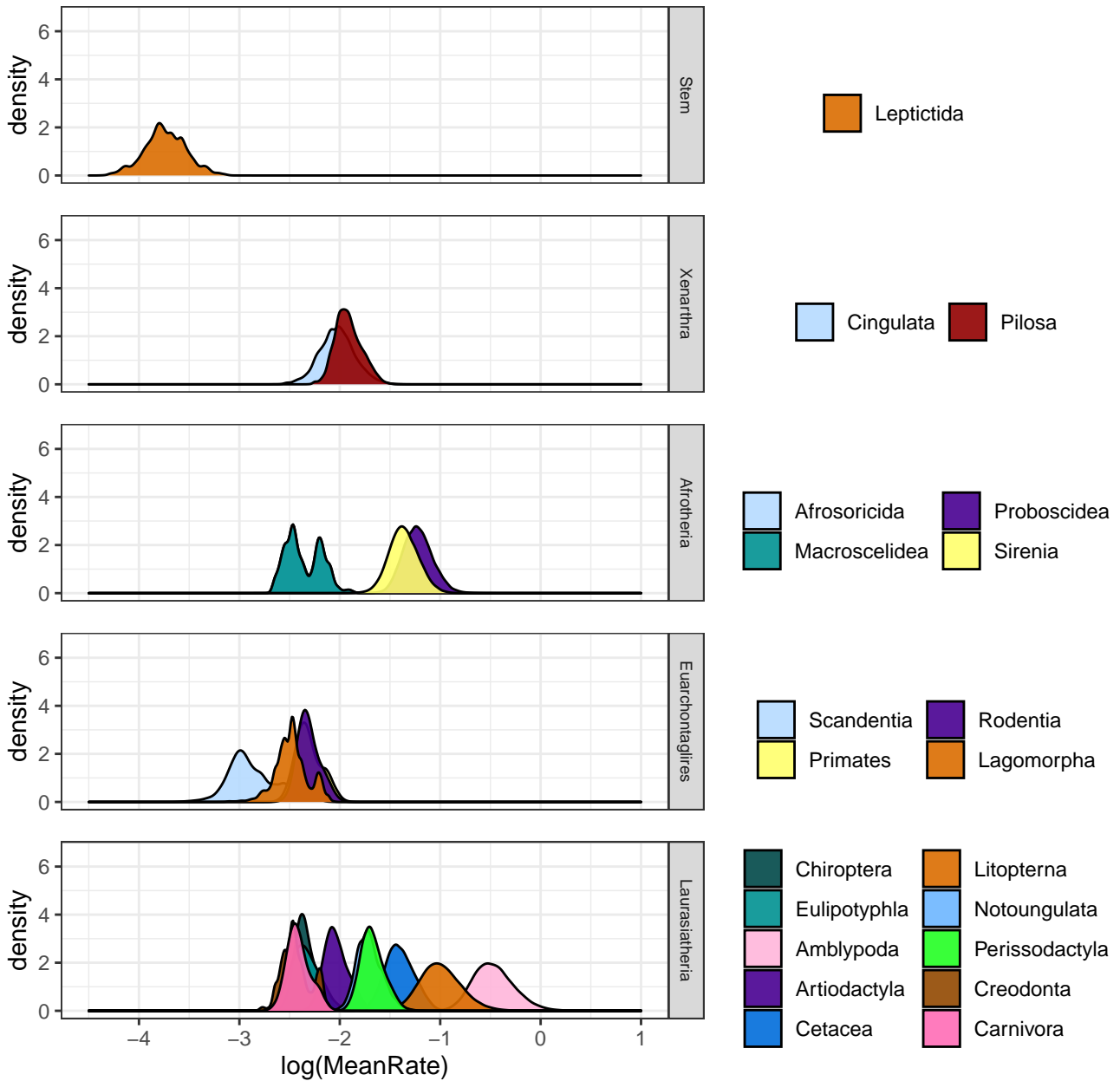


Fig. S5. N) Rates of evolution for terminal branches, subsetted into placental orders, for Tree Topology 3, Root Age = 75-80Ma.

Tree Topology 3: Root Age 80–85 Ma

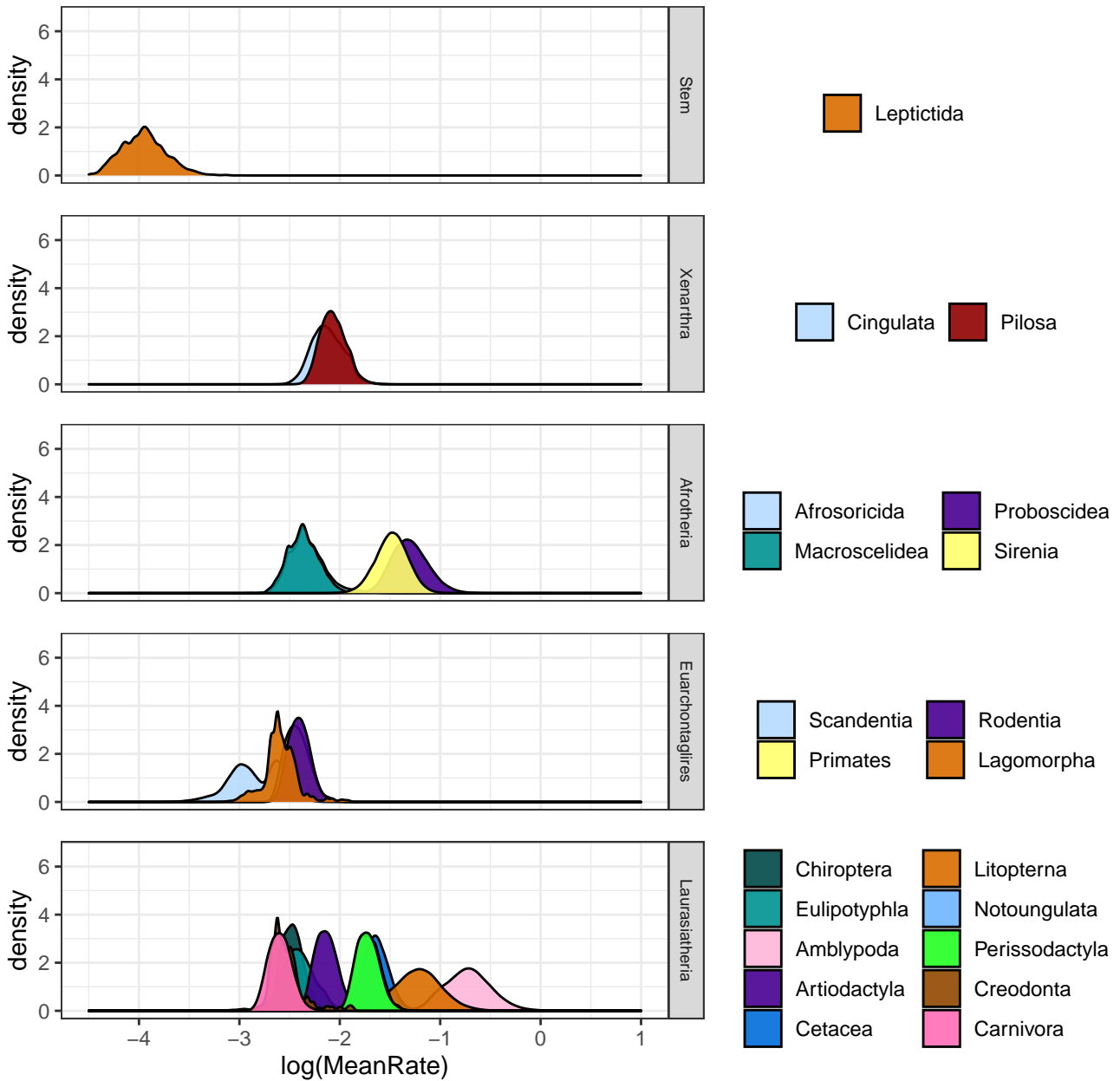


Fig. S5. O) Rates of evolution for terminal branches, subsetted into placental orders, for Tree Topology 3, Root Age = 80-85Ma.

Tree Topology 3: Root Age 85–90 Ma

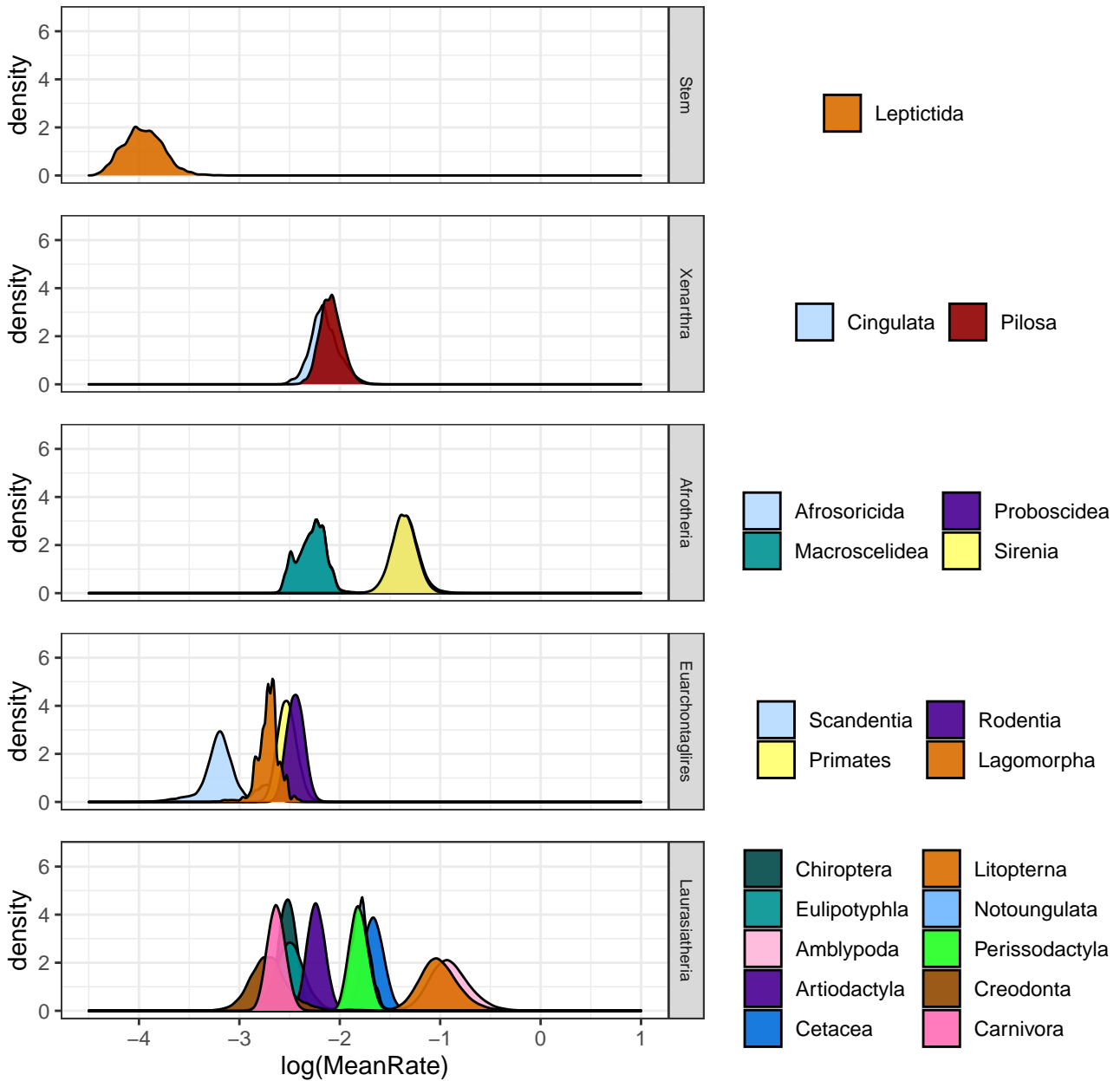


Fig. S5. P) Rates of evolution for terminal branches, subsetted into placental orders, for Tree Topology 3, Root Age = 85-90Ma.

Tree Topology 3: Root Age 90–95 Ma

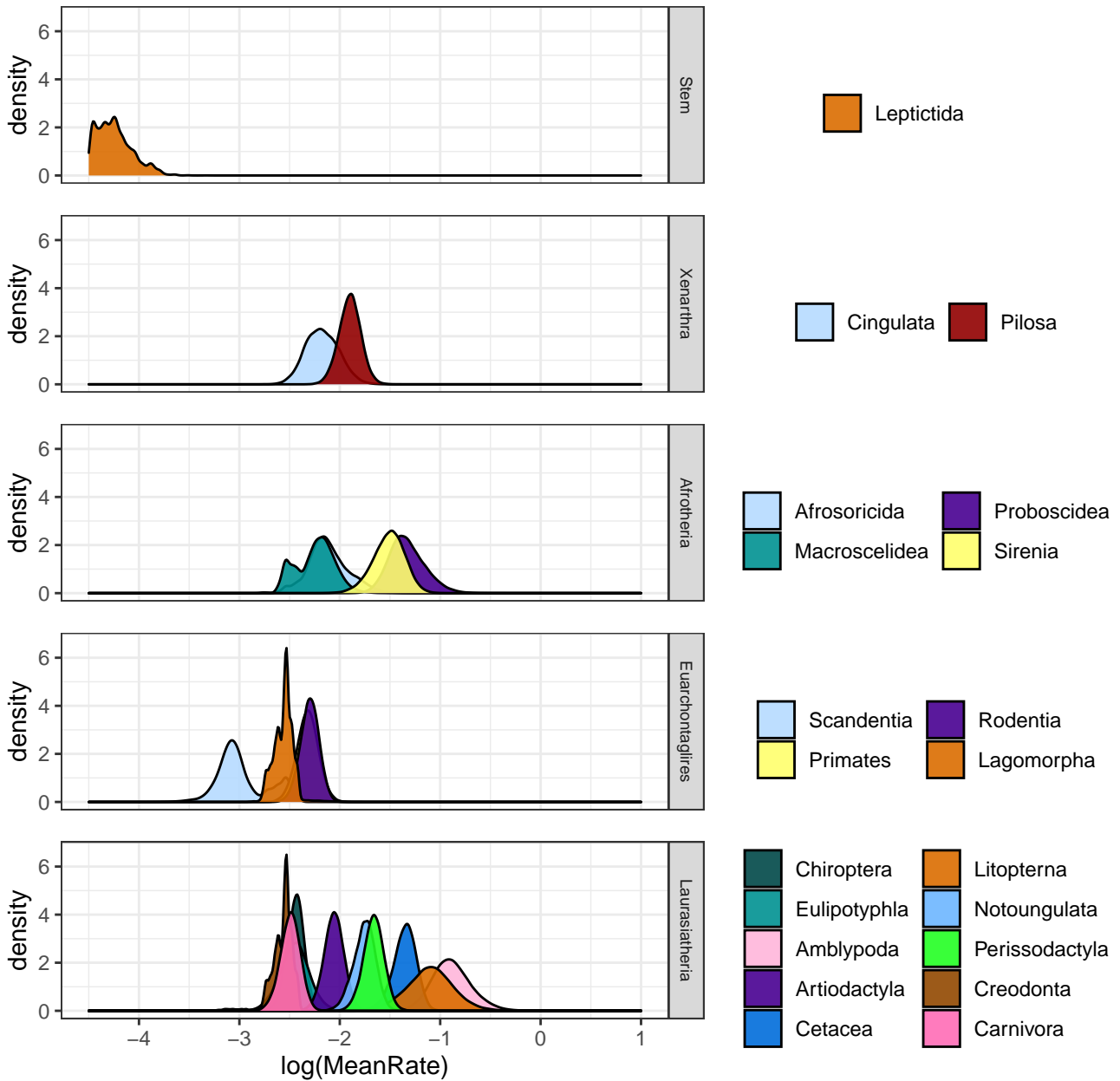


Fig. S5. Q) Rates of evolution for terminal branches, subsetted into placental orders, for Tree Topology 3, Root Age = 90-95Ma.

Tree Topology 3: Root Age 95–100 Ma

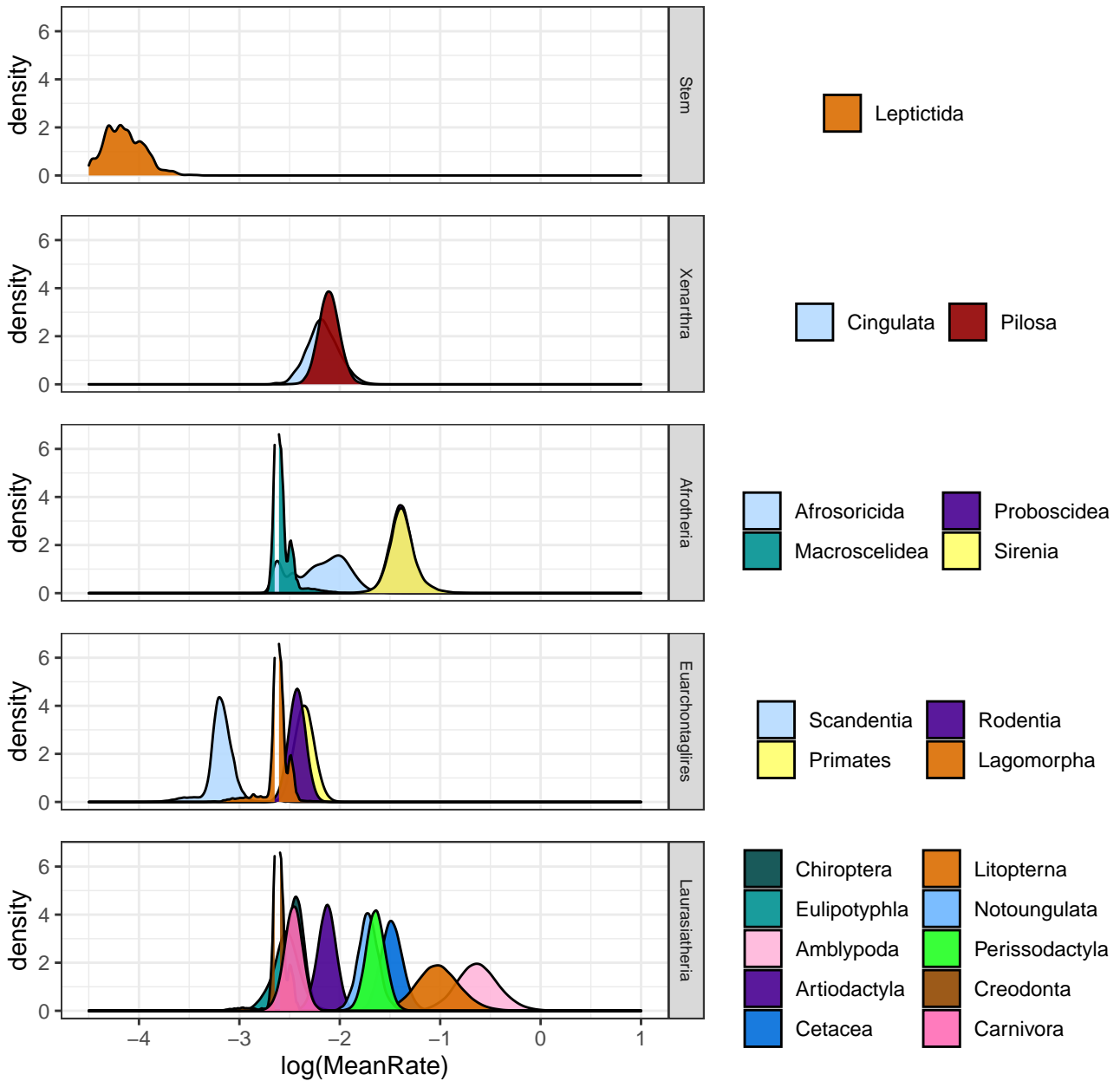


Fig. S5. R) Rates of evolution for terminal branches, subsetted into placental orders, for Tree Topology 3, Root Age = 95-100Ma.

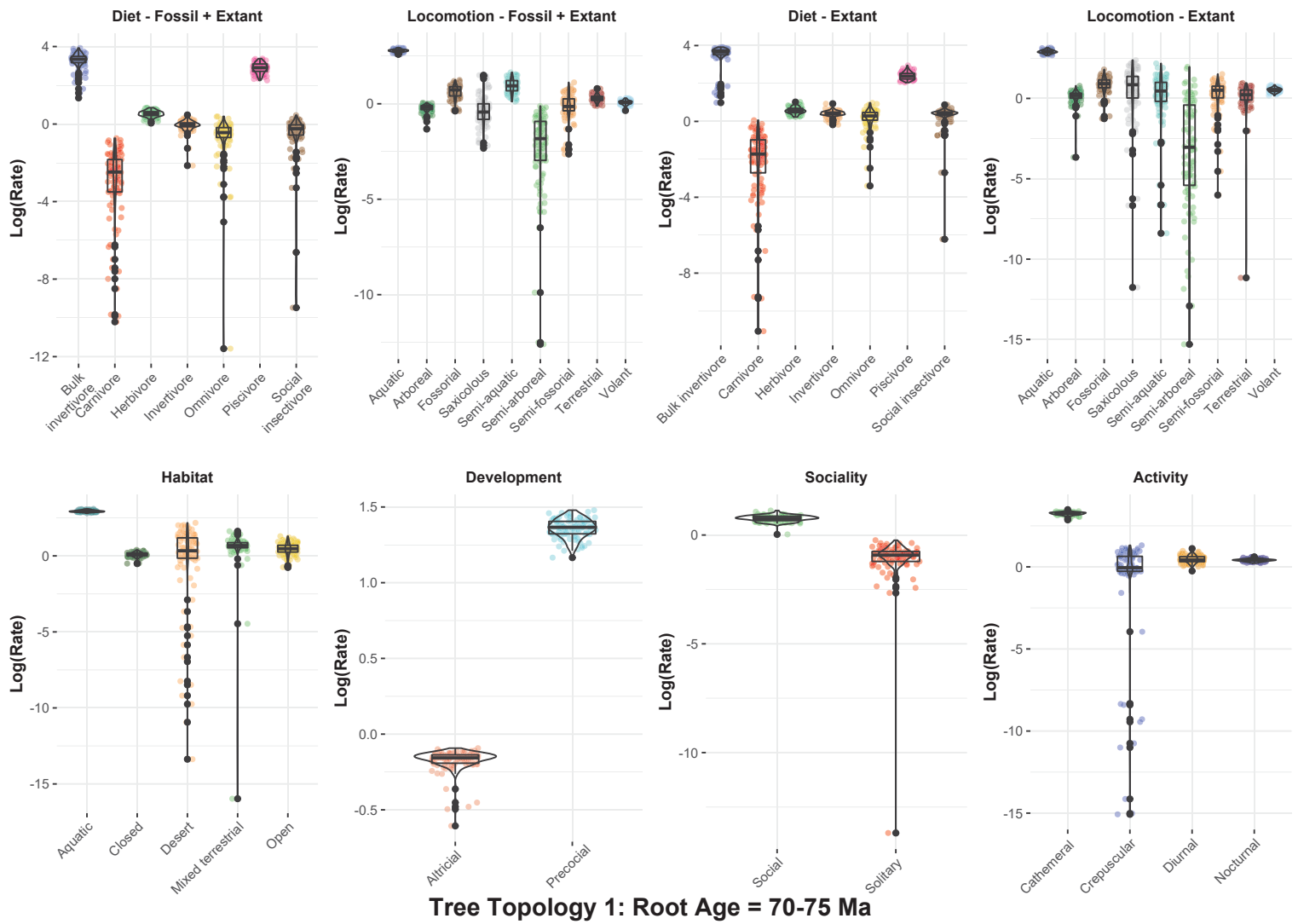


Fig. S7. A) Rates of evolution based on ecological and life history traits for placentals for Tree Topology 1, Root Age = 70-75Ma.

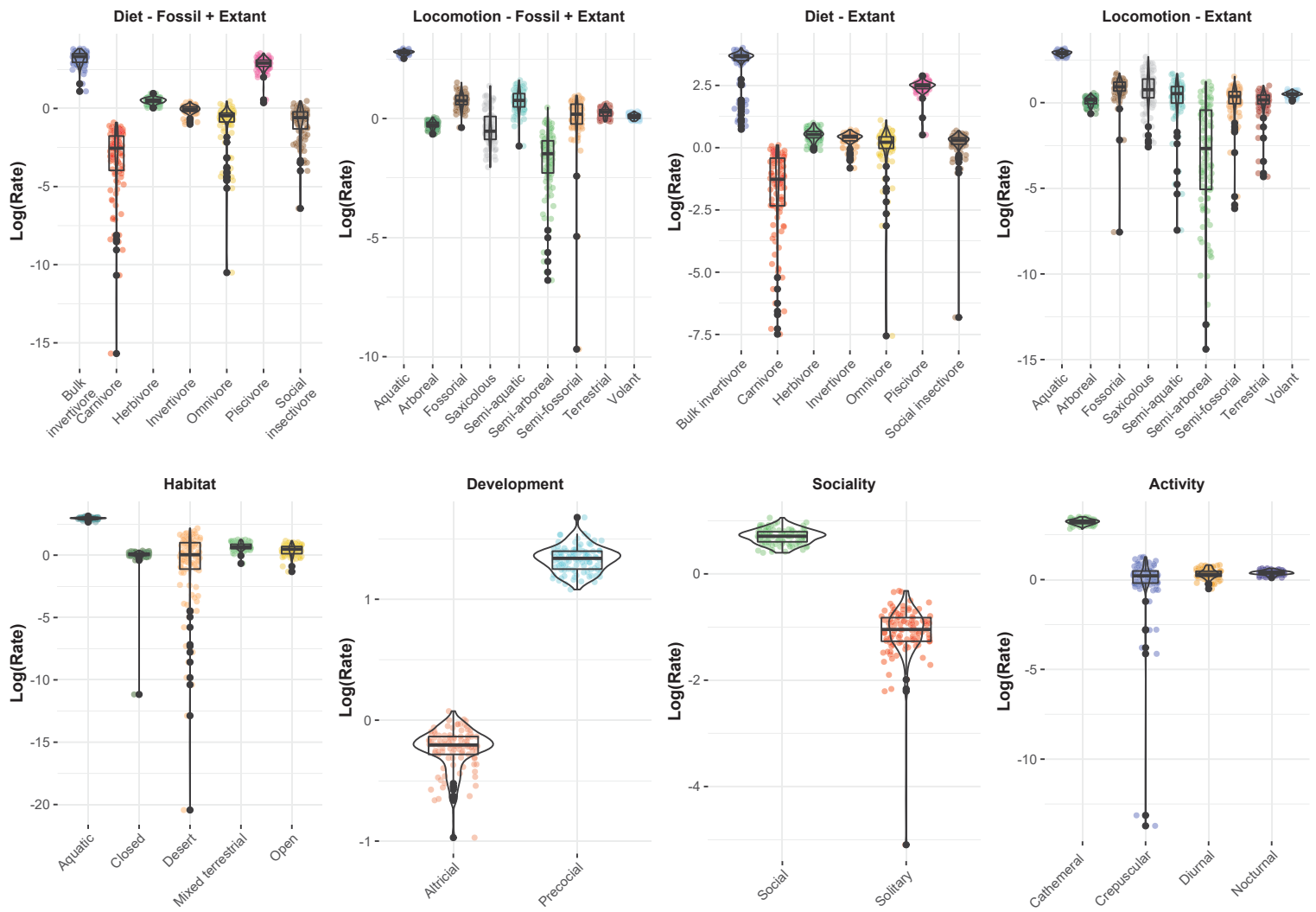


Fig. S7. B) Rates of evolution based on ecological and life history traits for placentals for Tree Topology 1, Root Age = 75-80Ma.

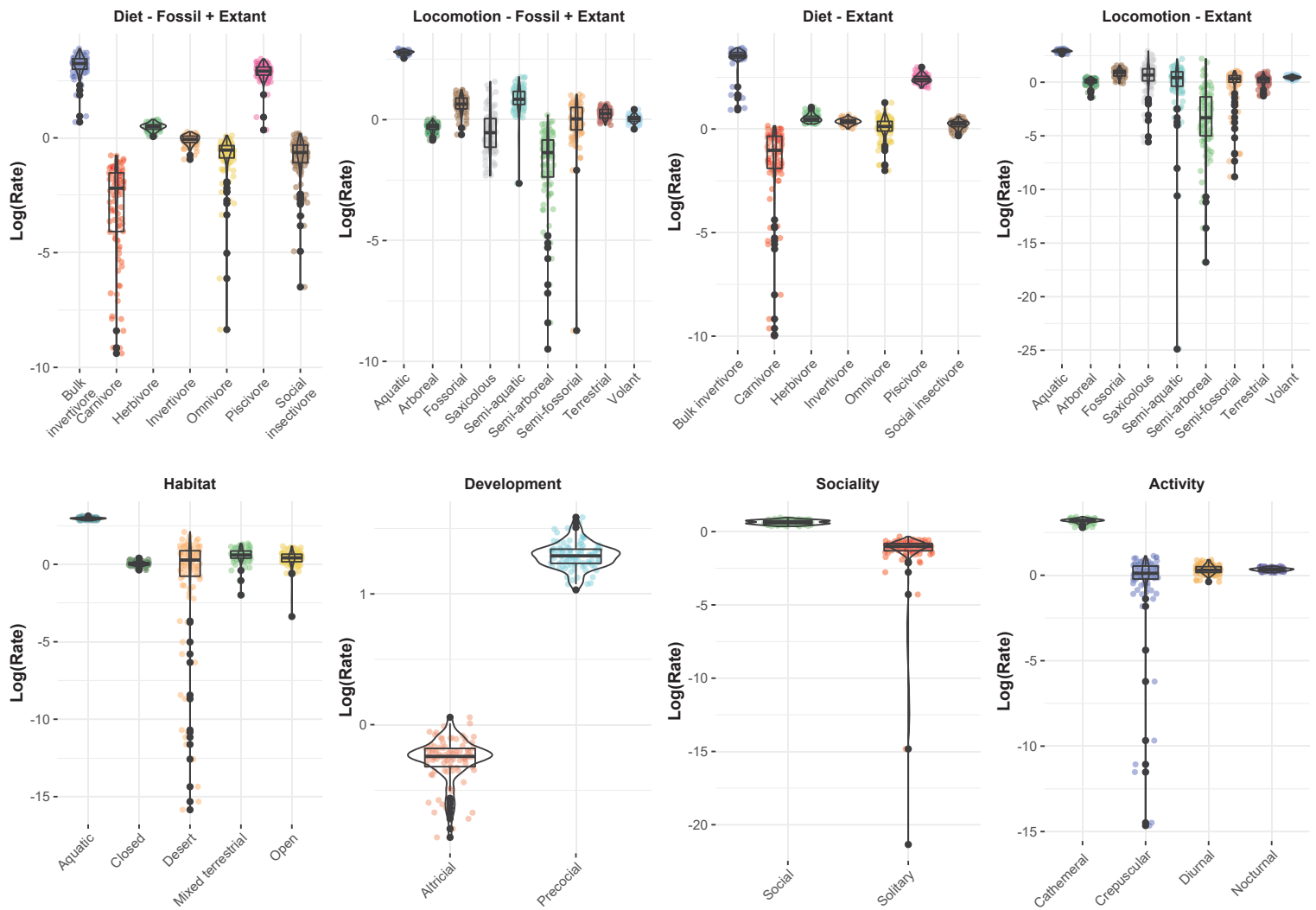


Fig. S7. C) Rates of evolution based on ecological and life history traits for placentals for Tree Topology 1, Root Age = 80-85Ma.

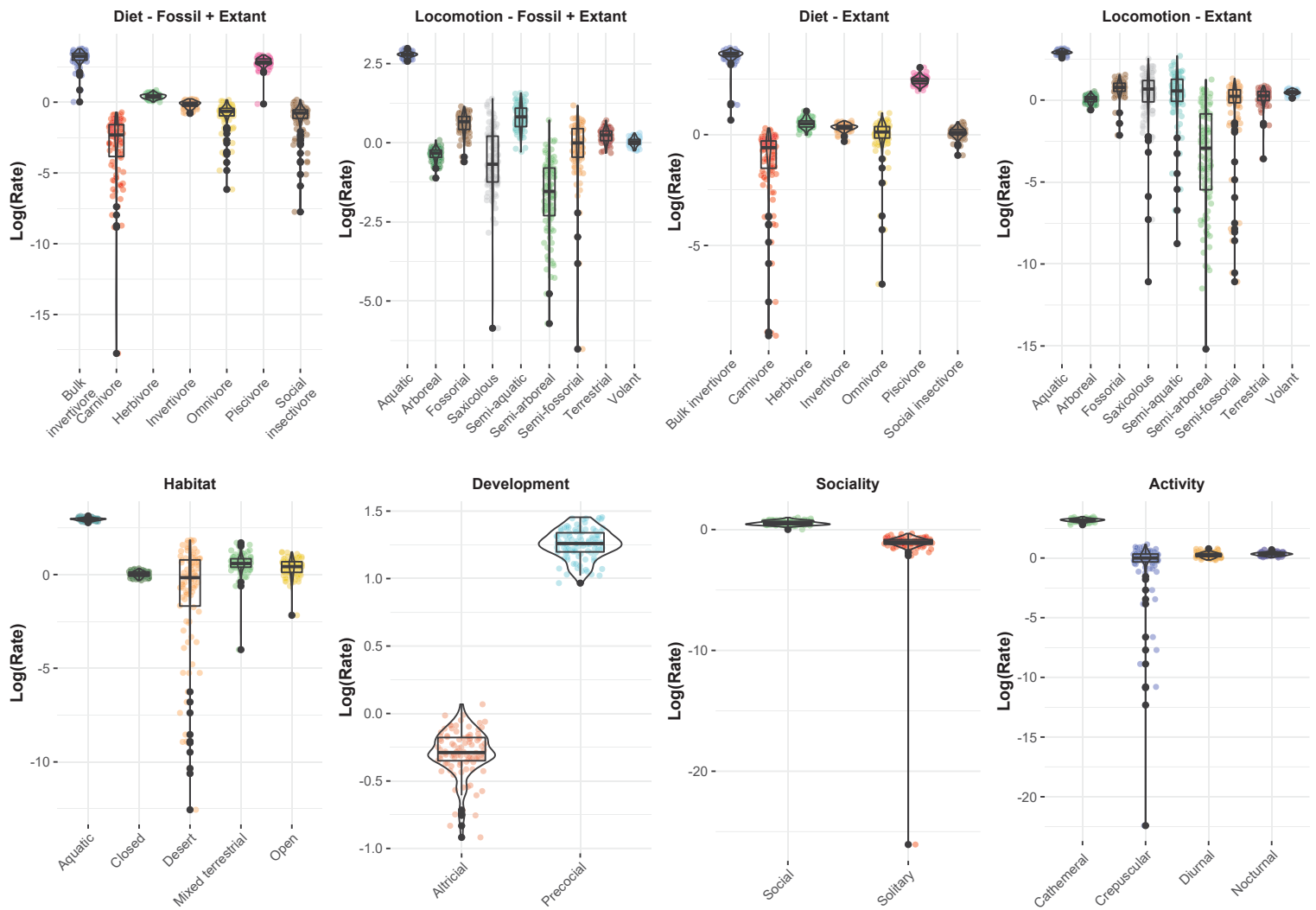


Fig. S7. D) Rates of evolution based on ecological and life history traits for placentals for Tree Topology 1, Root Age = 85-90Ma.

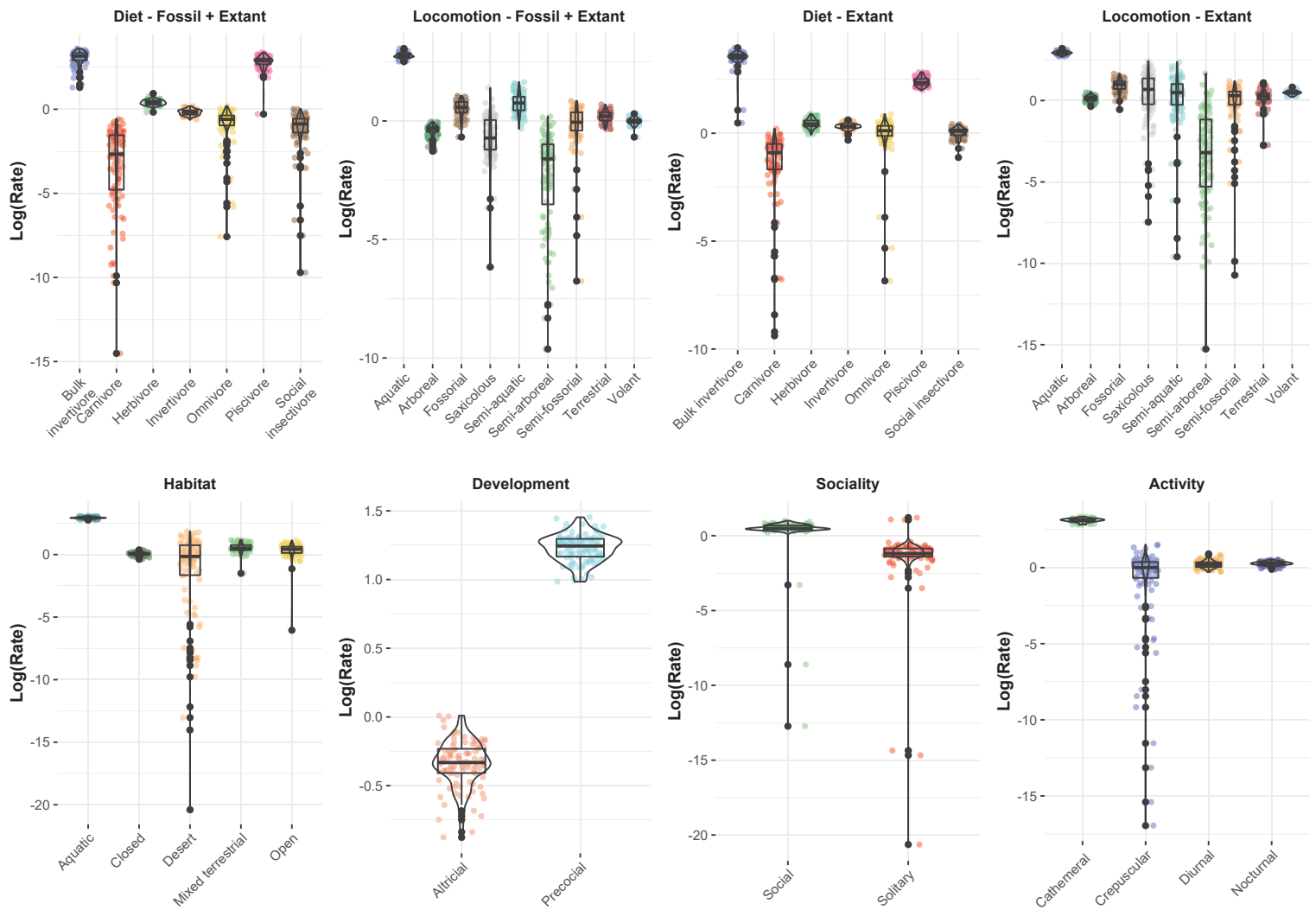


Fig. S7. E) Rates of evolution based on ecological and life history traits for placentals for Tree Topology 1, Root Age = 90-95Ma.

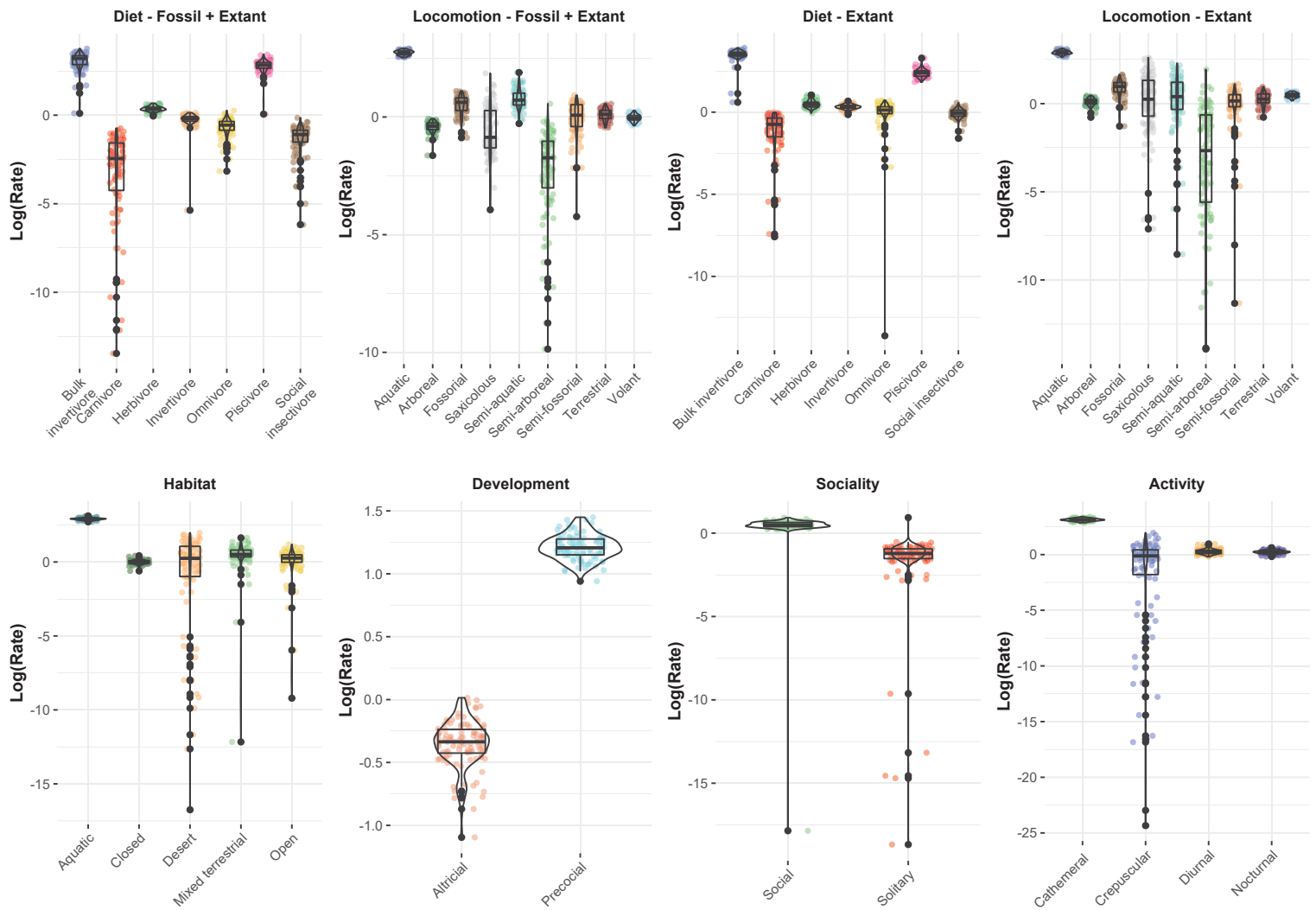


Fig. S7. F) Rates of evolution based on ecological and life history traits for placentals for Tree Topology 1, Root Age = 95-100Ma.

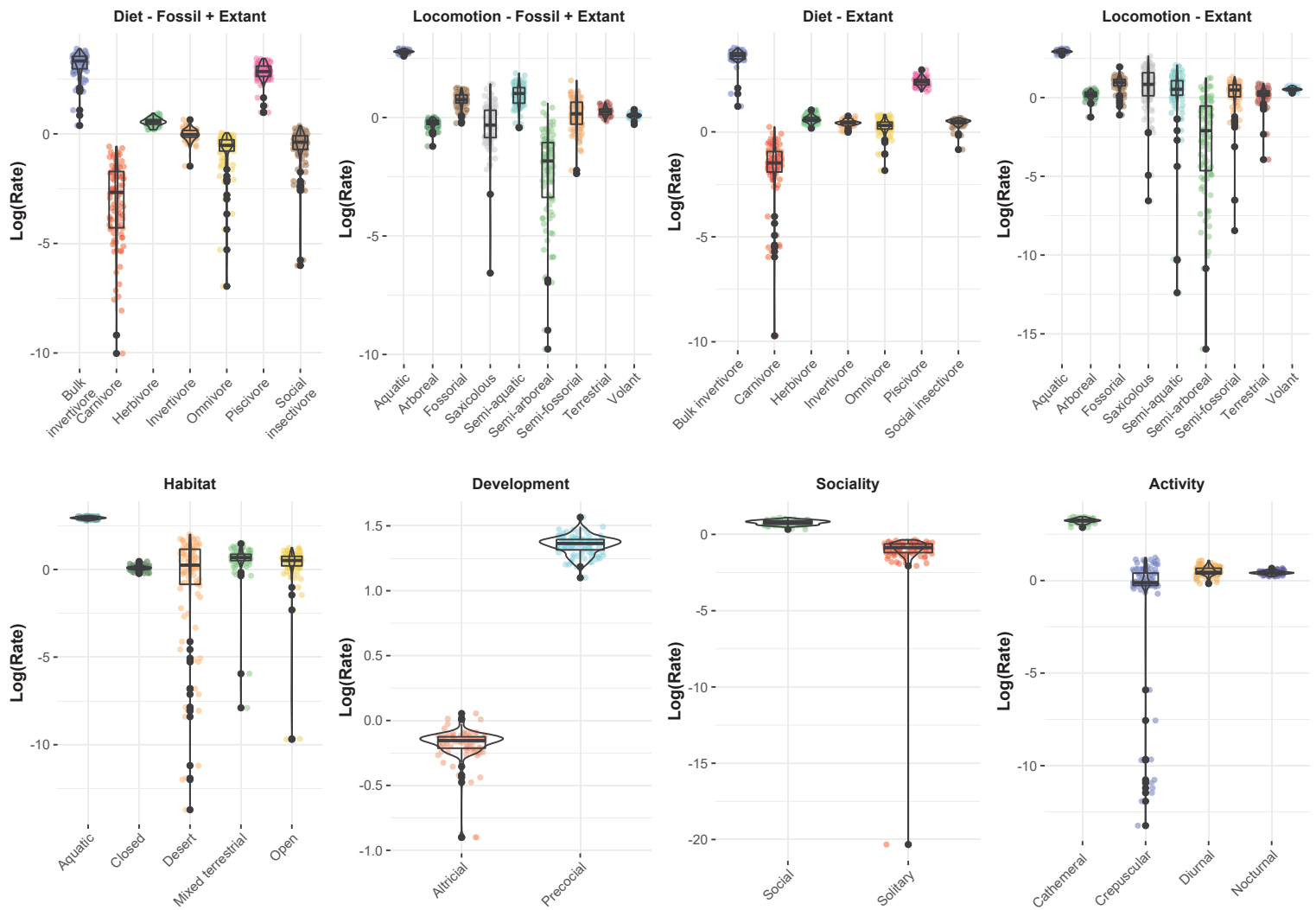


Fig. S7. G) Rates of evolution based on ecological and life history traits for placentals for Tree Topology 2, Root Age = 70-75Ma.

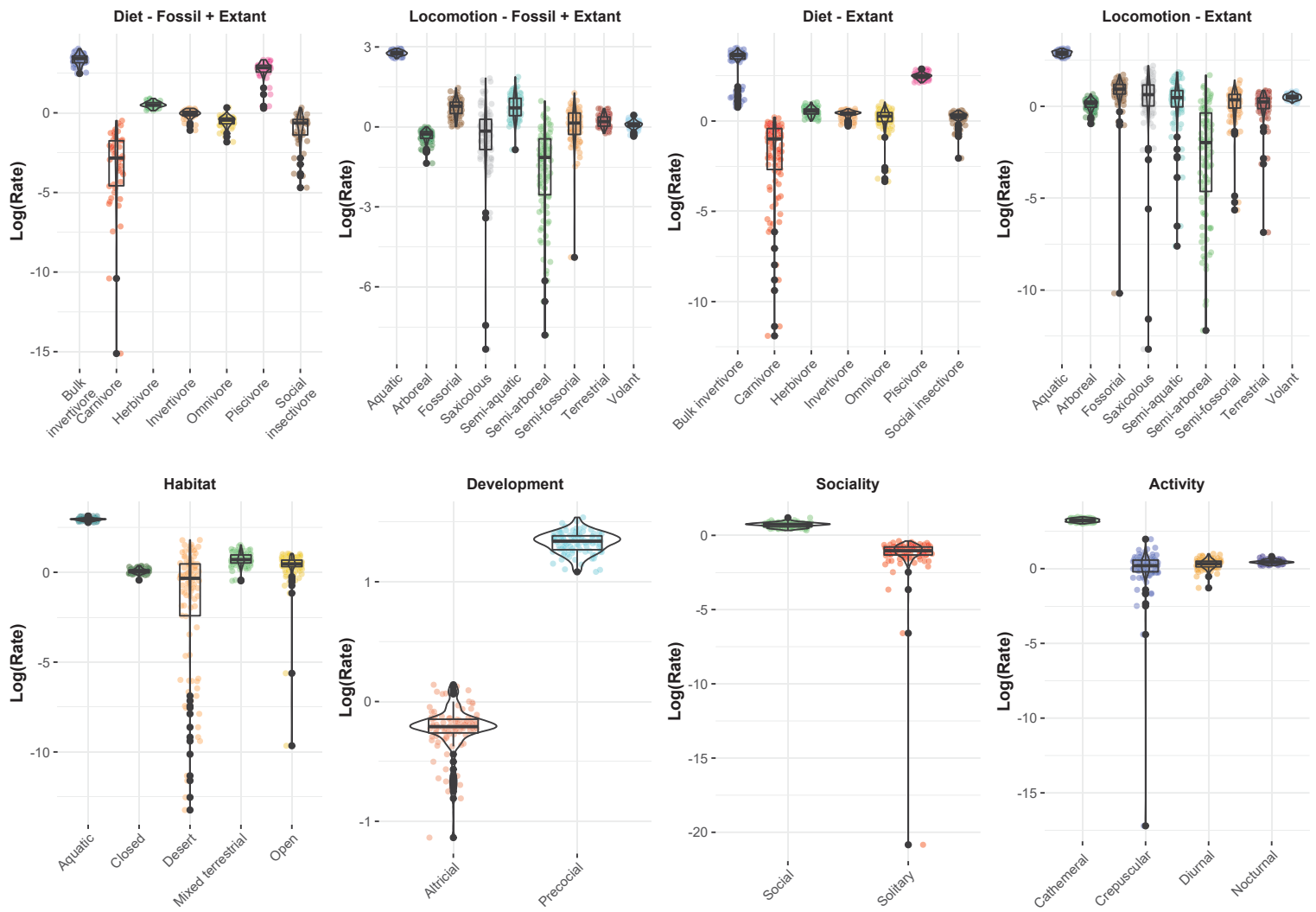


Fig. S7. H) Rates of evolution based on ecological and life history traits for placentals for Tree Topology 2, Root Age = 75-80Ma.

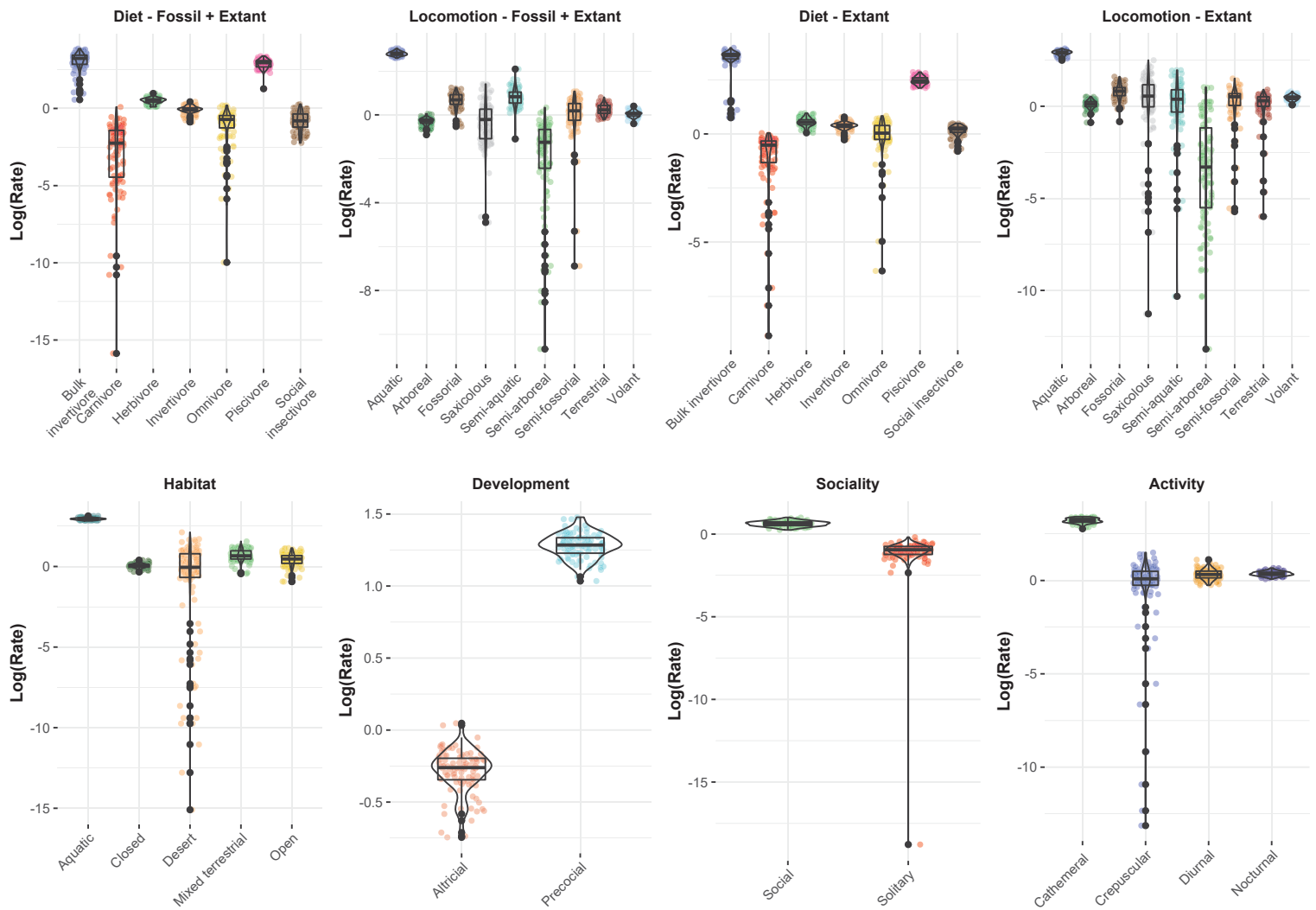


Fig. S7. I) Rates of evolution based on ecological and life history traits for placentals for Tree Topology 2, Root Age = 80-85Ma.

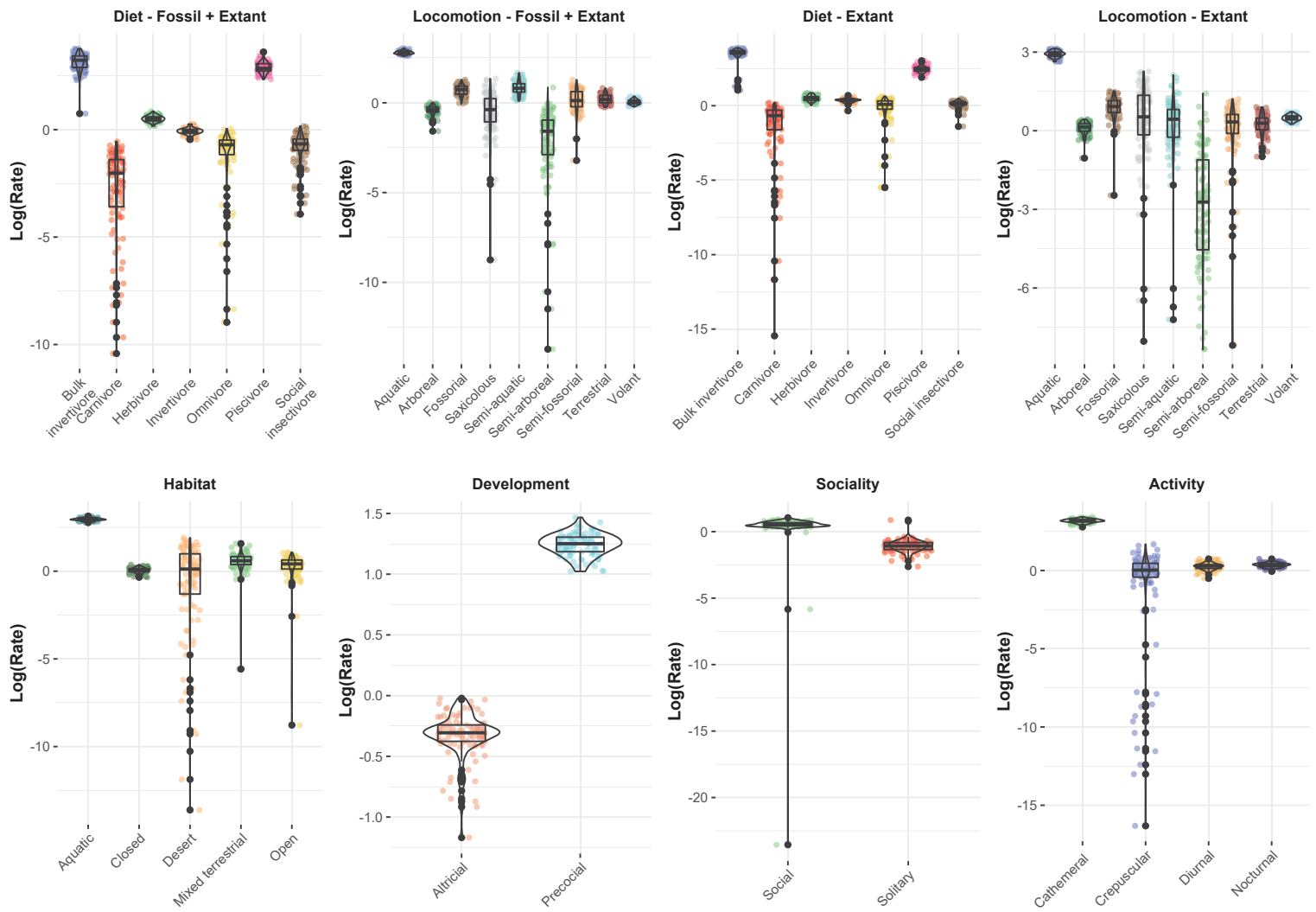


Fig. S7. J) Rates of evolution based on ecological and life history traits for placentals for Tree Topology 2, Root Age = 85-90Ma.

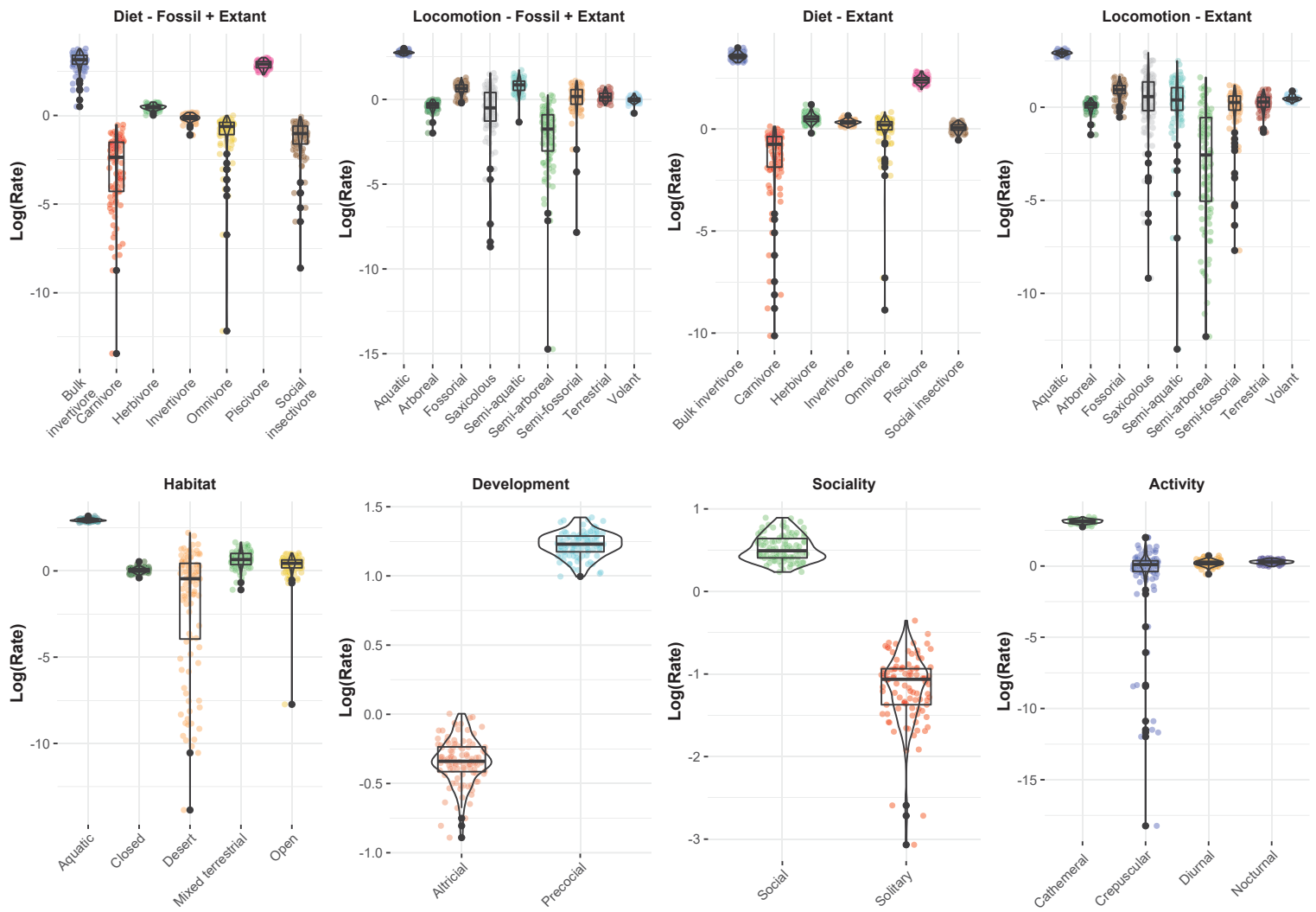


Fig. S7. K) Rates of evolution based on ecological and life history traits for placentals for Tree Topology 2, Root Age = 90-95Ma.

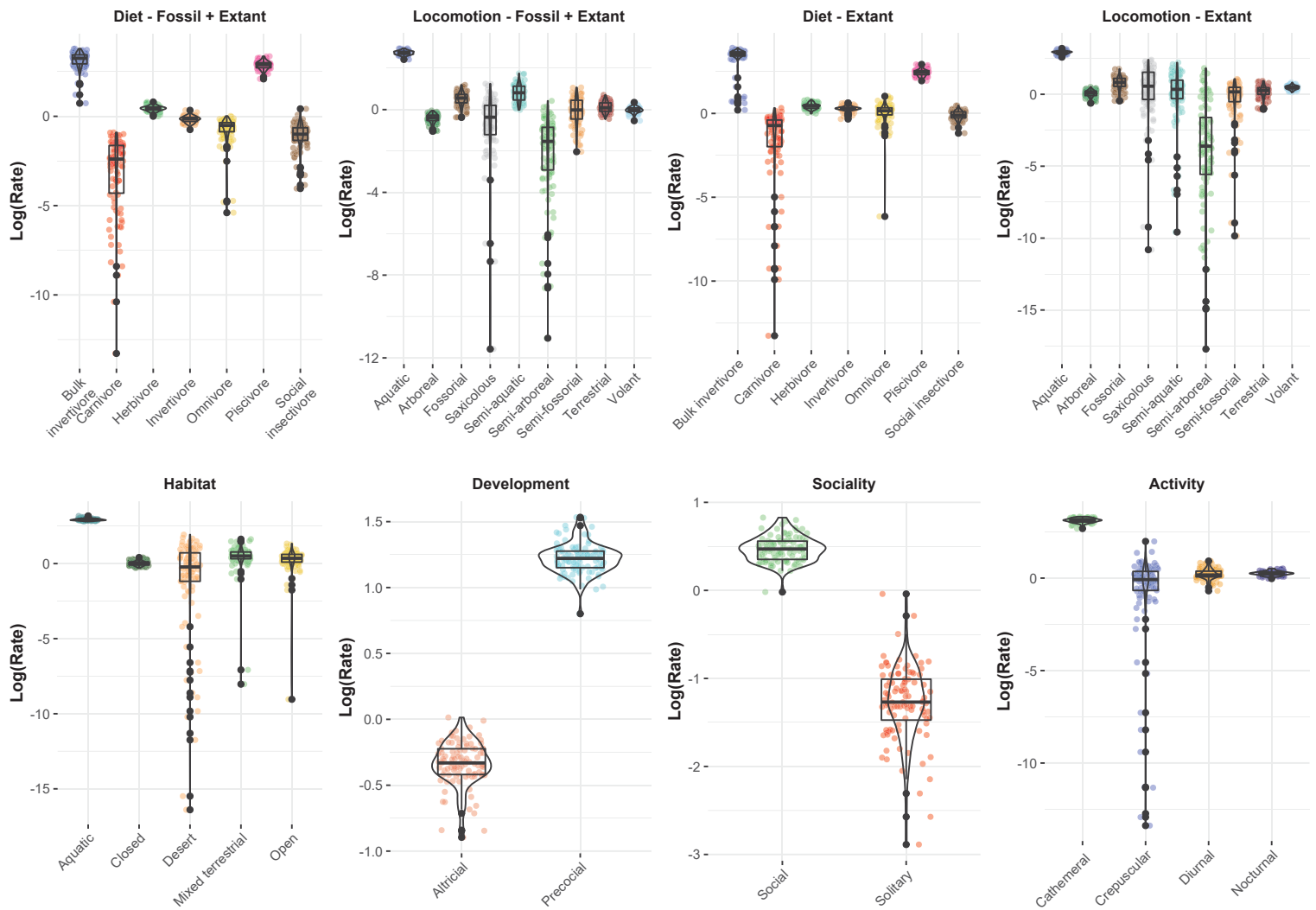


Fig. S7. L) Rates of evolution based on ecological and life history traits for placentals for Tree Topology 2, Root Age = 95-100Ma.

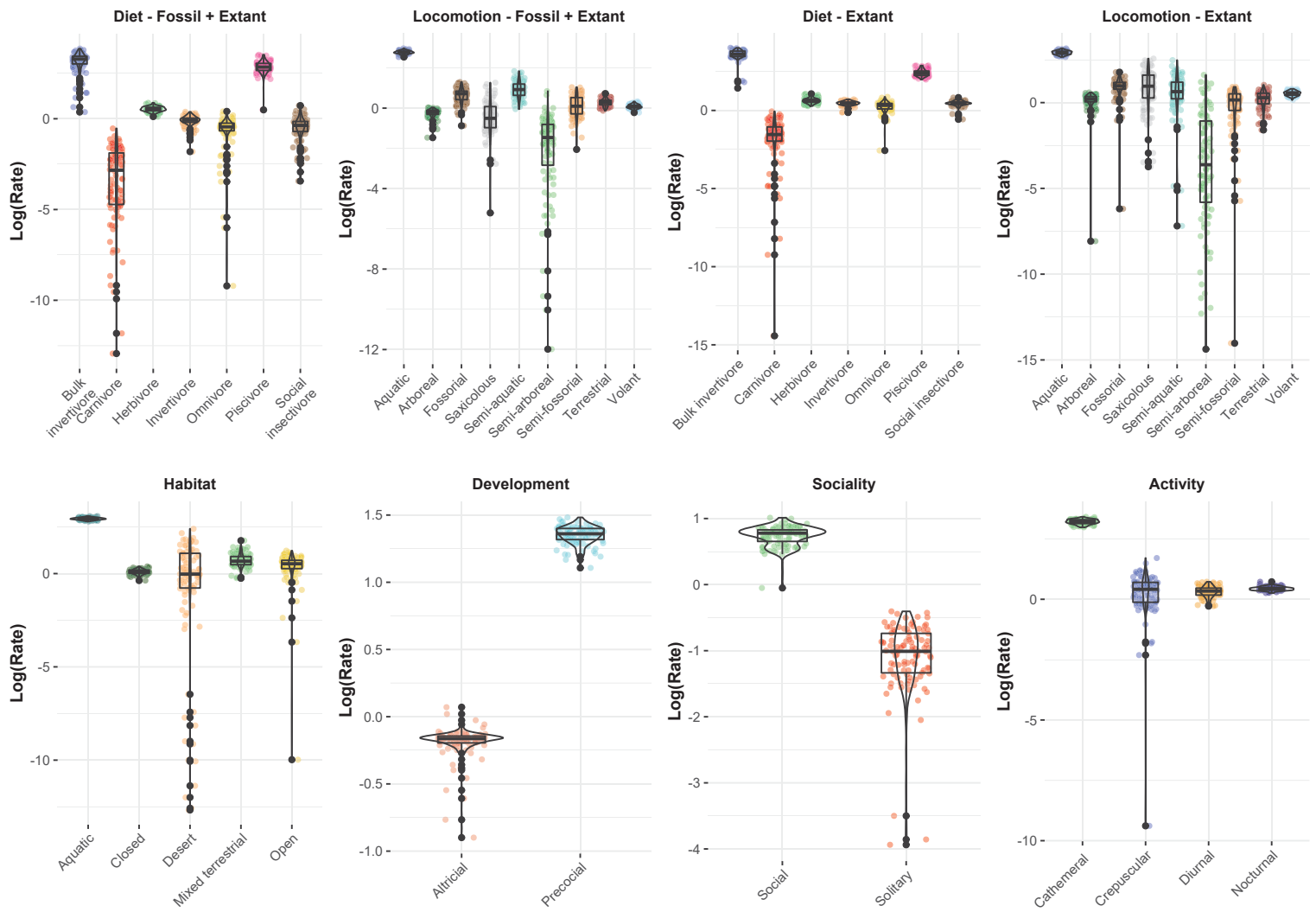


Fig. S7. M) Rates of evolution based on ecological and life history traits for placentals for Tree Topology 3, Root Age = 70-75Ma.

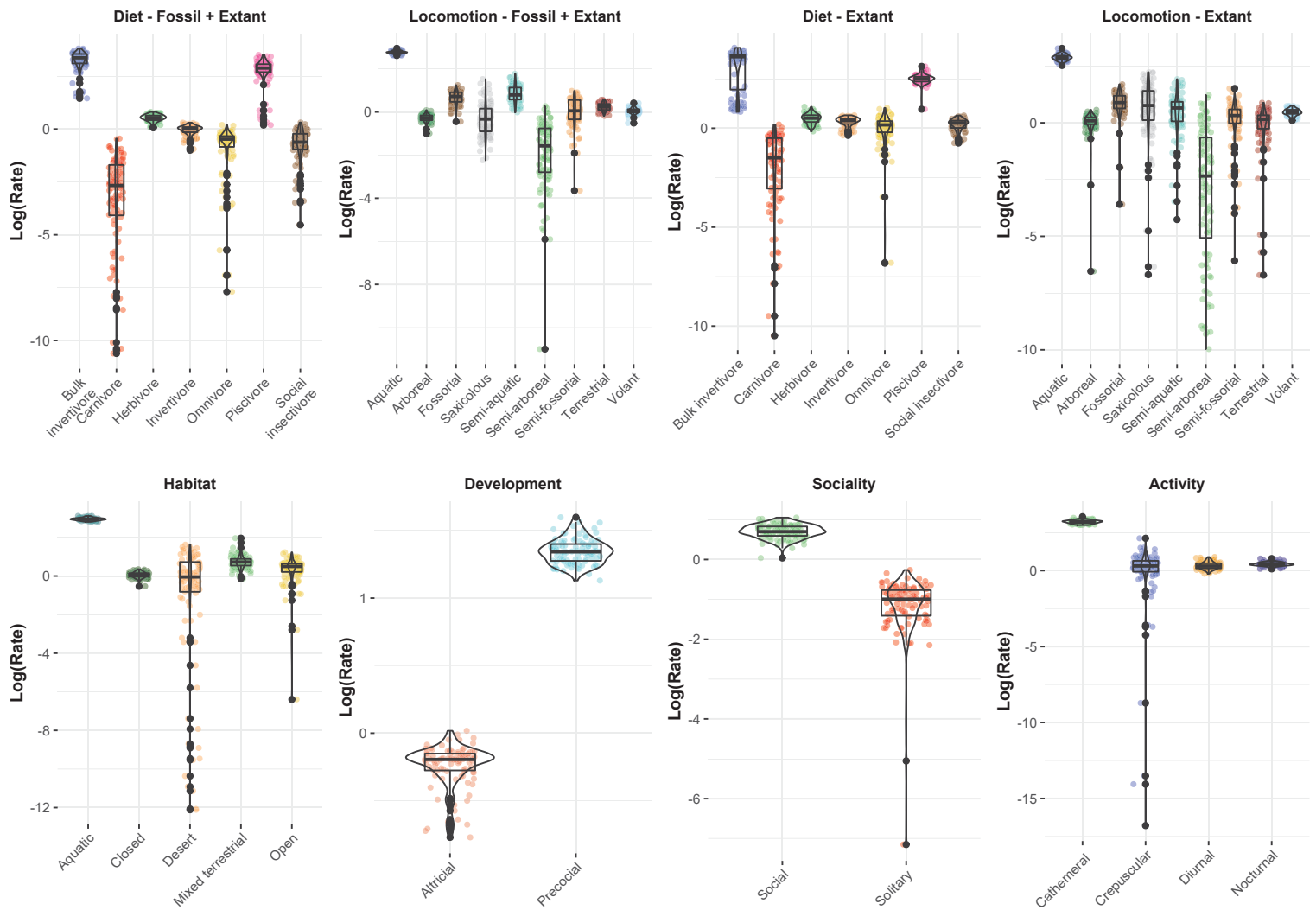


Fig. S7. N) Rates of evolution based on ecological and life history traits for placentals for Tree Topology 3, Root Age = 75-80Ma.

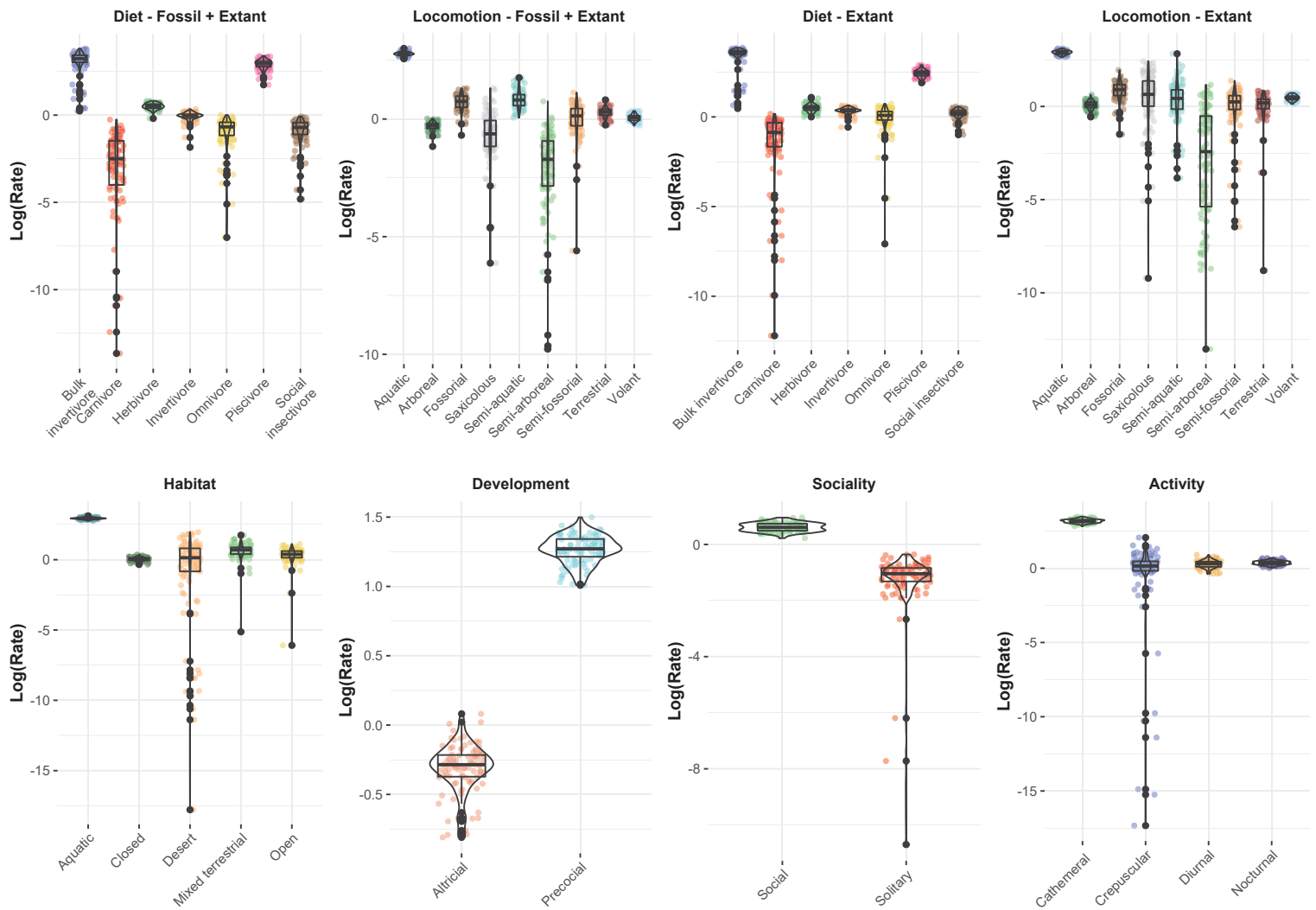


Fig. S7. O) Rates of evolution based on ecological and life history traits for placentals for Tree Topology 3, Root Age = 80-85Ma.

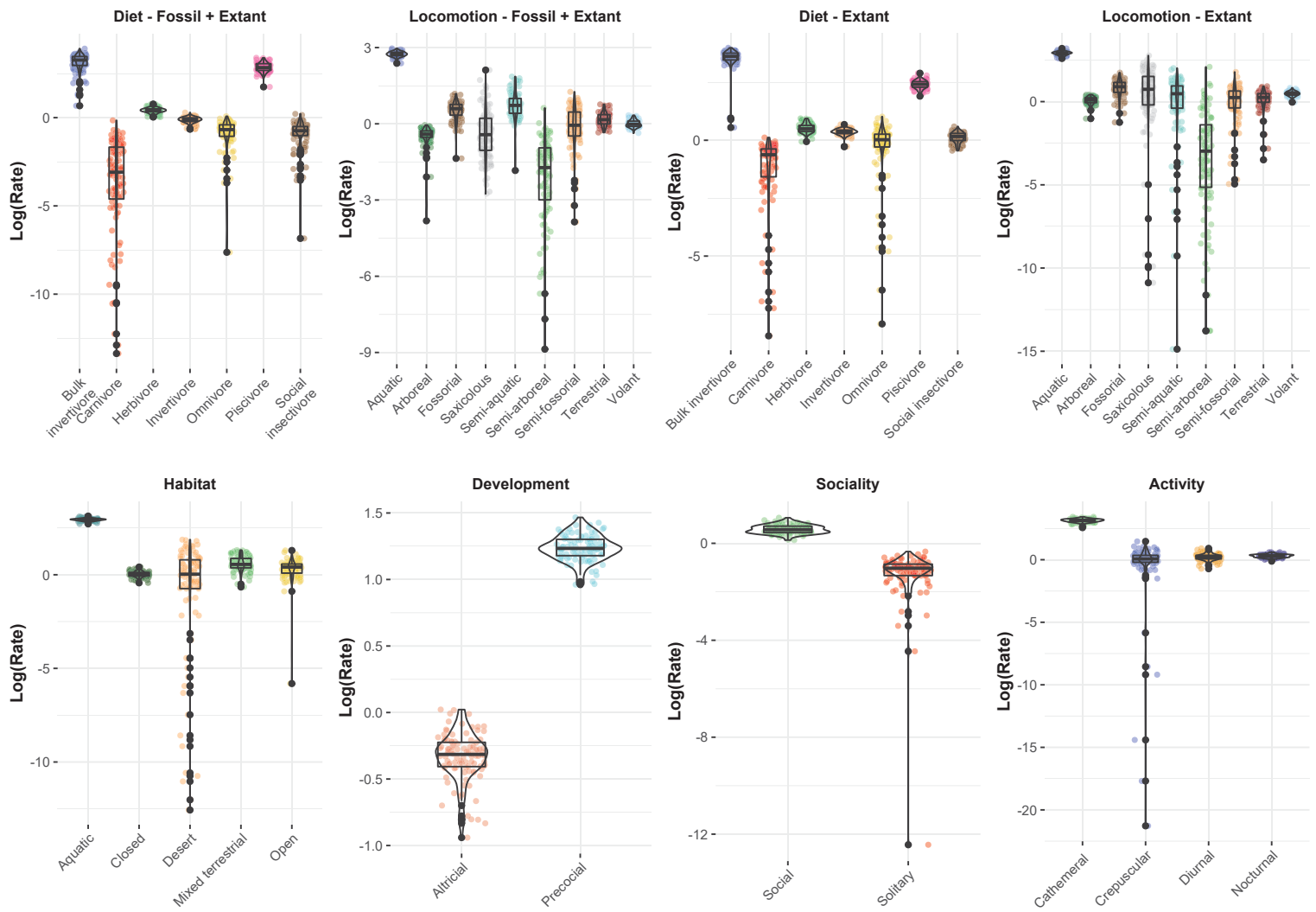


Fig. S7. P) Rates of evolution based on ecological and life history traits for placentals for Tree Topology 3, Root Age = 85-90Ma.

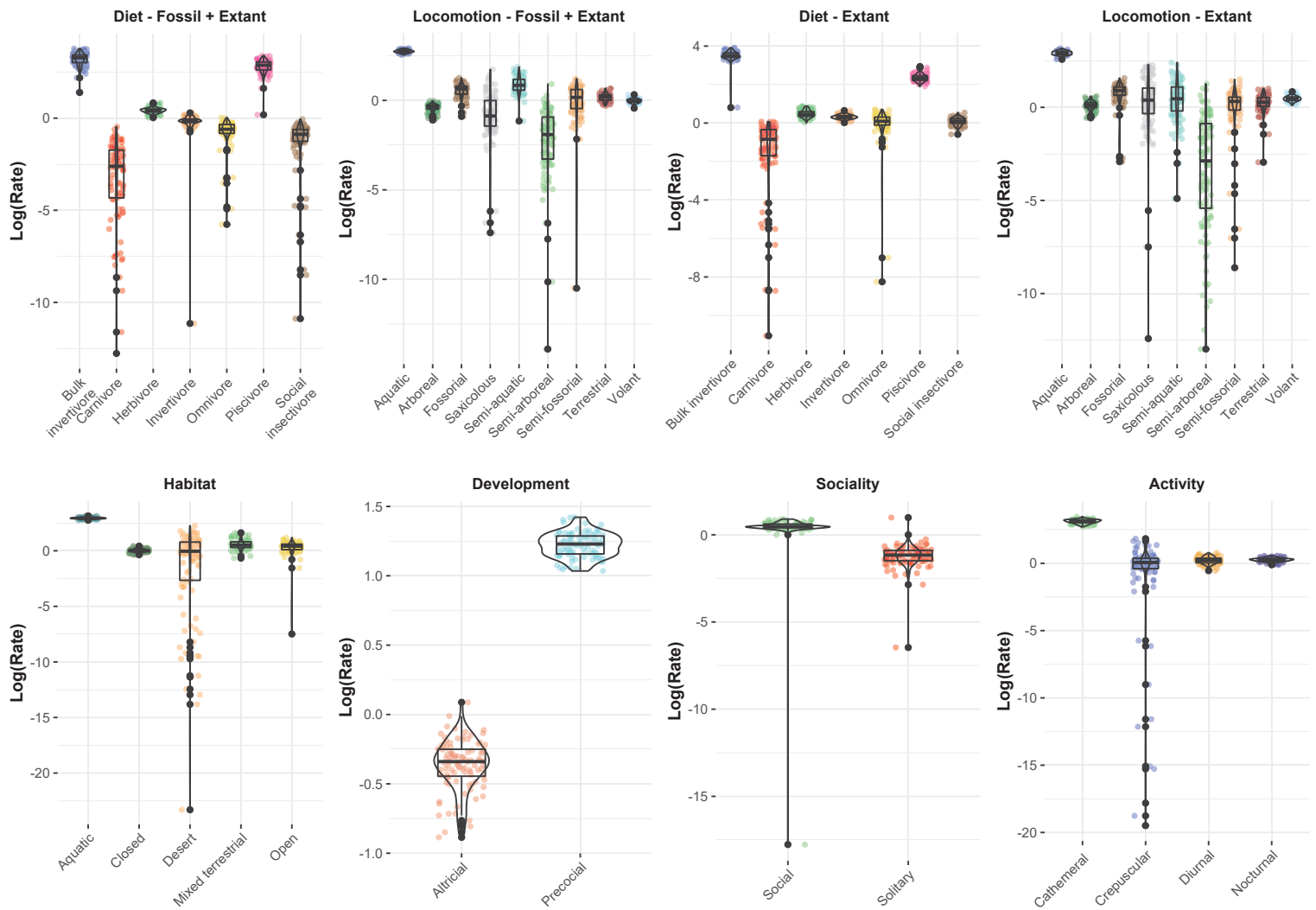


Fig. S7. Q) Rates of evolution based on ecological and life history traits for placentals for Tree Topology 3, Root Age = 90-95Ma.

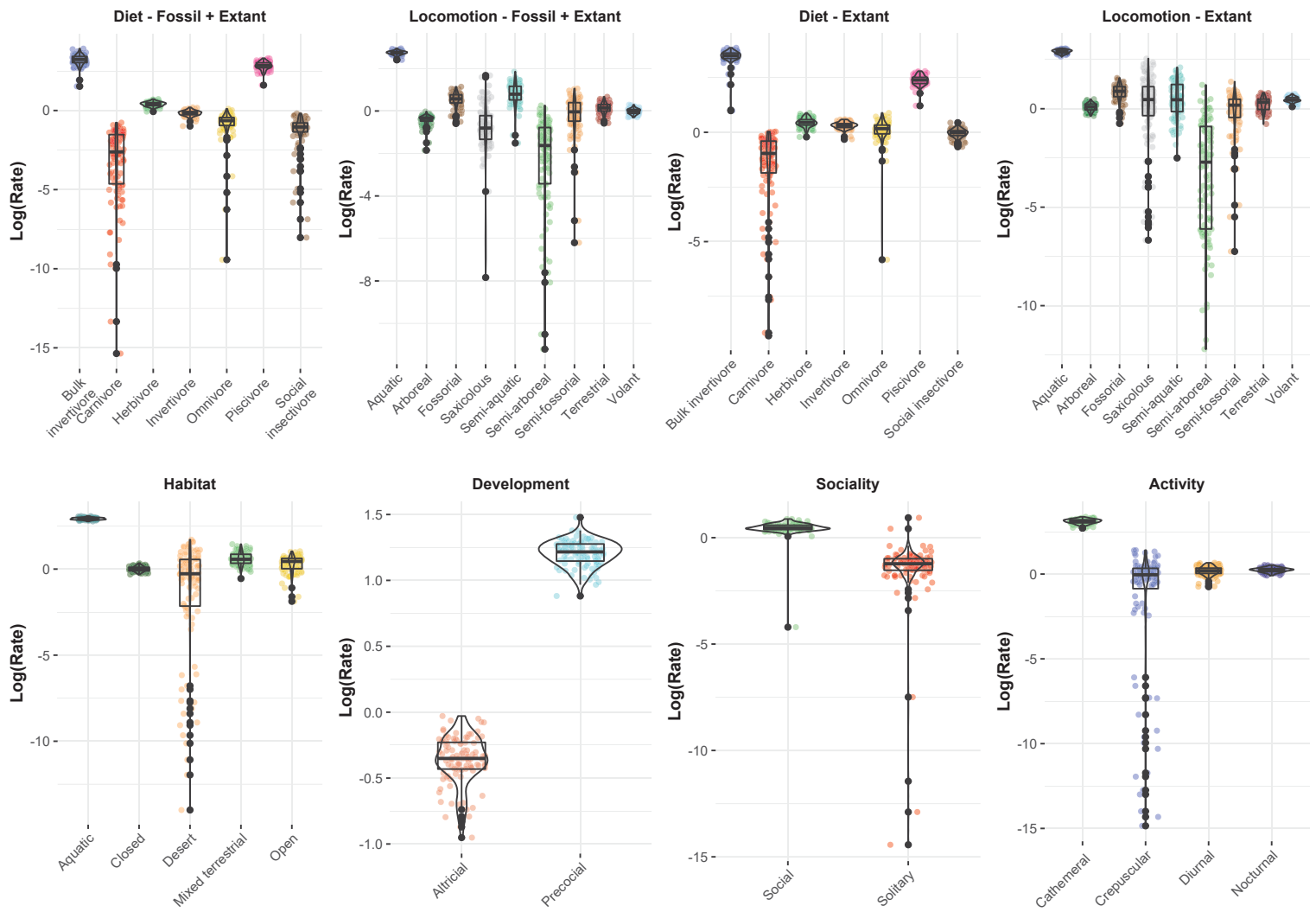


Fig. S7. R) Rates of evolution based on ecological and life history traits for placentals for Tree Topology 3, Root Age = 95-100Ma.

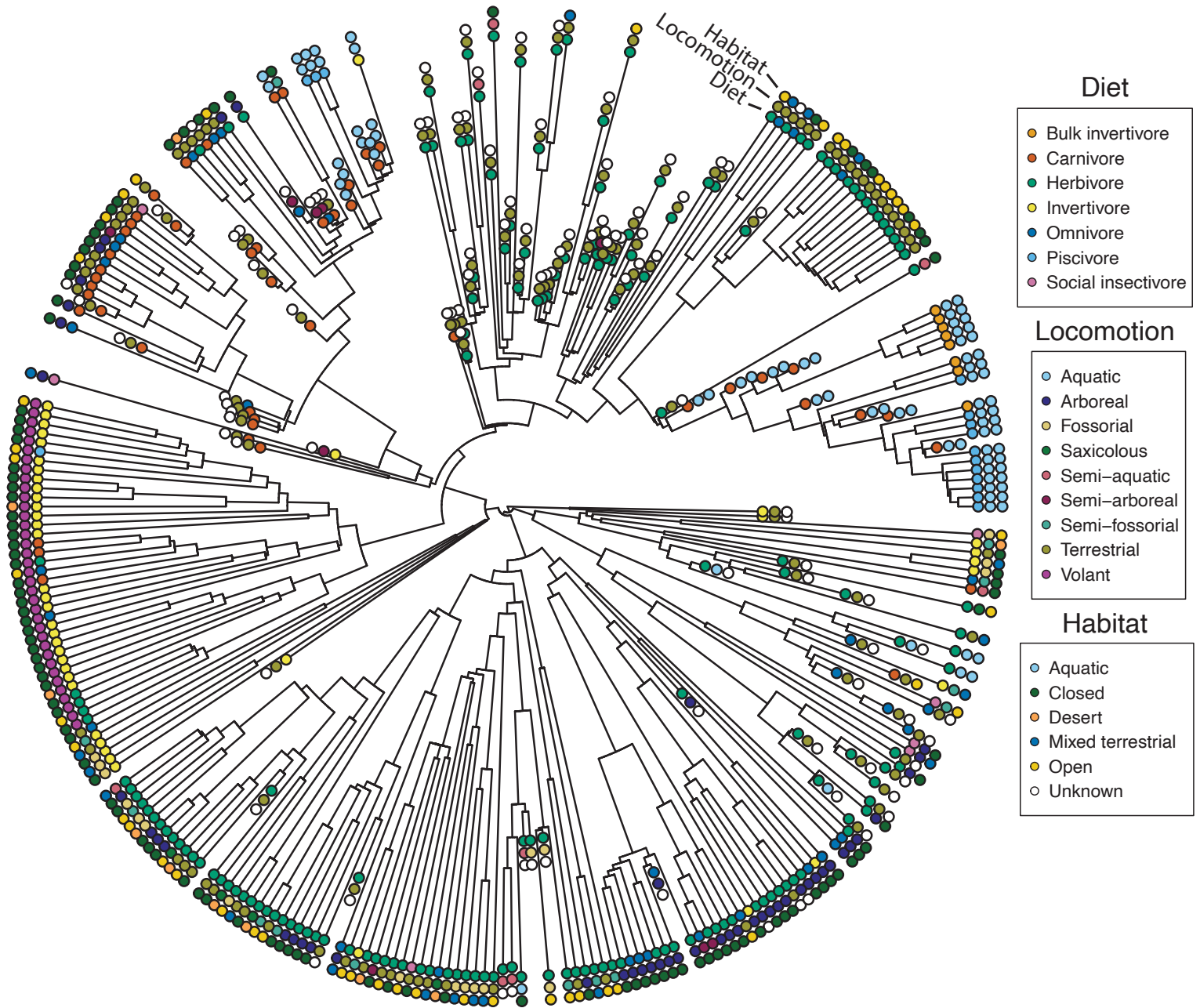


Fig. S8. A) Trait distributions for ecological traits, shown on Tree Topology 2, Root Age 80-85 Ma. Habitat traits are unknown for extinct taxa. Details of traits and references are provided in Table S1. Tree topology with species names is provided in Figure S4.

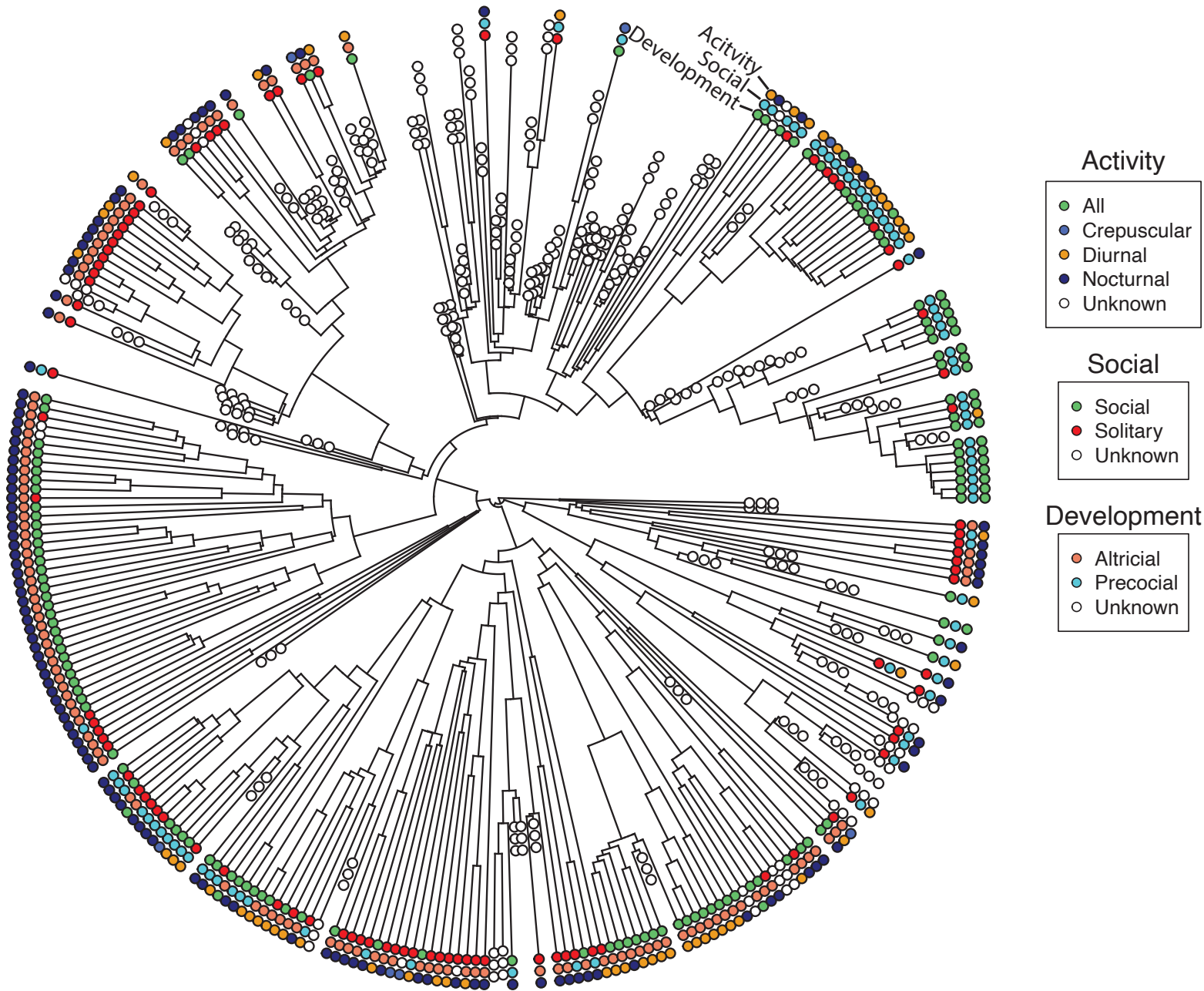


Fig. S8. B) Trait distributions for life history traits, shown on Tree Topology 2, Root Age 80-85 Ma. Traits are unknown for extinct taxa. Details of traits and references are provided in Table S1. Tree topology with species names is provided in Figure S4.

Table S1. Details of landmarks and curve sliding semi-landmarks.

Landmarks	Description	Element colour in Figure 1
1	Nasal: anteromedial	Turquoise
2	Nasal: anterolateral suture with premaxilla	
3	Nasal: posterolateral suture with frontal	
4	Nasal: posteromedial suture with frontal	
5	Premaxilla: anteromedial tip of rostrum,	Orange
6	Premaxilla: anterodorsal suture with nasal	
7	Premaxilla: posterodorsal suture with nasal and maxilla	
8	Premaxilla: posterolateral suture with maxilla, along tooth row	Dark orange
9	Maxilla: anterolateral suture with premaxilla, along tooth row	
10	Maxilla: anterodorsal suture with nasal and premaxilla	
11	Maxilla: posterodorsal/medial suture with nasal and frontal	
12	Maxilla/Lacrimal: posterodorsal junction with frontal along the orbit	
13	Maxilla: suture with jugal along the orbit	
14	Maxilla: ventral suture with jugal along the	
15	Maxilla: posterior end of tooth row	Green
16	Jugal: suture with maxilla along the orbit	
17	Jugal: ventral suture with maxilla along the zygomatic arch	
18	Jugal: posteroventral suture with squamosal	Pink
19	Frontal: anteromedial suture with nasal	
20	Frontal: posteromedial suture with parietal	
21	Frontal: posterolateral suture with parietal	
22	Frontal: postorbital process/bar tip	
23	Frontal: anterolateral suture with maxilla on orbit	
24	Frontal: anterodorsal suture with nasal and	Light green
25	Parietal: anteromedial suture with frontal	
26	Parietal: posteromedial suture with supraoccipital	
27	Parietal: posterolateral suture with squamosal and occipital	
28	Parietal: anterolateral suture with squamosal	
29	Parietal: anterolateral suture with frontal	Light blue
30	Squamosal: anterodorsal suture with parietal	
31	Squamosal: anteromedial junction of vault and zygomatic arch	
32	Squamosal: anterodorsal suture with jugal	
33	Squamosal: posteroventral/lateral suture with jugal	

34	Squamosal: anteromedial edge of glenoid	Yellow
35	Squamosal: posterolateral edge of glenoid	
36	Squamosal: posterolateral suture with occipital	Light blue
37	Squamosal: posterodorsal suture with parietal and occipital	
38	Posteromedial margin of skull roof	Pale yellow
39	Supraoccipital: anteromedial suture with parietal	
40	Occipital: opisthion	
41	Occipital condyle: dorsomedial	Red
42	Occipital condyle: dorsolateral	
43	Paraoccipital process	Pale yellow
44	Occipital: ventrolateral suture with squamosal	
45	Occipital: dorsolateral suture with squamosal and parietal	
46	Occipital condyle: ventrolateral	Red
47	Occipital condyle: ventromedial	
48	Basioccipital: basion	Purple
49	Basioccipital: anteromedial with basisphenoid	
50	Basioccipital: anterolateral with basisphenoid	
51	Basisphenoid: anteromedial with presphenoid	Dark grey
52	Basisphenoid: anterolateral with presphenoid	
53	Basisphenoid: posterolateral with basioccipital	
54	Basisphenoid: posteromedial suture with basioccipital	Blue
55	Palatine: posteromedial	
56	Palatine: anteromedial suture with maxilla	
57	Palatine: posteromedial suture with pterygoid	
58	Palatine: posteriolateral suture with maxilla	Hot pink
59	Pterygoid: posterior process	
60	Pterygoid: posterodorsal suture	Rose
61	Maxilla (ventral): posteromedial suture with palatine	
62	Maxilla (ventral): anteromedial suture with premaxilla	
63	Maxilla (ventral): anterolateral suture with premaxilla along tooth row	Light grey
64	Premaxilla (ventral): posteromedial suture with maxilla (or foramen)	
65	Premaxilla (ventral): anteromedial edge,	
66	Premaxilla (ventral): posterolateral suture with maxilla, along tooth row	

Curves	Description	From landmark	To landmark
1	Nasal: midline	1	4
2	Nasal: posterior	4	3
3	Nasal: lateral	3	2
4	Nasal: anterior	2	1
5	Premaxilla: anterior	5	6
6	Premaxilla: dorsal	6	7
7	Premaxilla: posterior	7	8
8	Premaxilla: lateral (ventral margin)	8	5
9	Maxilla: anterior	9	10
10	Maxilla: dorsal	10	11
11	Maxilla: posterodorsal to orbit	11	12
12	Maxilla: orbit	12	13
13	Maxilla: orbit to zygomatic	13	14
14	Maxilla: posteroventral	14	15
15	Maxilla: tooth row	15	9
16	Jugal: dorsal	16	18
17	Jugal: ventral	18	17
18	Jugal: anterior	17	16
19	Frontal: anteromedial	19	24
20	Frontal: anterolateral	24	23
21	Frontal: orbit	23	22
22	Frontal: postorbital process to vault along orbit	22	21
23	Frontal: posterior	21	20
24	Frontal: midline	20	19
25	Parietal: midline	25	26
26	Parietal: posterior	26	27
27	Parietal: lateral	27	28
28	Parietal: squamosal to frontal (where separated)	28	29
29	Parietal: anterolateral to midline	29	25
30	Glenoid: anterior	34	35
31	Glenoid: posterior	35	34
32	Squamosal: ventral zygomatic	32	33
33	Squamosal: dorsal zygomatic	33	32
34	Squamosal: anterior vault	31	30
35	Squamosal: dorsal vault	30	37
36	Squamosal: posterior vault	37	36
37	Squamosal: ventral vault	36	31
38	Supra/Occipital: midline to foramen magnum	39	40
39	Foramen magnum: dorsal	40	41
40	Exoccipital: dorsal	41	42
41	Occipital: dorsolateral to paraoccipital process	42	43
42	Occipital: paraoccipital to ventrolateral occipital	43	44

43	Occipital: ventrolateral to suture with squamosal	44	45
44	Supra/Occipital: dorsal	45	39
45	Exoccipital: medial	41	46
46	Exoccipital: ventral	46	47
47	Exoccipital: lateral	47	42
48	Basioccipital: midline	48	49
49	Basioccipital: anterior	49	50
50	Basioccipital: lateral	50	47
51	Basioccipital: posterior	47	48
52	Basisphenoid: midline	54	51
53	Basisphenoid: anterior	51	52
54	Basisphenoid: lateral	52	54
55	Basisphenoid: posterior	53	54
56	Palatine: midline	55	56
57	Palatine: lateral	56	58
58	Palatine: posterolateral to pterygoid	58	57
59	Palatine: pterygoid to posteromedial	57	55
60	Pterygoid: suture with palatine to process	57	59
61	Pterygoid: posterior	59	60
62	Pterygoid: dorsal	60	57
63	Maxilla (ventral): midline	61	62
64	Maxilla (ventral): anterior	62	63
65	Maxilla (ventral): lateral	63	58
66	Maxilla (ventral):posterior	58	61
67	Premaxilla (ventral): posterior	64	66
68	Premaxilla (ventral): lateral	66	65
69	Premaxilla (ventral): medial	65	64

Phylogenetic Regressions: Tree Topology 1, Extant Taxa only											Factors			
	Size	Diet	Locomotion	Habitat	Development	Activity	Social	Size:Diet	Size:Loc	Size:Hab	Size:Act	Size:Dev	Size:Soc	
Tree Topology 1: Root Age 70-75														
Pillai's Test Statistic	0.979	5.562	7.313	3.688	2.761	1.853	1.838	5.608	6.441	2.764	2.783	1.873	1.871	
SES	4.353	2.025	1.289	0.975	0.900	0.427	0.267	1.695	0.656	0.213	0.555	0.742	0.454	
P value	0.001	0.008	0.081	0.155	0.174	0.382	0.476	0.023	0.268	0.457	0.305	0.243	0.362	
Tree Topology 1: Root Age 75-80														
Pillai's Test Statistic	0.982	5.612	7.391	3.726	2.791	1.866	1.859	5.655	6.502	2.795	2.809	1.886	1.889	
SES	4.695	2.622	2.073	1.619	1.525	0.726	0.679	2.438	1.498	0.911	1.139	1.156	0.878	
P value	0.001	0.002	0.006	0.034	0.050	0.232	0.254	0.002	0.059	0.176	0.110	0.109	0.170	
Tree Topology 1: Root Age 80-85														
Pillai's Test Statistic	0.981	5.608	7.381	3.718	2.783	1.866	1.851	5.645	6.493	2.786	2.804	1.884	1.880	
SES	4.271	2.630	1.930	1.471	1.283	0.783	0.481	2.170	1.273	0.705	0.964	1.042	0.625	
P value	0.001	0.002	0.011	0.056	0.085	0.215	0.329	0.008	0.086	0.252	0.156	0.146	0.291	
Tree Topology 1: Root Age 85-90														
Pillai's Test Statistic	0.981	5.610	7.391	3.718	2.782	1.872	1.854	5.646	6.497	2.785	2.804	1.887	1.880	
SES	4.219	2.593	2.064	1.430	1.236	0.844	0.540	2.095	1.365	0.668	0.968	1.170	0.613	
P value	0.001	0.001	0.010	0.061	0.096	0.186	0.322	0.004	0.071	0.273	0.161	0.097	0.291	
Tree Topology 1: Root Age 90-95														
Pillai's Test Statistic	0.983	5.641	7.436	3.739	2.799	1.882	1.863	5.670	6.535	2.802	2.819	1.896	1.887	
SES	4.438	3.026	2.520	1.869	1.674	1.038	0.717	2.573	1.922	1.083	1.289	1.405	0.820	
P value	0.001	0.001	0.002	0.012	0.033	0.133	0.232	0.001	0.019	0.131	0.071	0.049	0.203	
Tree Topology 1: Root Age 95-100														
Pillai's Test Statistic	0.982	5.619	7.412	3.722	2.786	1.876	1.854	5.647	6.507	2.789	2.808	1.890	1.879	
SES	4.447	2.795	2.249	1.555	1.382	0.996	0.535	2.211	1.537	0.712	1.099	1.258	0.562	
P value	0.001	0.001	0.002	0.049	0.056	0.140	0.336	0.006	0.061	0.253	0.125	0.075	0.310	

Table S2. A) Phylogenetic regressions of ecological, developmental, and social traits on skull shape, assessed with extant taxa only (all factors), for Tree Topology 1.

Phylogenetic Regressions: Tree Topology 1, Full Dataset					
	Factors				
	Size	Diet	Locomotion	Size:Diet	Size:Loc
Tree Topology 1: Root Age 70-75					
Pillai's Test Statistic	0.974	5.387	7.059	5.289	7.006
SES	6.540	3.703	2.767	1.204	0.979
P value	0.001	0.001	0.003	0.109	0.177
Tree Topology 1: Root Age 75-80					
Pillai's Test Statistic	0.974	5.387	7.083	5.296	7.043
SES	6.717	3.626	2.985	1.356	1.378
P value	0.001	0.001	0.002	0.077	0.075
Tree Topology 1: Root Age 80-85					
Pillai's Test Statistic	0.974	5.413	7.069	5.305	7.001
SES	7.303	4.170	2.686	1.282	0.685
P value	0.001	0.001	0.002	0.091	0.264
Tree Topology 1: Root Age 85-90					
Pillai's Test Statistic	0.975	5.452	7.103	5.406	7.074
SES	6.909	4.584	2.808	2.483	1.364
P value	0.001	0.001	0.001	0.005	0.074
Tree Topology 1: Root Age 90-95					
Pillai's Test Statistic	0.974	5.416	7.110	5.339	7.090
SES	6.696	4.080	3.160	1.651	1.861
P value	0.001	0.001	0.002	0.040	0.033
Tree Topology 1: Root Age 95-100					
Pillai's Test Statistic	0.975	5.419	7.103	5.371	7.082
SES	6.980	4.037	3.043	2.167	1.689
P value	0.001	0.001	0.001	0.017	0.043

Table S2. B) Phylogenetic regressions of ecological, developmental, and social traits on skull shape, assessed with full dataset (for diet, locomotion, and size only), for Tree Topology 1.

Phylogenetic Regressions: Tree Topology 2, Extant Taxa only													
	Factors												
	Size	Diet	Locomotion	Habitat	Development	Activity	Social	Size:Diet	Size:Loc	Size:Hab	Size:Act	Size:Dev	Size:Soc
Tree Topology 2: Root Age 70-75													
Pillai's Test Statistic	0.981	5.605	7.381	3.715	2.781	1.867	1.851	5.642	6.492	2.783	2.803	1.885	1.879
SES	4.542	2.606	1.948	1.362	1.251	0.753	0.465	2.052	1.290	0.634	0.942	1.122	0.621
P value	0.001	0.001	0.014	0.069	0.084	0.231	0.373	0.009	0.091	0.279	0.171	0.112	0.297
Tree Topology 2: Root Age 75-80													
Pillai's Test Statistic	0.980	5.584	7.336	3.704	2.774	1.858	1.847	5.629	6.467	2.777	2.794	1.879	1.878
SES	4.364	2.427	1.525	1.146	1.134	0.553	0.452	2.008	1.017	0.504	0.801	0.975	0.600
P value	0.001	0.001	0.048	0.120	0.123	0.329	0.375	0.012	0.161	0.329	0.218	0.176	0.294
Tree Topology 2: Root Age 80-85													
Pillai's Test Statistic	0.980	5.584	7.331	3.706	2.777	1.856	1.849	5.633	6.469	2.780	2.796	1.879	1.882
SES	4.506	2.377	1.490	1.336	1.249	0.553	0.477	2.022	1.027	0.645	0.881	0.960	0.643
P value	0.001	0.001	0.040	0.075	0.100	0.328	0.343	0.013	0.148	0.277	0.188	0.168	0.269
Tree Topology 2: Root Age 85-90													
Pillai's Test Statistic	0.981	5.596	7.382	3.715	2.784	1.866	1.851	5.643	6.490	2.786	2.806	1.885	1.883
SES	4.573	2.402	1.958	1.411	1.418	0.786	0.503	2.160	1.268	0.762	0.970	1.141	0.673
P value	0.001	0.002	0.006	0.070	0.063	0.225	0.344	0.004	0.097	0.249	0.167	0.110	0.250
Tree Topology 2: Root Age 90-95													
Pillai's Test Statistic	0.981	5.608	7.379	3.725	2.790	1.866	1.856	5.650	6.496	2.792	2.809	1.885	1.885
SES	4.588	2.586	1.906	1.530	1.465	0.770	0.568	2.249	1.443	0.889	1.102	1.134	0.771
P value	0.001	0.001	0.010	0.050	0.058	0.238	0.306	0.005	0.068	0.195	0.123	0.105	0.227
Tree Topology 2: Root Age 95-100													
Pillai's Test Statistic	0.980	5.583	7.344	3.674	2.751	1.866	1.830	5.595	6.437	2.750	2.774	1.877	1.850
SES	4.320	2.323	1.616	0.740	0.660	0.709	0.093	1.444	0.549	-0.139	0.356	0.766	-0.022
P value	0.001	0.003	0.033	0.244	0.283	0.238	0.546	0.062	0.323	0.605	0.379	0.223	0.590

Table S2. C) Phylogenetic regressions of ecological, developmental, and social traits on skull shape, assessed with extant taxa only (all factors), for Tree Topology 2.

Phylogenetic Regressions: Tree Topology 2, Full Dataset					
	Factors				
	Size	Diet	Locomotion	Size:Diet	Size:Loc
Tree Topology 2: Root Age 70-75					
Pillai's Test Statistic	0.975	5.383	7.049	5.291	7.011
SES	6.888	3.629	2.481	1.185	0.965
P value	0.001	0.001	0.004	0.112	0.165
Tree Topology 2: Root Age 75-80					
Pillai's Test Statistic	0.974	5.383	7.044	5.298	7.044
SES	6.785	3.404	2.442	1.273	1.351
P value	0.001	0.001	0.007	0.092	0.087
Tree Topology 2: Root Age 80-85					
Pillai's Test Statistic	0.974	5.383	7.045	5.298	7.044
SES	6.879	3.478	2.474	1.243	1.410
P value	0.001	0.001	0.003	0.103	0.074
Tree Topology 2: Root Age 85-90					
Pillai's Test Statistic	0.974	5.424	7.097	5.315	7.018
SES	7.167	3.979	3.222	1.422	0.894
P value	0.001	0.001	0.001	0.061	0.186
Tree Topology 2: Root Age 90-95					
Pillai's Test Statistic	0.974	5.383	7.058	5.350	7.061
SES	6.756	3.711	2.549	1.928	1.622
P value	0.001	0.001	0.005	0.011	0.050
Tree Topology 2: Root Age 95-100					
Pillai's Test Statistic	0.975	5.401	7.092	5.305	7.030
SES	6.880	3.723	3.091	1.323	1.182
P value	0.001	0.001	0.001	0.093	0.113

Table S2. D) Phylogenetic regressions of ecological, developmental, and social traits on skull shape, assessed with full dataset (for diet, locomotion, and size only), for Tree Topology 2.

Phylogenetic Regressions: Tree Topology 3, Extant Taxa only

	Factors												
	Size	Diet	Locomotion	Habitat	Development	Activity	Social	Size:Diet	Size:Loc	Size:Hab	Size:Act	Size:Dev	Size:Soc
Tree Topology 3: Root Age 70-75													
Pillai's Test Statistic	0.979	5.566	7.315	3.692	2.763	1.853	1.839	5.614	6.443	2.767	2.785	1.873	1.871
SES	4.321	2.112	1.345	1.057	0.852	0.531	0.255	1.794	0.633	0.243	0.615	0.745	0.501
P value	0.001	0.004	0.069	0.141	0.190	0.330	0.481	0.018	0.287	0.440	0.300	0.234	0.348
Tree Topology 3: Root Age 75-80													
Pillai's Test Statistic	0.982	5.625	7.416	3.729	2.792	1.876	1.857	5.659	6.516	2.794	2.813	1.892	1.883
SES	4.505	2.859	2.315	1.696	1.515	0.974	0.584	2.318	1.617	0.838	1.148	1.303	0.684
P value	0.001	0.001	0.006	0.028	0.046	0.142	0.299	0.004	0.039	0.206	0.105	0.076	0.272
Tree Topology 3: Root Age 80-85													
Pillai's Test Statistic	0.982	5.615	7.408	3.729	2.795	1.869	1.859	5.651	6.505	2.797	2.814	1.887	1.890
SES	4.467	2.735	2.294	1.692	1.587	0.833	0.683	2.326	1.488	1.026	1.227	1.197	0.826
P value	0.001	0.002	0.003	0.031	0.036	0.195	0.258	0.004	0.053	0.146	0.099	0.102	0.192
Tree Topology 3: Root Age 85-90													
Pillai's Test Statistic	0.979	5.564	7.336	3.688	2.763	1.857	1.838	5.608	6.445	2.765	2.786	1.875	1.869
SES	4.440	2.170	1.549	1.024	0.864	0.584	0.221	1.701	0.676	0.194	0.558	0.829	0.440
P value	0.001	0.009	0.041	0.154	0.208	0.300	0.473	0.028	0.245	0.458	0.319	0.219	0.372
Tree Topology 3: Root Age 90-95													
Pillai's Test Statistic	0.981	5.590	7.367	3.709	2.778	1.861	1.847	5.630	6.477	2.780	2.799	1.880	1.879
SES	4.511	2.481	1.821	1.277	1.181	0.619	0.397	2.008	1.126	0.525	0.952	0.902	0.606
P value	0.001	0.002	0.010	0.083	0.103	0.287	0.388	0.009	0.118	0.332	0.176	0.176	0.296
Tree Topology 3: Root Age 95-100													
Pillai's Test Statistic	0.981	5.609	7.385	3.717	2.784	1.867	1.853	5.641	6.490	2.786	2.806	1.885	1.879
SES	4.465	2.680	2.035	1.400	1.337	0.741	0.484	2.205	1.238	0.640	1.077	1.095	0.594
P value	0.001	0.002	0.007	0.078	0.082	0.233	0.347	0.004	0.104	0.277	0.125	0.113	0.300

Table S2. E) Phylogenetic regressions of ecological, developmental, and social traits on skull shape, assessed with extant taxa only (all factors), for Tree Topology 3.

Phylogenetic Regressions: Tree Topology 3, Full Dataset					
	Factors				
	Size	Diet	Locomotion	Size:Diet	Size:Loc
Tree Topology 3: Root Age 70-75					
Pillai's Test Statistic	0.974	5.385	7.060	5.291	7.003
SES	6.761	3.812	2.763	1.260	0.961
P value	0.001	0.001	0.001	0.095	0.153
Tree Topology 3: Root Age 75-80					
Pillai's Test Statistic	0.974	5.426	7.083	5.370	7.053
SES	6.533	3.719	2.791	2.284	1.427
P value	0.001	0.001	0.001	0.006	0.061
Tree Topology 3: Root Age 80-85					
Pillai's Test Statistic	0.975	5.406	7.119	5.349	7.067
SES	6.533	3.980	3.359	1.973	1.645
P value	0.001	0.001	0.001	0.018	0.040
Tree Topology 3: Root Age 85-90					
Pillai's Test Statistic	0.974	5.409	7.106	5.301	7.030
SES	6.896	3.980	3.325	1.295	1.187
P value	0.001	0.001	0.001	0.090	0.114
Tree Topology 3: Root Age 90-95					
Pillai's Test Statistic	0.974	5.436	7.116	5.356	7.061
SES	6.914	4.065	3.268	1.896	1.466
P value	0.001	0.001	0.001	0.015	0.062
Tree Topology 3: Root Age 95-100					
Pillai's Test Statistic	0.974	5.418	7.082	5.361	7.041
SES	6.626	4.212	2.957	2.015	1.244
P value	0.001	0.001	0.001	0.009	0.103

Table S2. F) Phylogenetic regressions of ecological, developmental, and social traits on skull shape, assessed with full dataset (for diet, locomotion, and size only), for Tree Topology 3.

Data S1. (separate file)

Specimen details and species trait data.